Electronic Supplementary Material (ESI) for Chemical Science.
This journal is © The Royal Society of Chemistry 2022

Supporting Information for

Direct Observation of Reversible Bond Homolysis by 2D EXSY NMR

Satoshi Takebayashi[a,*], Robert R. Fayzullin[b], and Richa Bansal[a]

[a] Science and Technology Group, Okinawa Institute of Science and Technology Graduate University, 1919-1 Tancha, Onna-son, Okinawa 904-0495, Japan

[b] Arbuzov Institute of Organic and Physical Chemistry, FRC Kazan Scientific Center, Russian Academy of Sciences, 8 Arbuzov Street, Kazan 420088, Russian Federation

[*]Correspondence to: satoshi.takebayashi@oist.jp

Table of Contents

1. General considerations and materials

All reactions were carried out under an N_2 atmosphere using an MBRAUN glovebox, UNILAB Plus SP, equipped with an MB-20-G gas purifier, and an MB-LMF-2/40-REG regenerable solvent trap, and an MB-GS-35 -35 °C freezer, or using standard Schlenk techniques. All glassware was dried overnight at 170 °C and cooled down under a vacuum in the glovebox antechamber. All solvents were reagent grade or higher. n-Pentane (≥99.0%), hexane (≥95.0%, n-hexane with minor amount of isomers of methylpentane, and methylcyclopentane), n-heptane (≥99.0%), dichloromethane (≥99.5%), benzene (≥99.7%), toluene (≥99.8%), acetonitrile (≥99.8%), methanol (≥99.8%), tetrahydrofuran (Sigma-Aldrich 401757-1L, anhydrous, ≥99.9%, inhibitor-free), diethyl ether (≥99.5% with 3ppm BHT), hexamethyldisiloxane (Sigma-Aldrich 205389-500ML, ≥98%) were dried for more than two days over MS3A (dried in a 200°C oven for overnight and cooled under vacuum overnight in the glovebox antechamber) in the glovebox and kept in the glovebox. Common chemicals were purchased and were used as received unless stated otherwise. $Co_2(CO)_8$ (stabilized with 1-5% hexane, >99%) was purchased from TCI at the beginning of this study and kept in the glovebox freezer during this study (about six months). 2,2,6,6-Tetramethyl-1-piperidinyloxy (TEMPO, ≥98.0%) was purchased from Nacalai Tesque Inc and kept in the glovebox freezer. White crystals of 1,3-bis(2,6-diisopropylphenyl)imidazolidin-2-ylidene (**SIPr**),[1] 1,3-bis(2,6-diethylphenyl)imidazolidin-2-ylidene (**SIEt**),[2] and 1,3-bis(2,6-dimethylphenyl)imidazolidin-2-ylidene (**SIMe**)[3] were prepared from the corresponding imidazolium chloride (for **SIPr**) or bromide (for **SIEt** and **SIMe**) using the literature procedure and stored at -35 °C. 1,3-Bis(4-diethylamino-2,6-dimethylphenyl)-4,5-dihydroimidazolium chloride (**NEt_2-SIMe-HCl**) was prepared according to a literature method.[4] Complex 1 was prepared according to a literature method[5]. Celite filtration was carried out using a pipet, cotton wool, and Celite®545, which was dried in a 170 °C oven overnight, cooled down under a vacuum overnight in the glovebox antechamber and kept in the glovebox. The dimensions of the 20 mL vial are 60 mm in height and 28 mm in outer diameter, and the Teflon coated stirring bar is 15 mm long and 5 mm in diameter.

2. Analysis methods

NMR spectroscopy:

All deuterated solvents were purchased and dried over MS3A for more than two days in the glovebox and kept in the glovebox. NMR spectra were recorded using Bruker Avance III-400N, Avance III NEO 500 equipped with a cryoprobe, and JEOL JNM-ECZ600R/M3 spectrometers. ^1H and $^{13}C\{^1H\}$ NMR chemical shifts are reported in parts per million (δ) relative to TMS with the residual solvent signal ($CDCl_3$: 7.26 (^1H) and 77.16 (^{13}C) ppm, C_6D_6: 7.16 (^1H) and 128.06 (^{13}C) ppm, THF-d_8: 1.72 (^1H) and 25.31 (^{13}C) ppm, toluene-d_8: 2.08 (^1H) and 20.43 (^{13}C) ppm, DMSO-d_6: 2.50 (^1H) and 39.52 (^{13}C) ppm, methanol-d_4: 3.31 (^1H) and 49.00 (^{13}C) ppm) as the internal reference. ^2H NMR chemical shifts are reported in parts per million (δ) relative to residual solvent signal (THF-d_8: 1.72 (^1H)) as the internal reference.

NMR peak assignments of diamagnetic compounds were made using ^1H-^1H-gCOSY, ^1H-^{13}C-HMQC, and ^1H-^{13}C-HMBC NMR experiments. Abbreviations for NMR spectra are s (singlet), d (doublet), t (triplet), q (quartet), quint (quintet) sep (septet), dd (doublet of doublet), td (doublet of triplet), dq (doublet of quartet), m (multiplet), and br (broad). Air-sensitive NMR samples were prepared in a nitrogen glovebox using a J. Young NMR tube or a standard NMR tube sealed with a septum and parafilm. High-pressure NMR experiments were conducted using Wilmad 524-PV-7 (O.D.:5 mm, I.D.: 3.46 mm, recommended

maximum pressure: 10.3 bar) or 528-PV-6 (O.D.:5 mm, I.D.: 4.24 mm, recommended maximum pressure: 6.9 bar).

NMR measurement of paramagnetic complexes:

^{1}H NMR of paramagnetic complexes (typically 20 mM solution) was measured with delay time (d1) of 0.1 s, time-domain data points (td) of 128k, and scan number of 1-128. Wide spectral width (sw) of 200 to 400 ppm was used to ensure the detection of paramagnetically shifted signals. ^{13}C{^{1}H} NMR experiments were not attempted on paramagnetic complexes. ^{1}H NMR signals were assigned based on integration value.

Measurement of the effective magnetic moment by Evans' method:

Measurement of the effective magnetic moment by Evans' method was carried out using glass capillaries containing C_6D_6 (measurement in C_6D_6) or 1,3,5-trimethoxybenzene in toluene-d_8 (measurement in toluene-d_8) as external standards.

FTIR spectroscopy:

IR spectra were recorded using a Nicolet iS5 FT-IR spectrophotometer and are reported in the frequency of absorption (cm^{-1}). Abbreviations for FT-IR spectra are s (strong), m (medium), and w (weak).

High-resolution mass spectrometry (HRMS):

HRMS were recorded using a Thermo Scientific LTQ-Orbitrap mass spectrometer, using Electro Spray Ionization (ESI) mode. Attempts to measure HRMS of most of the air-sensitive cobalt complexes resulted in the detection of decomposed complexes.

Elemental analyses:

Elemental analyses were conducted using Exeter Analytical CE-440 Elemental Analyzer. All samples were weighed and sealed in tin cups in a nitrogen glovebox. N_2 gas in the tin cups was replaced by argon by three vacuum argon refill cycles. All the samples were analyzed using an autosampler under a He atmosphere.

EPR spectroscopy:

EPR samples were prepared in a nitrogen glovebox using 5 mm outer diameter quartz EPR tubes sealed with rubber septums and parafilm for sealing. X-band EPR spectra were recorded using a JEOL JES-X330 X-band EPR spectrometer equipped with JEOL ES-CT470 electrical heating and systems.

UV-Vis spectroscopy:

UV-Vis spectra were recorded using a Cary 60 UV-Vis spectrophotometer and quartz cuvettes (pathlength: 10 mm x 10 mm) equipped with a screw cap.

2. Preparation of NHC ligands

1,3-Bis(2,4,6-trimethylphenyl)-4,5-dihydroimidazol-2-ylidene (SIMes)

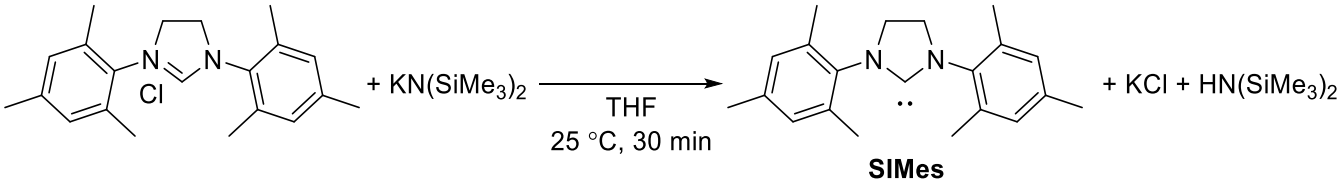

SIMes

SIMes is a well-known compound; however, its preparation and isolation from imidazolium salt are not clearly reported according to Scifinder searcing.[3,6] It was prepared using a modified procedure of ref. 3. In a nitrogen glovebox, a 20 mL vial equipped with a Teflon coated stirring bar was charged with 1,3-Bis(2,4,6-trimethylphenyl)-4,5-dihydroimidazolium chloride (786.7 mg, 2.29 mmol), and $KN(SiMe_3)_2$ (480.3 mg, 2.41 mmol). 8 mL THF was then added to the vial at 25 °C. The suspension was stirred for 1 h at 25 °C. Formation of faint yellow solution and fine precipitate of KCl was observed. The suspension was filtered through Celite , and the Celite was washed with THF. The clear yellow solution was concentrated, and faint yellow solid was obtained. Yield: 677.5 mg, 97%. The crude solid was pure enough to be used for the complex formation. The clean formation of the carbene was confirmed by ^{1}H NMR (Figure S1).

^{1}H NMR (400.15 MHz, C_6D_6, 298 K): δ 1.91 (12H, s, 4 *ortho*-C*H*$_3$), 2.21 (6H, s, 2 *para*-C*H*$_3$), 2.86 (4H, br, 2 C*H*$_2$), 6.74 (4H, pseudo d due to small unresolved coupling constant, *meta*-C*H*).

1,3-Bis(4-bromo-2,6-dimethylphenyl)-4,5-dihydroimidazol-2-ylidene (Br-SIMe)

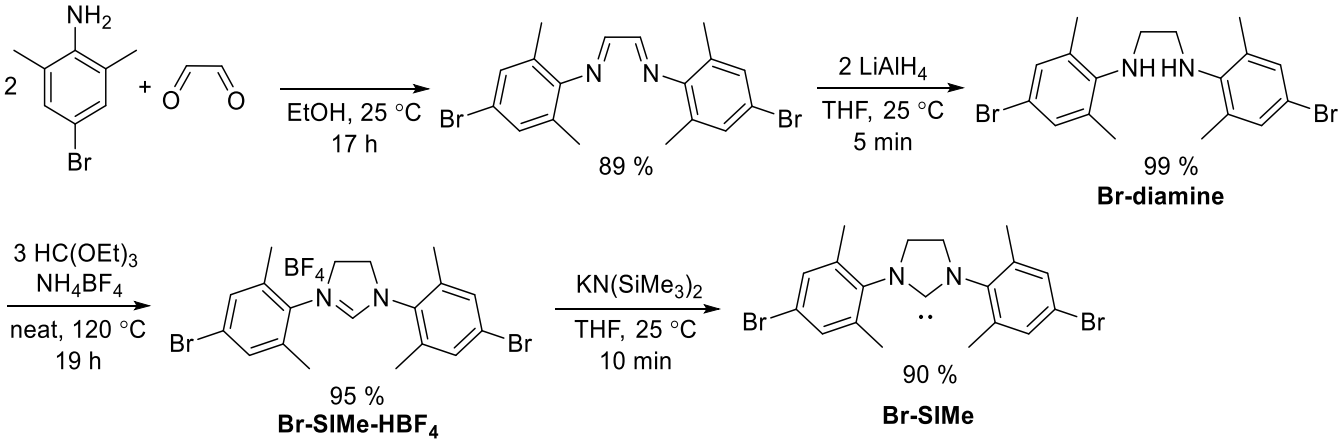

Br-SIMe is a known compound; however, its preparation from HBF_4 salt is not known.[7]

A 100 mL round bottom flask equipped with a Teflon coated stirring bar was charged with 4-bromo-2,6-dimethylaniline (4.0311 g, 20.0 mmol), glyoxal (40 % in water, 1.4545 g, 10.0 mmol), 20 mL ethanol, and three drops of formic acid. Argon was flushed into the flask, and the flask was closed with a glass stopper. The mixture was stirred for 17 h at 25 °C. The resulting yellow solid was filtered, washed with 10 mL ethanol, and dried under vacuum (2.7487 g). The concentration of filtrate gave 2nd crop of the solid (1.0241 g). Total yield: 3.7728 g, 89 %. It is a known compound.[8]

The diimine (3.7728 g, 8.94 mmol) was added to a 250 mL round bottom flask equipped with a Teflon coated stirring bar. The flask was brought into a nitrogen glovebox, and the yellow solid was dissolved in 40 mL THF. To the clear, orange solution was added $LiAlH_4$ (680.3 mg, 17.9 mmol) portionwise at 25 °C. Formation of H_2 and mild heating of the solution were observed. The solution color

changed to dark brown and then a faint yellow. The mixture was stirred for 5 min at 25 °C. The flask was brought outside the glovebox, and the reaction was quenched by dropwise addition of 4 mL MeOH at 0 °C while stirring the flask (Caution! exothermic reaction with evolution of H_2). The resulting slurry with a stirring bar was slowly concentrated to dryness using a rotary evaporator to avoid bumping. To the resulting yellow solid was added ca. 50 mL dichloromethane, and the mixture was stirred until the solid broke up to fine powder. The resulting yellow suspension was vacuum filtered using Celite packed in a fritted glass funnel. The flask and the solids were washed a few times to quantitatively filter the product. The resulting clear yellow solution was concentrated to dryness to obtain a yellow solid of diamine product. Yield: 3.7772 g, 99 %. The clean formation of the diamine product (**Br-diamine**) was confirmed by ^{1}H NMR (Figure S2). No further characterization was conducted. It is a known compound.[8]
^{1}H NMR (400.15 MHz, $CDCl_3$, 298 K): δ 2.26 (12H, s, 4 *ortho*-C*H*$_3$), 3.15 (4H, s, 2 C*H*$_2$), 3.30 (2H, br, overlapping with CH_2 signal, 2 N*H*), 7.13 (4H, s, 4 *meta*-C*H*).

The diamine (3.7772 g, 8.86 mmol), NH_4BF_4 (933.6 mg, 8.90 mmol), and $HC(OEt)_3$ (3.9573 g, 26.7 mmol) were charged in a 250 mL round bottom flask equipped with a Teflon coated stirring bar. The mixture was stirred for 19 h at 120 °C. To the resulting suspension was added ca. 50mL diethyl ether. The resulting off-white solid was filtered, washed with ether, and dried under a vacuum. Yield: 4.3953 g, 95%. The clean formation of imidazolium salt (**Br-SIMe-HBF$_4$**) was confirmed by comparison of ^{1}H NMR spectra with that of known HCl salt[9] (Figure S3).
^{1}H NMR (400.15 MHz, DMSO-d_6, 298 K): δ 2.38 (12H, s, 4 *ortho*-C*H*$_3$), 4.46 (4H, s, 2C*H*$_2$), 7.55 (4H, s, 4 *meta*-C*H*), 8.99 (1H, s, NCHN).

In a nitrogen glovebox, the imidazolium salt (527.2 mg, 1.01 mmol) and $KN(SiMe_3)_2$ (206.6 mg, 1.04 mmol) were weighed in a 20 mL vial equipped with a Teflon coated stirring bar. To the stirred mixture was added 4 mL C_6H_6 at 25 °C. The mixture was stirred for 30 min at 25 °C, concentrated to dryness, redissolved in diethyl ether, and filtered through a plug of Celite. The resulting brown solution was concentrated to obtain an orange solid. Yield: 390.6 mg, 90%. The crude solid was pure enough to be used for the complex formation. The clean formation of the carbene was confirmed by ^{1}H NMR (Figure S4).[7]
^{1}H NMR (400.15 MHz, C_6D_6, 298 K): δ 2.03 (12H, s, 4 *ortho*-C*H*$_3$), 3.05 (4H, s, 2C*H*$_2$), 7.18 (4H, s, overlapping with C_6D_6 signal, 4 *meta*-C*H*).

1,3-Bis(4-ethoxy-2,6-dimethylphenyl)-4,5-dihydroimidazolium chloride (EtO-SIMe-HCl)

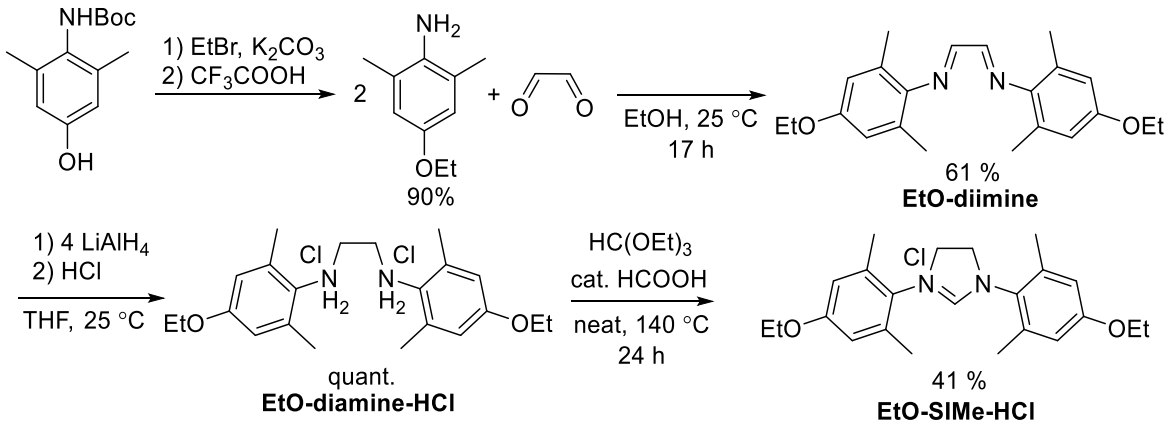

A 250 mL round bottom flask equipped with a Teflon coated stirring bar was charged with *tert*-butyl (4-hydroxy-2,6-dimethylphenyl)carbamate[10] (5.4379 g, 22.9 mmol) and 50 mL dry acetone. To the flask

was added K_2CO_3 (6.4 g, 46.3 mmol) and EtBr (2.6 mL, 34.8 mmol). Argon was flushed into the flask, and the flask was closed with a glass stopper. The mixture was stirred at 65 °C. EtBr (1.3 mL, 17.4 mmol) was added after 24h and 48 h. The conversion was checked each day using GC-MS, and full conversion was achieved after three days. The resulting yellow solution was vacuum filtered using Celite packed in a fritted glass funnel, and the flask and Celite were washed with acetone. The concentration of acetone solution gave brown oil. To a 100 mL flask containing the brown oil were added 30 mL CH_2Cl_2 and 10 mL CF_3COOH. The solution was stirred for 4 h at 25 °C. GC-MS analysis of the solution after four h showed full conversion of the carbamate to 4-ethoxy -2,6-dimethylanilne. Yield: 3.3965 g, 90%. The formation of 4-ethoxy -2,6-dimethylanilne was confirmed by ^{1}H NMR (Figure S5). No further characterization was conducted.

^{1}H NMR (400.15 MHz, C_6D_6, 298 K): δ 1.36 (3H, t, $^3J_{HH}$ = 7.0 Hz, OCH_2CH_3), 2.17 (12H, s, 2 *ortho*-CH_3), 3.0 (not integrable very broad signal, NH_2), 3.95 (2H, q, $^3J_{HH}$ = 7.0 Hz, OCH_2CH_3), 6.56 (2H, s, 2 *meta*-C*H*).

A 100 mL round bottom flask equipped with a Teflon coated stirring bar was charged with 4-ethoxy-2,6-dimethylaniline (3.3965 g, 20.6 mmol), glyoxal (40 % in water, 1.4857 g, 10.2 mmol), 20 mL ethanol, and a drop of formic acid. Argon was flushed into the flask, and the flask was closed with a glass stopper. The mixture was stirred for 16 h at 25 °C. The resulting yellow solid was filtered, washed with 10 mL ethanol, and dried under vacuum to give a yellow solid of **EtO-diimine**. Yield: 2.0434 g, 61 %. The formation of **EtO-diimine** was confirmed by ^{1}H, ^{13}C{^{1}H}, HSQC, and HMBC NMR, and HRMS. Figure S6 shows ^{1}H and ^{13}C{^{1}H}NMR spectra of **EtO-diimine**.

^{1}H NMR (500.13 MHz, $CDCl_3$, 298 K): δ 1.41 (6H, t, $^3J_{HH}$ = 7.0 Hz, $2OCH_2CH_3$), 2.19 (12H, s, 4 *ortho*-CH_3), 4.02 (4H, q, $^3J_{HH}$ = 7.0 Hz, $2OCH_2CH_3$), 6.64 (4H, s, 4 *meta*-C*H*), 8.10 (2H, s, 2N=C*H*).

^{13}C{^{1}H} NMR (125.76 MHz, $CDCl_3$, 298 K): δ 15.08 (s, $2OCH_2CH_3$) 18.89 (s, 4 *ortho*-CH_3), 63.61 (s, $2OCH_2CH_3$), 114.40 (s, 4 *meta*-CH), 128.77 (s, 4 *ortho*-*C*), 143.31 (s, 2*C*N), 156.20 (s, 2 *para*-*C*), 163.54 (s, 2N=*C*H).

HRMS (ESI$^+$): Calcd for $C_{22}H_{29}N_2O_2$ ($[M+H]^+$): 353.2229. Found: 321.2211.

The diimine (2.0434 g, 6.24 mmol) was added to a 250 mL round bottom flask equipped with a Teflon coated stirring bar. The flask was brought into a nitrogen glovebox, and the yellow solid was dissolved in 40 mL THF. To the clear, orange solution was added $LiAlH_4$ (1 g, 26 mmol) portionwise at 25 °C. Formation of H_2 and mild heating of the solution were observed. The solution color changed to dark brown and then a faint yellow. The mixture was stirred for 5 min at 25 °C. The flask was brought outside the glovebox, and the reaction was quenched by dropwise addition of MeOH at 0 °C while stirring the flask until the formation of H_2 stopped (Caution! exothermic reaction with evolution of H_2). The resulting slurry with a stirring bar was slowly concentrated to dryness using a rotary evaporator to avoid bumping. To the resulting yellow solid was added ca. 50 mL dichloromethane and the mixture was stirred until the solid broke up and formed fine powder. The resulting yellow suspension was vacuum filtered using Celite charged in a fritted glass funnel. The flask and the solids were washed a few times to quantitatively filter the product. The resulting clear yellow solution was concentrated to dryness to obtain a yellow solid of diamine product. The product contained 4% (determined by ^{1}H NMR) of unreduced **EtO-diimine**. Thus, the $LiAlH_4$ reduction described above was repeated. After the second reduction, an off-white solid of **EtO-diamine** was obtained (2.1557 g, quant.). The formation of **EtO-diamine** was confirmed by ^{1}H, ^{13}C{^{1}H}, HSQC, and HMBC NMR, and HRMS. Figure S7 shows ^{1}H and ^{13}C{^{1}H}NMR spectra of **EtO-diamine**.

^{1}H NMR (500.13 MHz, $CDCl_3$, 298 K): δ 1.38 (6H, t, $^3J_{HH}$ = 7.0 Hz, 2OCH$_2$C*H$_3$*), 2.21 (12H, s, 4 *ortho*-C*H$_3$*), 3.08 (4H, s, 2C*H$_2$*), 3.13 (2H, br, overlapping with a CH_2 signal, 2N*H*), 3.97 (4H, q, $^3J_{HH}$ = 7.0 Hz, 2OC*H$_2$*CH$_3$), 6.58 (4H, s, 4 *meta*-C*H*).
^{13}C{^{1}H} NMR (125.76 MHz, $CDCl_3$, 298 K): δ 15.13 (s, 2OCH$_2$*C*H$_3$) 18.79 (s, 4 *ortho*-*C*H$_3$), 49.63 (s, 2*C*H$_2$), 63.64 (s, 2O*C*H$_2$CH$_3$), 114.78 (s, 4 *meta*-*C*H), 131.98 (s, 4 *ortho*-*C*), 139.25 (s, 2*C*N), 154.31 (s, 2 *para*-*C*).
HRMS (ESI$^+$): Calcd for $C_{22}H_{33}N_2O_2$ ([M+H]$^+$): 357.2542. Found: 321.2529.

EtO-diamine (2.1557 g, 6.50 mmol) was dissolved in CH_2Cl_2 and 35% $HCl_{(aq)}$ (1 mL, 15 mmol) was added. The resulting white suspension was concentrated to dryness by a rotary evaporator to obtain a white solid of **EtO-diamine-HCl** quantitatively. The formation of **EtO-diamine-HCl** was confirmed by ^{1}H and ^{13}C{^{1}H}NMR (Figure S8).
^{1}H NMR (500.13 MHz, methanol-*d*$_4$, 298 K): δ 1.39 (6H, t, $^3J_{HH}$ = 7.0 Hz, 2OCH$_2$C*H$_3$*), 2.51 (12H, s, 4 *ortho*-C*H$_3$*), 3.87 (4H, s, 2C*H$_2$*), 4.04 (4H, q, $^3J_{HH}$ = 7.0 Hz, 2OC*H$_2$*CH$_3$), 6.78 (4H, s, 4 *meta*-C*H*).
^{13}C{^{1}H} NMR (125.76 MHz, methanol-*d*$_4$, 298 K): δ 15.01 (s, 2OCH$_2$*C*H$_3$) 18.47 (s, 4 *ortho*-*C*H$_3$), 47.54 (s, 2*C*H$_2$), 64.87 (s, 2O*C*H$_2$CH$_3$), 116.93 (s, 4 *meta*-*C*H), 126.70 (br s, 4 *ortho*-*C*), 134.65 (s, 2*C*N), 160.75 (s, 2 *para*-*C*).

EtO-diamine-HCl (813.7 mg, 1.89 mmol), formic acid (3 drops), and 10 mL $HC(OEt)_3$ were charged in a 50 mL round bottom flask equipped with a Teflon coated stirring bar. The mixture was stirred for 24 h at 140 °C. To the resulting suspension was added ca. 50mL diethyl ether. The resulting white solid was filtered, washed with diethyl ether and ethyl acetate, and dried under a vacuum. Yield: 313.0 mg, 41%. The formation of **EtO-SIMe-HCl** was confirmed by ^{1}H, ^{13}C{^{1}H}, HSQC, and HMBC NMR, and HRMS. Figure S9 shows ^{1}H and ^{13}C{^{1}H}NMR spectra of **EtO-SIMe-HCl**.
^{1}H NMR (500.13 MHz, $CDCl_3$, 298 K): δ 1.40 (6H, t, $^3J_{HH}$ = 7.0 Hz, 2OCH$_2$C*H$_3$*), 2.41 (12H, s, 4 *ortho*-C*H$_3$*), 4.00 (4H, q, $^3J_{HH}$ = 7.0 Hz, 2OC*H$_2$*CH$_3$), 4.60 (4H, s, 2 C*H$_2$*), 6.65 (4H, s, 4 *meta*-C*H*), 9.09 (1H, s, NC*H*N).
^{13}C{^{1}H} NMR (125.76 MHz, $CDCl_3$, 298 K): δ 14.84 (s, 2OCH$_2$*C*H$_3$) 18.59 (s, 4 *ortho*-*C*H$_3$), 52.36 (s, 2 *C*H$_2$), 63.87 (s, 2O*C*H$_2$CH$_3$), 115.09 (s, 4 *meta*-*C*H), 125.43 (s, 4 *ortho*-*C*), 136.89 (s, 2*C*N), 159.95 (s, 2 *para*-*C*), 160.22 (s, N*C*HN).
HRMS (ESI$^+$): Calcd for $C_{23}H_{31}N_2O_2$ ([M-Cl]$^+$): 367.2386. Found: 367.2381.

1,3-Bis(4-diethylamino-2,6-trimethylphenyl)-4,5-dihydroimidazol-2-ylidene (NEt$_2$-SIMe)

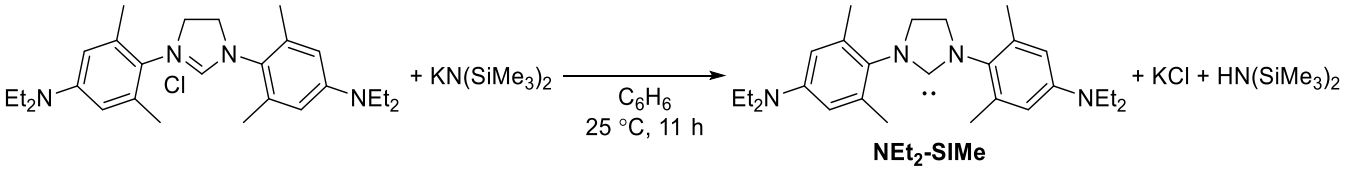

In a nitrogen glovebox, a 20 mL vial equipped with a Teflon coated stirring bar was charged with 1,3-Bis(4-diethlamino-2,6-trimethylphenyl)-4,5-dihydroimidazolium chloride[4] (136.7 mg, 0.299 mmol), and $KN(SiMe_3)_2$ (66.9 mg, 0.335 mmol). 6 mL benzene was then added to the vial at 25 °C. The suspension was stirred for 11 h at 25 °C. The formation of yellow solution and fine precipitate of KCl was observed. The solution was concentrated to dryness, and the product was extracted using diethyl ether. The concentration of the ether solution gave a brown solid of crude product. The solid was washed three times with ca. 5 mL cold pentane and dried to obtain an off-white solid of pure **NEt$_2$-SIMe**. Yield: 54.1 mg,

43%. The clean formation of the carbene was confirmed by ^{1}H and ^{13}C{^{1}H} NMR and HRMS (Figure S10).
^{1}H NMR (500.13 MHz, $CDCl_3$, 298 K): δ 0.99 (12H, t, $^{3}J_{HH}$ = 7.0 Hz, 2N(CH_2CH_3)$_2$), 2.43 (12H, s, 4 *ortho*-CH_3), 3.08 (8H, q, $^{3}J_{HH}$ = 7.0 Hz, 2N(CH_2CH_3)$_2$), 3.39 (4H, s, 2 CH_2), 6.53 (4H, s, 4 *meta*-C*H*).
^{13}C{^{1}H} NMR (125.76 MHz, $CDCl_3$, 298 K): δ 12.89 (s, 2N(CH_2CH_3)$_2$) 19.09 (s, 4 *ortho*-CH_3), 44.59 (s, 2N(CH_2CH_3)$_2$), 51.41 (s, 2 CH_2), 112.41 (s, 4 *meta*-CH), 131.81 (s, 2CN), 137.29 (s, 4 *ortho*-*C*), 146.83(s, 2 *para*-*C*), 244.47 (s, NCN).
HRMS (ESI^{+}): Calcd for $C_{27}H_{11}N_4$ ([M+H]$^{+}$): 421.3331. Found: 421.3316.

Preparation of Co and Ni complexes

Preparation of [Co(SIMes)(CO)$_3$]$_2$ (2-Mes)

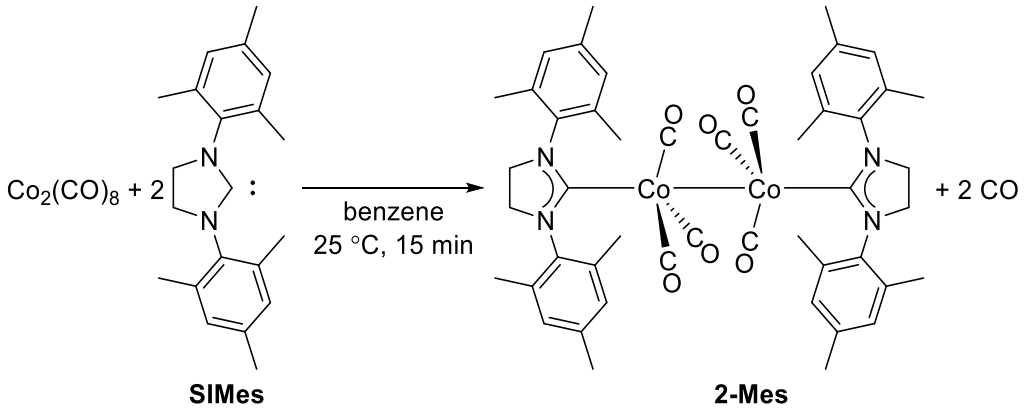

In a nitrogen glovebox, a 20 mL vial equipped with a Teflon coated stirring bar was charged with $Co_2(CO)_8$ (85.4 mg, 0.250 mmol) and 1,3-Bis(2,4,6-trimethylphenyl)imidazolidin-2-ylidene (**SIMes**) (153.3 mg, 0.500 mmol). 5 mL benzene was then added to the vial at 25 °C. The vial was quickly attached to a vacuum line, and the solution was kept under a slight static vacuum (until the solution started to boil) to minimize CO contamination of the glovebox. Rapid CO evolution was observed when benzene was added. Brown solution and precipitate were formed after stirring the solution for 15 min at 25 °C. 10 mL n-pentane was added to the brown suspension while stirring to precipitate more product. The brown precipitate of **2-Mes** was washed with 6 mL n-pentane and dried under vacuum. Yield: 214.4 mg, 95%.
Figures S11-13 and S36 show ^{1}H and ^{13}C{^{1}H}NMR, FTIR, and UV-Vis spectra of **2-Mes**.
^{1}H NMR (500.13 MHz, C_6D_6, 298 K): δ 2.08 (12H, s, 4 *para*-CH_3), 2.23 (24H, s, 8 *ortho*-CH_3), 3.01 (8H, s, 4 CH_2), 6.78 (8H, s, 8 *meta*-C*H*).
^{13}C{^{1}H} NMR (125.76 MHz, C_6D_6, 298 K): δ 18.29 (s, 8 *ortho*-CH_3), 21.08 (s, 4 *para*-CH_3), 51.07 (s, 4 CH_2) , 129.82 (s, 8 *meta*-CH), 136.97 (s, 8 *ortho*-*C*), 137.83 (s, 4CN), 137.92 (s, 4 *para*-*C*), 205.40 (s, 6CO), 216.38 (s, 2NCN).
FTIR (KBr pellet, cm^{-1}): 2024 (w, CO), 1965 (s, CO), 1947 (s, CO), 1911 (s, CO).
UV-Vis (in THF, 25 °C): λ_{max} = 369 nm (Co-Co σ-σ* transition. ε was not calculated as [dimer] is unknown).
Elemental analysis: Calcd: C:64.14, H:5.83, N:6.23. Found: C:64.00, H:5.56, N:6.20.
HRMS (ESI$^{+/-}$): Only a free SIMes ligand signal was detected.

Preparation of [Co(SIMes)(TEMPO)(CO)](3)

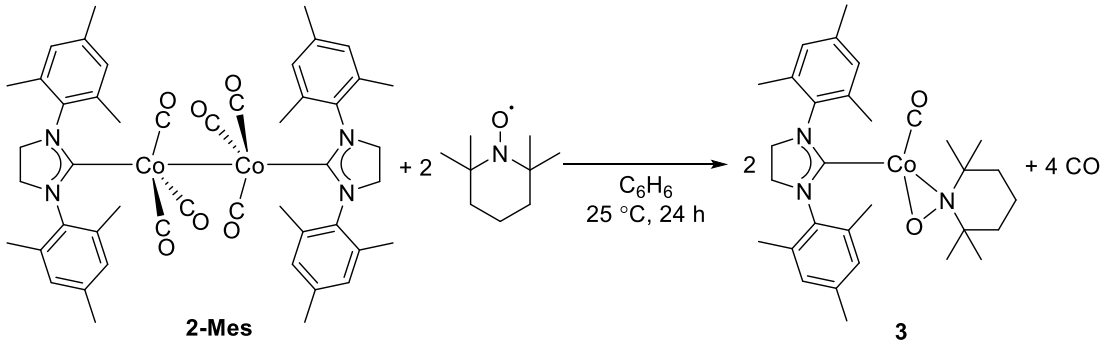

In a nitrogen glovebox, a 20 mL vial equipped with a Teflon coated stirring bar was charged with **2-Mes** (22.9 mg, 0.0255 mmol) and TEMPO (7.9 mg, 0.051 mmol). 2 mL benzene was added to the vial at 25 °C. The brown solution was stirred for 24 h at 25 °C. The resulting dark red solution was filtered through Celite, and the Celite was washed with benzene. The concentration of the solution gave dark red oil. Dark red crystals of **3** were formed upon the addition of pentane to the oil. The suspension was kept at -35 °C overnight to obtain more crystal. The crystal was washed with 3 mL n-heptane pre-cool at -35 °C and dried under vacuum. Yield: 23.5 mg, 84%.
Figures S14-16 show ^{1}H and ^{13}C{^{1}H}NMR and FTIR spectra of **3**.
^{1}H NMR (500.13 MHz, C_6D_6, 298 K): δ 1.04 (1H, m, $CH_2CH_2CH_2$), 1.09 (12H, s, 4 CH_3 moieties of the TEMPO ligand), 1.25 (2H, m, $CH_2CH_2CH_2$), 1.31 (1H, m, $CH_2CH_2CH_2$), 1.56 (2H, m, $CH_2CH_2CH_2$), 2.17 (6H, s, 2 *para*-CH_3), 2.42 (12H, s, 4 *ortho*-CH_3), 3.29 (4H, s, NCH_2CH_2N), 6.85 (4H, s, 4 *meta*-C*H*).
^{13}C{^{1}H} NMR (125.77 MHz, C_6D_6, 298 K): δ 17.61 (s, $CH_2CH_2CH_2$), 18.39 (s, 4 *ortho*-CH_3), 21.12 (s, 2 *para*-CH_3), 24.27 (s, 2 CH_3 moiety of the TEMPO ligand), 32.49 (s, 2 CH_3 moiety of the TEMPO ligand), 38.03 (s, $CH_2CH_2CH_2$), 50.92 (s, NCH_2CH_2N), 64.15 (s, CMe_2NCMe_2), 129.50 (s, 4 *meta*-CH), 137.08 (s, 2 *para*-*C*), 137.47 (s, 4 *ortho*-*C*), 138.16 (s, 2 *C*N), 204.48 (s, *C*O), 224.00 (s, N*C*N).
FTIR (Thin film, cm^{-1}): 1965 (m, CO), 1947 (m, CO), 1911 (s, CO).
Elemental analysis: Calcd: C:67.74, H:8.07, N:7.65. Found: C:67.73, H:7.94, N:7.61.
HRMS (ESI$^{+/-}$): Only a free SIMes ligand signal was detected.

Preparation of [Ni(SIMes)(CO)$_3$](4)

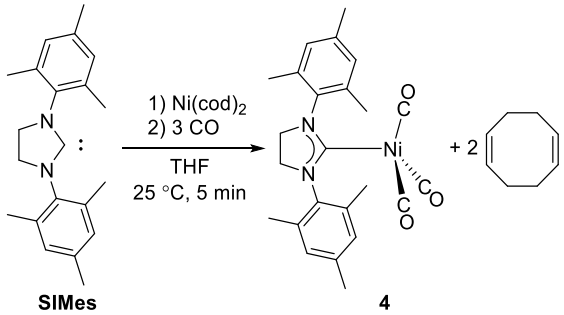

It is a known compound; however, its preparation from $Ni(cod)_2$ is not known[11]. In a nitrogen glovebox, a 50 mL Schlenk tube equipped with a Teflon coated stirring bar was charged with $Ni(cod)_2$ (27.6 mg, 0.100 mmol), 1,3-Bis(2,4,6-trimethylphenyl)imidazolidin-2-ylidene (**SIMes**) (30.3 mg, 0.099

mmol), and 4 mL THF at 25 °C. The dark wine-red solution was stirred for 5 min at 25 °C. Nitrogen in the tube was removed by a freeze-pump-thaw cycle, and 1 atm of CO was added to the tube. The solution color changed to yellow as soon as the solution was stirred. The solution was concentrated to dryness, and the solid was extracted using pentane. The concentration of pentane extract gave a yellow crystalline solid of **4**. Yield: 44.1 mg, 99%. Clean formation of **4** was confirmed by ^{1}H NMR (Figure S17).[11]
^{1}H NMR (400.15 MHz, C_6D_6, 298 K): δ 2.12 (6H, s, 2 *para*-C*H*$_3$), 2.20 (12H, s, 4 *ortho*-C*H*$_3$), 3.14 (4H, s, 4 C*H*$_2$), 6.83 (4H, s, 8 *meta*-C*H*).

Preparation of [Co(SIMe)(CO)$_3$]$_2$ (2-Me)

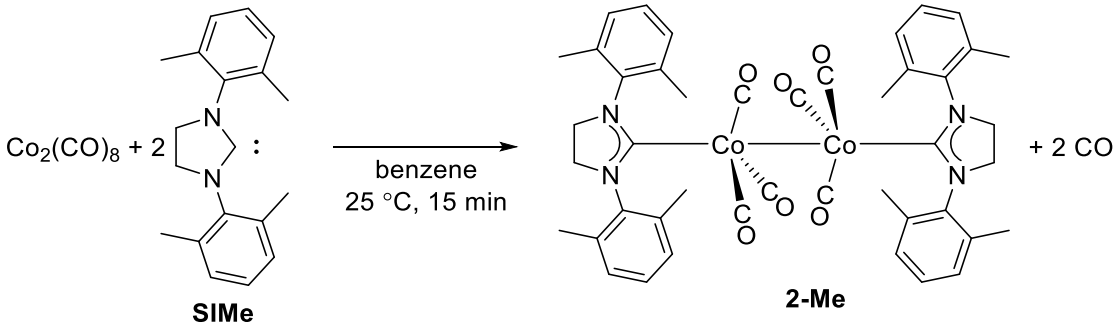

In a nitrogen glovebox, a 20 mL vial equipped with a Teflon coated stirring bar was charged with $Co_2(CO)_8$ (86.0 mg, 0.251 mmol) and 1,3-Bis(2,6-dimethylphenyl)imidazolidin-2-ylidene (**SIMe**) (278.8 mg, 1.00 mmol). 3 mL benzene was then added to the vial at 25 °C. The vial was quickly attached to a vacuum line, and the solution was kept under a slight static vacuum (until the solution started to boil) to minimize CO contamination of the glovebox. Rapid CO evolution was observed when benzene was added. Brown solution was formed after stirring the solution for 15 min at 25 °C. The solution was passed through a plug of Celite, and the Celite was washed with benzene. The combined benzene solution was concentrated to ca. 2 mL. 10 mL n-pentane was layered into the brown solution, and the solution was left overnight at 25 °C. Brown crystal of **2-Me** was decanted, washed with 6 mL n-pentane, and dried under vacuum (55.3 mg). The combined benzene/n-pentane solution was kept at -35°C for overnight to obtain the second crop of the product (73.7 mg)—the combined yield: 129.0 mg, 61%.
Figures S18-20 and S36 show ^{1}H and ^{13}C{^{1}H}NMR, FTIR, and UV-Vis spectra of **2-Me**.
^{1}H NMR (500.13 MHz, C_6D_6, 298 K): δ 2.22 (24H, s, 8C*H*$_3$), 2.97 (8H, s, 4C*H*$_2$), 6.96 (8H, distorted pseudo doublet with roofing effect, 8 *meta*-C*H*), 7.00 (4H, distorted dd with roofing effect, $^{3}J_{HH}$ = 5.8, 8.7 Hz, 4 *para*-C*H*).
^{13}C{^{1}H} NMR (125.76 MHz, C_6D_6, 298 K): δ 18.32 (s, 8*C*H$_3$), 50.87 (s, 4*C*H$_2$) , 128.68 (s, 4 *para*-*C*H), 129.11 (s, 8 *meta*-*C*H), 137.39 (s, 8 *ortho*-*C*), 140.16 (s, 4*C*N), 205.27 (s, 6*C*O), 215.98 (s, 2N*C*N).
FTIR (KBr pellet, cm^{-1}): 1959 (m, CO), 1939 (m, CO), 1915 (s, CO).
UV-Vis (in THF, 25 °C): λ_{max} = 372 nm (Co-Co σ-σ* transition. ε was not calculated as [dimer] is unknown).
Elemental analysis: Calcd: C:62.71, H:5.26, N:6.65. Found: C:62.63, H:4.97, N:6.67.
HRMS (ESI$^{+/-}$): Only a free SIMe ligand signal was detected.

Preparation of [Co(SIEt)(CO)$_3$]$_2$ (2-Et)

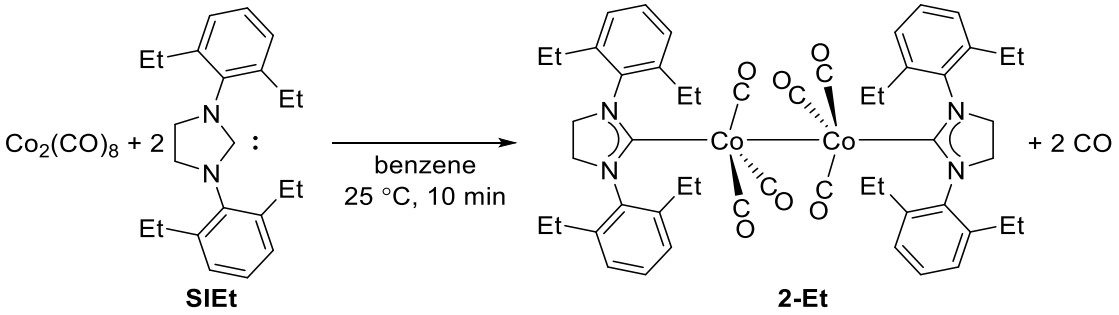

In a nitrogen glovebox, a 20 mL vial equipped with a Teflon coated stirring bar was charged with $Co_2(CO)_8$ (85.9 mg, 0.251 mmol) and 1,3-Bis(2,6-diethylphenyl)imidazolidin-2-ylidene (**SIEt**) (182.3 mg, 0.545 mmol). 3 mL benzene was then added to the vial at 25 °C. The vial was quickly attached to a vacuum line, and the solution was kept under a slight static vacuum (until the solution started to boil) to minimize CO contamination of the glovebox. Rapid CO evolution was observed when benzene was added. Brown solution and brown precipitate were formed after stirring the solution for 10 min at 25 °C. The solution was passed through a plug of Celite, and the Celite was washed with benzene. 12 mL n-pentane was added to the suspension while stirring it. Brown powder of **2-Et** was decanted, washed with 6 mL n-pentane, and dried under vacuum. Yield: 180.4 mg, 75%.
Figures S21-23 and S36 show ^{1}H and ^{13}C{^{1}H}NMR, FTIR, and UV-Vis spectra of **2-Et**.
^{1}H NMR (500.13 MHz, C_6D_6, 298 K): δ 1.22 (24H, t, $^3J_{HH}$ = 7.6 Hz, 8CH_2CH_3), 2.51 (8H, dq, $^2J_{HH}$ = 15.1 Hz, $^3J_{HH}$ = 7.6 Hz, 8CH_2CH$_3$), 2.84 (8H, dq, $^2J_{HH}$ = 15.1 Hz, $^3J_{HH}$ = 7.6 Hz, 8CH_2CH$_3$), 3.16 (8H, s, 4CH_2), 7.06 (8H, d, $^3J_{HH}$ = 7.6 Hz, 8 *meta*-C*H*), 7.16 (4H, overlapping with residual C_6D_5H signal, 4 *para*-C*H*).
^{13}C{^{1}H} NMR (125.76 MHz, C_6D_6, 298 K): δ 14.65 (s, 8CH$_2$*C*H$_3$), 24.17 (s, 8*C*H$_2$CH$_3$), 52.33 (s, 4*C*H$_2$) , 126.77 (s, 8 *meta*-*C*H), 129.10 (s, 4 *para*-*C*H), 139.21 (s, 4 *C*N), 142.66 (s, 8 *ortho*-*C*), 204.84 (s, 6*C*O), 217.54 (s, 2N*C*N).
FTIR (KBr pellet, cm^{-1}): 1960 (m, CO), 1942 (2, CO), 1928 (s, CO).
UV-Vis (in THF, 25 °C): λ_{max} = 372 nm (Co-Co σ-σ* transition. ε was not calculated as [dimer] is unknown).
Elemental analysis: Calcd: C:65.40, H:6.33, N:5.87. Found: C:65.70, H:6.22, N:5.91.
HRMS (ESI$^{+/-}$): Only a free SIEt ligand signal was detected.

Preparation of [Co(SIPr)(CO)$_3$]$_2$ (2-^{i}Pr)

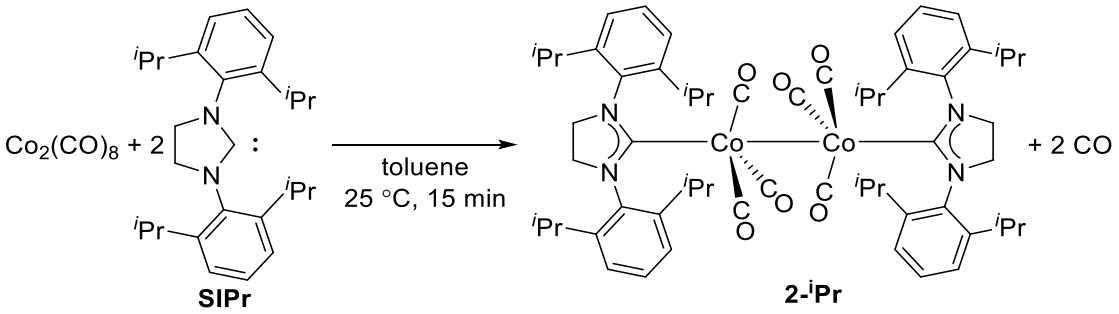

In a nitrogen glovebox, a 20 mL vial equipped with a Teflon coated stirring bar was charged with $Co_2(CO)_8$ (34.6 mg, 0.102 mmol) and 1,3-Bis(2,6-diisopropylphenyl)imidazolidin-2-ylidene (**SIPr**) (78.1

mg, 0.200 mmol). 2 mL toluene was then added to the vial at 25 °C. The vial was quickly attached to a vacuum line, and the solution was kept under a slight static vacuum (until the solution started to boil) to minimize CO contamination of the glovebox. Rapid CO evolution was observed when toluene was added. Brown solution and crystalline precipitate were formed after stirring the solution for 15 min at 25 °C. 6 mL n-pentane were added to the brown suspension while stirring to precipitate more product. The suspension was kept at -35 °C for overnight to precipitate more crystals. The brown crystal of **2-^{i}Pr** was washed with 6 mL n-pentane and dried under vacuum. Yield: 101.5 mg, 95%.
Figures S24-26 and S36 show ^{1}H and ^{13}C{^{1}H}NMR, FTIR, and UV-Vis spectra of **2-^{i}Pr**.
^{1}H NMR (500.13 MHz, C_6D_6, 298 K): δ 1.06 (24H, d, $^{3}J_{HH}$ = 7.0 Hz, 8CH(C*H*$_3$)), 1.54 (24H, d, $^{3}J_{HH}$ = 7.0 Hz, 8CH(C*H*$_3$)), 3.22 (8H, sept, $^{3}J_{HH}$ = 7.0 Hz, 8C*H*(CH_3)), 3.37 (8H, s, 4C*H*$_2$), 7.09 (8H, d, $^{3}J_{HH}$ = 7.5 Hz, 8 *meta*-C*H*), 7.20 (4H, t, $^{3}J_{HH}$ = 7.5 Hz, 4 *para*-C*H*).
^{13}C{^{1}H} NMR (125.76 MHz, C_6D_6, 298 K): δ 23.54 (s, 8CH(*C*H_3)), 26.32 (s, 8CH(*C*H_3)), 28.80 (s, 8*C*H(CH_3)), 53.76 (s, 4*C*H_2) , 124.92 (s, 8 *meta*-*C*H), 129.72 (s, 4 *para*-*C*H), 138.13 (s, 4*C*N), 147.59 (s, 8 *ortho*-*C*), 204.81 (s, 6*C*O), 218.75 (s, 2N*C*N).
FTIR (KBr pellet, cm^{-1}): 1962 (s, CO), 1943 (s, CO).
UV-Vis (in THF, 25 °C): λ_{max} = 381 nm (Co-Co σ-σ* transition. ε was not calculated as [dimer] is unknown).
Elemental analysis: Calcd: C:67.53, H:7.18, N:5.25. Found: C:67.63, H:6.99, N:5.07.
HRMS (ESI$^{+/-}$): Only a free SIPr ligand signal was detected.

Preparation of [Co(Br-SIMe)(CO)$_3$]$_2$ (2-Br)

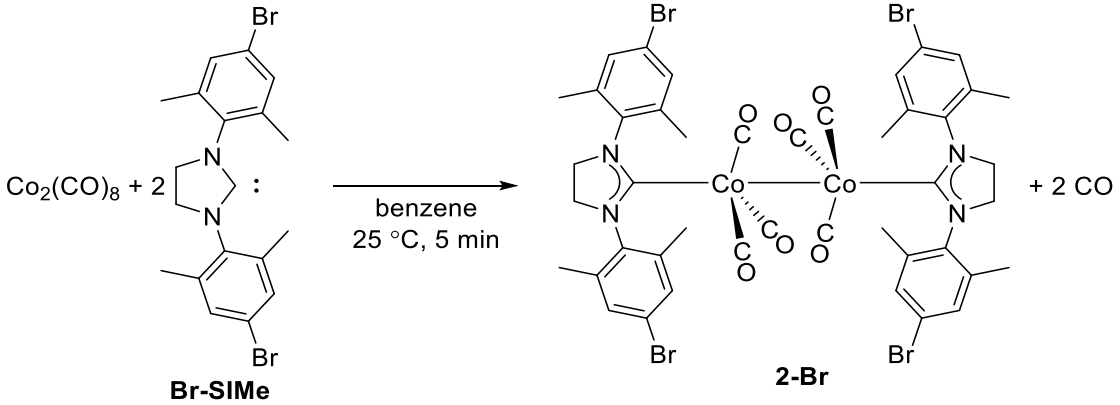

In a nitrogen glovebox, a 20 mL vial equipped with a Teflon coated stirring bar was charged with $Co_2(CO)_8$ (40.4 mg, 0.118 mmol) and 1,3-Bis(4-bromo-2,6-dimethylphenyl)imidazolidin-2-ylidene (**Br-SIMe**) (118.5 mg, 0.272 mmol). 4 mL benzene was then added to the vial at 25 °C. The vial was quickly attached to a vacuum line, and the solution was kept under a slight static vacuum (until the solution started to boil) to minimize CO contamination of the glovebox. Rapid CO evolution was observed when benzene was added. Dark brown solution and green oil were formed after stirring the solution for 5 min at 25 °C. The solution was passed through a plug of Celite, and the Celite was washed with benzene. The combined benzene solution was concentrated to dryness to obtain brown crystalline solid and green oil. The green oil was removed from the solid by washing with ca. 2 mL MeOH, and the brown solid of **2-Br** was dried under vacuum. Yield: 75.7 mg, 48%.
Figures S27-29 and S36 show ^{1}H and ^{13}C{^{1}H}NMR, FTIR, and UV-Vis spectra of **2-Br**.

^{1}H NMR (500.13 MHz, C_6D_6, 298 K): δ 1.97 (24H, s, 8C*H*$_3$), 2.79 (8H, s, 4C*H*$_2$), 7.14 (8H, s, 8 *meta*-C*H*).
^{13}C{^{1}H} NMR (125.76 MHz, C_6D_6, 298 K): δ 17.92 (s, 8*C*H$_3$), 50.59 (s, 4*C*H$_2$) , 122.50 (s, 4 *para*-*C*Br), 132.06 (s, 8 *meta*-*C*H), 138.98 (s, 4*C*N), 139.51 (s, 8 *ortho*-*C*), 205.07(s, 6*C*O), 216.46 (s, 2N*C*N).
FTIR (KBr pellet, cm^{-1}): 1961 (s, CO), 1944 (s, CO), 1929 (s, CO).
UV-Vis (in THF, 25 °C): λ_{max} = 371 nm (Co-Co σ-σ* transition. ε was not calculated as [dimer] is unknown).
Elemental analysis: Calcd: C:45.63, H:3.48, N:4.84. Found: C:45.33, H:3.10, N:4.96.
HRMS (ESI$^{+/-}$): Only a free Br-SIMe ligand signal was detected.

Preparation of [Co(EtO-SIMe)(CO)$_3$]$_2$ (2-OEt)

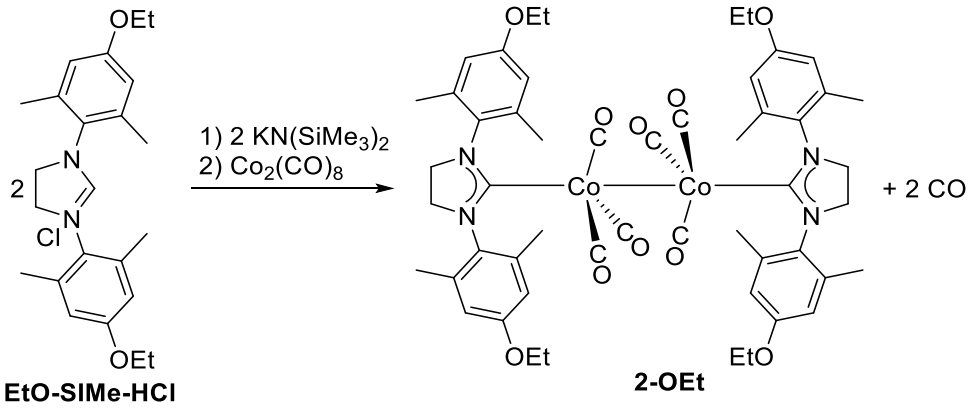

In a nitrogen glovebox, a 20 mL vial equipped with a Teflon coated stirring bar was charged with KN(SiMe$_3$)$_2$ (62.8 mg, 0.315 mmol) and 1,3-Bis(4-ethoxy-2,6-dimethylphenyl)-4,5-dihydroimidazolium chloride (**EtO-SIMe-HCl**) (129.7 mg, 0.322mmol). 4 mL THF was then added to the vial at 25 °C. The solution was stirred for 20 min at 25 °C and concentrated to dryness. Then, $Co_2(CO)_8$ (54.4 mg, 0.159 mmol) and 4 mL benzene were added. The vial was quickly attached to a vacuum line, and the solution was kept under a slight static vacuum (until the solution started to boil) to minimize CO contamination of the glovebox. Rapid CO evolution was observed when benzene was added. A dark brown solution was formed after stirring the solution for 1 h at 25 °C. The solution was concentrated to dryness to obtain a mixture of brown and green solid. The addition of benzene to the mixture of solids formed a brown solution and green oil. The solution was passed through a plug of basic alumina using benzene to remove green oil. The concentration of the resulting brown solution gave a brown solid of **2-OEt**. Yield: 30.7 mg, 19%.
Figures S30-32 and S36 show ^{1}H and ^{13}C{^{1}H}NMR, FTIR, and UV-Vis spectra of **2-OEt**.
^{1}H NMR (500.13 MHz, C_6D_6, 298 K): δ 1.14 (12H, t, $^3J_{HH}$ = 7.0 Hz, 4OCH$_2$C*H*$_3$), 2.24 (24H, s, 8 *ortho*-C*H*$_3$), 3.04 (8H, s, 2 C*H*$_2$), 3.60 (8H, q, $^3J_{HH}$ = 7.0 Hz, 2OC*H*$_2$CH$_3$), 6.68 (8H, s, 4 *meta*-C*H*).
^{13}C{^{1}H} NMR (125.76 MHz, C_6D_6, 298 K): δ 14.89 (s, 4OCH$_2$*C*H$_3$) 18.67 (s, 4 *ortho*-*C*H$_3$), 51.25 (s, 4 *C*H$_2$), 63.25 (s, 4O*C*H$_2$CH$_3$), 114.89 (s, 8 *meta*-*C*H), 133.66 (s, 4*C*N), 138.60 (s, 8 *ortho*-*C*), 159.02 (s, 2 *para*-*C*OEt), 205.50 (s, 6*C*O), 217.61 (s, 2N*C*N).
FTIR (thin film, cm^{-1}): 1957 (m, CO), 1935 (s, CO), 1909 (m, CO).
UV-Vis (in THF, 25 °C): λ_{max} = 370 nm (Co-Co σ-σ* transition. ε was not calculated as [dimer] is unknown).
Elemental analysis: Calcd: C:61.30, H:5.94, N:5.50. Found: C:61.32, H:5.66, N:5.45.
HRMS (ESI$^{+/-}$): Only a free EtO-SIMe ligand signal was detected.

Preparation of [Co(NEt$_2$-SIMe)(CO)$_3$]$_2$ (2-NEt$_2$)

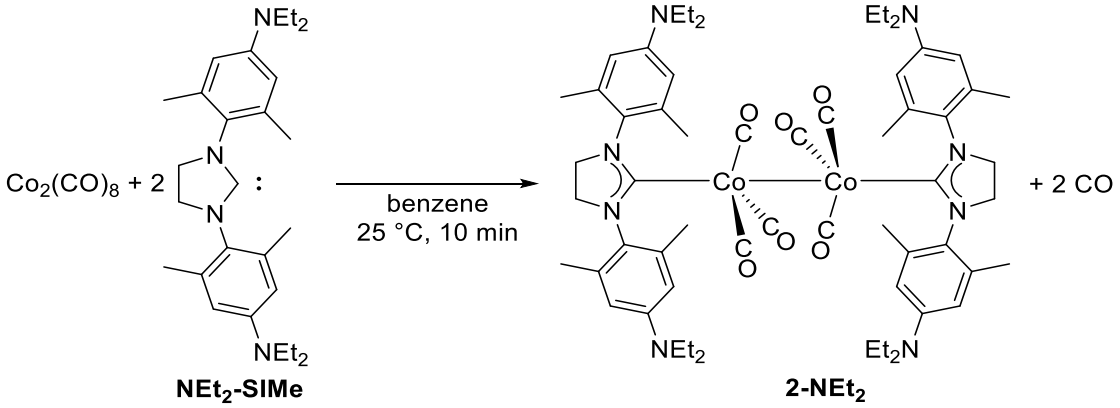

In a nitrogen glovebox, a 20 mL vial equipped with a Teflon coated stirring bar was charged with **NEt$_2$-SIMe** (44.7 mg, 0.106mmol) and $Co_2(CO)_8$ (16.9 mg, 0.049 mmol). 4 mL benzene was then added to the vial at 25 °C. The vial was quickly attached to a vacuum line, and the solution was kept under a slight static vacuum (until the solution started to boil) to minimize CO contamination of the glovebox. Rapid CO evolution was observed when benzene was added. A dark brown solution was formed after stirring the solution for 10 min at 25 °C. The solution was concentrated to dryness and passed through a plug of basic alumina using benzene to remove the green oil byproduct. The concentration of the resulting brown solution gave a brown solid of **2-NEt$_2$**. Yield: 29.8 mg, 53%.

Figures S33-36 show ^{1}H and ^{13}C{^{1}H}NMR, FTIR, and UV-Vis spectra of **2-NEt$_2$**.

^{1}H NMR (500.13 MHz, C_6D_6, 298 K): δ 1.00 (24H, t, $^3J_{HH}$ = 7.0 Hz, 2N(CH_2CH_3)$_2$), 2.32 (24H, s, 8CH_3), 3.07 (16H, q, $^3J_{HH}$ = 7.0 Hz, 2N(CH_2CH_3)$_2$), 3.23 (8H, s, 4CH_2), 6.49 (8H, s, 8 *meta*-C*H*).

^{13}C{^{1}H} NMR (125.76 MHz, C_6D_6, 298 K): δ 12.82 (s, 4CH_2CH_3), 19.10 (s, 8CH_3), 44.76 (s, 4CH_2CH_3) 51.53 (s, 4CH_2) , 112.93 (s, 8 *meta*-*C*H), 130.37 (s, 4*C*N), 137.86 (s, 8 *ortho*-*C*), 147.75 (s, 4 *para*-*C*NEt$_2$), 205.63 (s, 6*C*O), 218.59 (s, 2N*C*N).

FTIR (thin film, cm^{-1}): 1941 (s, CO), 1913 (s, CO), 1883 (s, CO).

UV-Vis (in THF, 25 °C): λ_{max} = 364 nm (Co-Co σ-σ* transition. ε was not calculated as [dimer] is unknown).

Elemental analysis: Calcd: C:63.93, H:7.15, N:9.94. Found: C:63.77, H:6.93, N:9.80.

HRMS (ESI$^{+/-}$): Only a free NEt$_2$-SIMe ligand signal was detected.

5. Studies of monomer-dimer equilibrium

^{1}H NMR measurement of [Co(NHC)(CO)$_3$]$_2$ complexes at variable temperatures.
In a nitrogen glovebox, [Co(NHC)(CO)$_3$]$_2$ (4.2-5.7 mg, 0.0050 mmol) was weighed in a 4 mL vial. To the vial was then added 0.50 mL C_6D_6, and the vial was closed tightly by a plastic cap with a polypropylene liner (for **2-Br**, complex (2.7 mg, 0.0023 mmol) and 0.70 mL C_6D_6 was used due to low solubility of this complex). The complex was dissolved completely by gently heating the solution with a heat gun, cooled to room temperature, and transferred to a J. Young NMR tube. Eleven ^{1}H NMR spectra were recorded between 24.0 and 69.9 °C (roughly every 5°C increment) using a Bruker Avance III NEO 500 NMR spectrometer equipped with a cryoprobe. The temperature was calibrated using dry ethylene glycol, and the accuracy of the temperatures is estimated to be ± 1 K.[12] Figures S37-43 show stacked ^{1}H NMR spectra of [Co(NHC)(CO)$_3$]$_2$ measured at temperatures between 24.0 and 69.9 °C.

Variable temperatures magnetic susceptibility measurement of 2-Mes and 1 using Evans' method
Solution magnetic susceptibilities of **2-Mes** and **1** were measured using 0.010 M (**2-Mes**) and 0.020 M (**1**) C_6D_6 solutions. C_6D_6 in a sealed glass capillary was used as an external standard. Evans' method was conducted using Bruker Avance III NEO 500 NMR spectrometer equipped with a cryoprobe. Table S1 shows the temperature-dependent change of effective magnetic moment (μ_{eff}) of **2-Mes** and **1** without diamagnetic correction and consideration of temperature dependence of solvent density. Effective magnetic moment (μ_{eff}) of **2-Mes** (value calculated assuming 100% dissociation of the dimer to the radical species **2-Mes***) increases on increasing temperature. In contrast, no significant change of μ_{eff} was observed when a solution of **1** was heated. Table S1 shows the temperature-dependent change of effective magnetic moment (μ_{eff}) of solution of **2-Mes** and **1**.

Table S1. Temperature-dependent change of effective magnetic moment (μ_{eff}) of solution of **2-Mes** and **1**.

Temperature (K)	μ_{eff} of **2-Mes** (μ_B)	μ_{eff} of **1** (μ_B)
297.18	0.74	1.82
301.68	0.73	1.82
306.18	0.76	1.81
310.67	0.77	1.81
315.26	0.81	1.81
319.85	0.84	1.81
324.45	0.88	1.80
329.03	0.92	1.80
333.72	0.98	1.80
338.41	1.03	1.80
343	1.09	1.80

^{1}H NMR measurement of 2-Mes at variable temperatures under 3 bar CO.
In a nitrogen glovebox, **2-Mes** (4.5 mg, 0.0050 mmol) was weighed in a 4 mL vial. To the vial was then added 0.50 mL C_6D_6, and the vial was closed tightly by a plastic cap with a polypropylene liner. The complex was dissolved completely by gently heating the solution with a heat gun, cooled to room temperature, and transferred to a high-pressure NMR tube (Wilmad 528-PV-6). The tube was pressurized

by 3 bar CO. Eleven ^{1}H NMR spectra were recorded between 24.0 and 69.9 °C (roughly every 5°C increment) using a Bruker Avance III NEO 500 NMR spectrometer equipped with a cryoprobe. No formation of free SIMes ligand was detected in ^{1}H NMR spectra. Temperature-dependent reversible formation of the broad signals was not affected by the CO pressure. Figure S44 shows stacked ^{1}H NMR spectra of **2-Mes** complexes measured at temperatures between 24.0 and 69.9 °C under 3 bar CO.

^{1}H NMR measurement of 2-Mes under variable concentrations.

In a nitrogen glovebox, **2-Mes** (5.0 mg, 0.0056 mmol) was dissolved in 1.00 mL C_6D_6, to form 5.6 mM solution. 0.25 mL of 5.6 mM solution was diluted with 0.25 mL of C_6D_6 to form 2.8 mM solution. 0.05 mL of 5.6 mM solution was diluted with 0.45 mL of C_6D_6 to form 0.56 mM solution. 0.50 ml C_6D_6 was added to 0.50 mL 0.56 mM solution to form 0.28 mM solution.^{1}H NMR spectra of solutions with different concentrations were recorded at 298 K, and the ratio of **2-Mes** and **2-Mes*** was determined using the integration of 4-methyl signals from SIMes ligands. Table S2 shows ratios of **2-Mes** and **2-Mes*** in four different concentrations.

Table S2. Monomer: dimer ratios of **2-Mes** in four different concentrations.

Concentration of **2-Mes** (mM)	**2-Mes***(%)	**2-Mes** (%)
5.6	2.8	97.2
2.8	3.9	96.1
0.56	7.8	92.2
0.28	10.0	90.0

EPR measurement of 2-Mes and 1 at variable temperatures.

Variable temperature EPR measurement of **2-Mes** was conducted using 10.0 mM C_6D_6 solution of **2-Mes** (concentration of **2-Mes** without consideration of the formation of **2-Mes***). Variable temperature EPR measurement of **1** was conducted using 20.0 mM C_6D_6 solution of **1**. The temperature of the EPR cavity was controlled using JEOL ES-CT470 N_2 gas heating system. The temperature at the bottom of the samples tube was set to 293.15, 303.15, 313.15, 323.15, 333.15, and 343.15 ± 0.15 K. Actual temperature of the center of the sample solution (± 0.7 K) was determined by measuring the temperature of dummy toluene sample using TENMARS TM-80N thermometer equipped with a TP-03 type-K thermocouple wire directly inserted to the center of toluene sample and was 292.65, 301.05, 309.55, 318.05, 326.25, and 334.75 ± 0.7 K. Integration values were calculated by double integration of the first derivative EPR spectra using a JEOL JES-X330 software. The measurement parameters employed were as follows: microwave power, 1 mW; experimental frequency, 9.078 GHz; center field, 316 mT; sweep width, ±150 mT; sweep time, 60 s; time constant, 0.1 s; modulation frequency, 100kHz; modulation width, ±0.5 mT, receiver gain, 100 dB for **2-Mes**, 30 dB for **1**; and a number of the scan, 1. The measurement of **2-Mes** was conducted twice. Integration values of **1** at each measurement temperature were used as standard values for 20.0 mM monomeric **2-Mes** radical at each temperature. Concentrations of monomeric **2-Mes** at each temperature were calculated by comparison of standard value and actual integration value of **2-Mes** solution. Figure S45 shows the temperature-dependent change of EPR spectra of **2-Mes**.

Temperature-dependent reversible formation of 2-Mes* observed using variable temperature EPR.

Repeating heating and cooling of the EPR sample of **2-Mes** (3.40 M in toluene) showed a reversible increase and decrease in the EPR signal. Figure S46 shows Temperature dependent reversible formation of **2-Mes*** detected as a change of EPR double integration values.

Variable temperatures UV-Vis measurement of 2-Mes.

Variable temperature UV-Vis spectra of **2-Mes** were recorded using 0.12 g/L benzene solution of **2-Mes** in a quartz cuvette (pathlength: 10 mm x 10 mm) equipped with a screw cap and a magnetic stirring bar. The temperature of the solution was regulated using Peltier thermostatted cell holder equipped with a magnetic stirrer. The temperature at the bottom of the cuvette was reported with an accuracy of ±0.2 °C. Changes in UV-Vis spectra of **2-Mes** on heating and cooling were shown in Figure S47

^{1}H NMR measurement of 2-Mes at 137.3 °C under 5 bar N_2.

In a nitrogen glovebox, **2-Mes** (4.5 mg, 0.0050 mmol) was weighed in a 4 mL vial. To the vial was then added 0.50 mL toluene-d_8, and the vial was closed tightly by a plastic cap with a polypropylene liner. The complex was dissolved completely by gently heating the solution with a heat gun, cooled to room temperature, and transferred to a high-pressure NMR tube (Wilmad 528-PV-6). The tube was pressurized by 5 bar nitrogen to increase the boiling temperature of toluene-d_8. ^{1}H NMR spectra were recorded using a Bruker Avance III NEO 500 NMR spectrometer equipped with a cryoprobe. Probe temperature was increased gradually, and ^{1}H NMR spectra were recorded at 37.5, 55.9, 74.5, 93.1, 110.6, 128.5, and 137.5 °C. Signals from monomer and dimer were broadened on temperature increase and merged into three broad signals at 110.6 °C. Spectrum recorded at 137.3 °C showed four broad signals with the expected integration ratio of 4:4:6:12. The signals were assigned based on ^{1}H NMR integration values and EXSY NMR. Small new diamagnetic signals appeared above 120 °C due to the gradual thermal decomposition of the complex.

Figure S48 shows a ^{1}H NMR spectrum of **2-Mes*** recorded at 137.3 °C. Figure S49 shows stacked ^{1}H NMR spectra of **2-Mes** measured at temperatures between 24.0 and 137.3 °C.

^{1}H NMR (500.13 MHz, toluene-d_8, 410.5 K) of **2-Mes***: δ 2.72 (12H, br, 4 *ortho*-CH_3), 2.82 (4H, br, 2 CH_2, partially overlapping with *an ortho*-CH_3 signal), 3.59 (6H, br, 2 *para*-CH_3), 7.15 (4H, br, 4 *meta*-C*H*).

2D DOSY NMR of 2-Mes in the presence of 4 as an internal standard.

In a nitrogen glovebox, **2-Mes** (4.4 mg, 0.0049 mmol) and $Me_3SiOSiMe_3$ (1.0 µL) were dissolved in 1.0 mL C_6D_6. 0.50 mL of this solution was then added to a vial containing **4** (2.5 mg, 0.0056 mmol), and the solution was transferred to a J. Young NMR tube. 2D DOSY NMR spectra were measured at 298 K using a Bruker Avance III NEO 500 NMR spectrometer equipped with a cryoprobe. LED-bipolar gradients pulse program (ledbpgp2s) was used with gradient diffusion delay (d20) of 0.03 s and the recycle delay (d1) of 3 s. A 2D DOSY spectrum and a detailed list of acquisition and fitting parameters are available in Figures S50-52.

2D EXSY NMR of $[Co(NHC)(CO)_3]_2$ complexes.
2D EXSY NMR experiments were conducted using Bruker Avance III NEO 500 or Avance III-400N NMR spectrometers. A phase-sensitive 2D NOESY pulse program (noesygpphpp) was used with a mixing time (d8) of 0.3 s and the recycle delay (d1) of 2 s. d8 of 0.1 s and d1 of 1 s was used for the measurement of **2-Br**. Figures S53-59 show 2D EXSY NMR spectra of $[Co(NHC)(CO)_3]_2$ complexes and detailed acquisition parameters.

Calculation of enthalpy ($\Delta H°$, BDE), entropy ($\Delta S°$), and Gibbs free energy (ΔG_{298}, BDFE) of Co-Co bond dissociation using ^{1}H NMR integration at variable temperatures.
BDE, ΔS, and BDFE of Co-Co bond dissociation

$$\underset{\textbf{dimer}}{[Co(NHC)(CO)_3]_2} \overset{K_{eq}}{\rightleftharpoons} 2\ \underset{\textbf{monomer}}{[Co(NHC)(CO)_3]}$$

were calculated using Van't Hoff equation

$$lnK_{eq} = -\frac{\Delta H^\circ}{R}\left(\frac{1}{T}\right) + \frac{\Delta S^\circ}{R} \qquad (1)$$

K_{eq}: Equilibrium constant $= \dfrac{[\mathbf{monomer}]^2}{[\mathbf{dimer}]}$

R: Ideal gas constant (8.314 $J \cdot K^{-1} \cdot mol^{-1}$)

T: Temperature(K)

and Gibbs free energy equation.

$$\Delta G = \Delta H° - T\Delta S° \qquad (2)$$

[**monomer**] and [**dimer**] were calculated using an integration of ^{1}H NMR signals from monomers and dimers and an initial concentration of **2-Mes** (0.010 M). The raw thermodynamic data and van't Hoff plots ($\ln K_{eq}$ vs. $1/T$) based on NMR-determined monomer-dimer equilibrium constants of $[Co(NHC)(CO)_3]_2$ complexes are available in Supplementary Data File 1. The signals used for the concentration calculations are indicated with * in Figures S37-43.

Calculation of enthalpy ($\Delta H°$, BDE), entropy ($\Delta S°$), and Gibbs free energy (ΔG_{298}, BDFE) of Co-Co bond dissociation using the integration of EPR spectra at variable temperatures.
BDE, ΔS, and BDFE of Co-Co bond dissociation were calculated using Van't Hoff equation 1 and Gibbs free energy equation 2.

[**monomer**] and [**dimer**] were calculated by the equations 3:

$$[\boldsymbol{monomer}] = 20.0 * \frac{EPR\ integration\ value\ of\ \mathbf{2}}{EPR\ integration\ value\ of\ \mathbf{1}} \qquad (3)$$

$$[\boldsymbol{dimer}] = \frac{20.0 - [\boldsymbol{monomer}]}{2}$$

Double integration of the first derivative EPR spectra of **2-Mes** and **1** at 292.65, 301.05, 309.55, 318.05, 326.25, and 334.75 ± 0.7 K (actual solution temperature) were used as EPR integration values. The raw

thermodynamic data and van't Hoff plot (lnK_{eq} vs. 1/T) based on EPR-determined monomer-dimer equilibrium of complex **2-Mes** are available in Supplementary Data File (vant Hoff plot data.xlsx).

Calculation of activation enthalpy ($\Delta H^{\ddagger}$), entropy ($\Delta S^{\ddagger}$), and Gibbs free energy ($\Delta G^{\ddagger}_{298}$) of Co-Co bond dissociation using temperature-dependent line broadening of ^{1}H NMR spectra.
$\Delta H^{\ddagger}$, $\Delta S^{\ddagger}$, $\Delta G^{\ddagger}_{298}$ of Co-Co bond dissociation were calculated using the Eyring equation and

$$ln\left(\frac{k}{T}\right) = -\frac{\Delta H^{\ddagger}}{R}\left(\frac{1}{T}\right) + \frac{\Delta S^{\ddagger}}{R} + \ln\left(\frac{k_B}{h}\right) \qquad (4)$$

k: rate constant (s^{-1})
R: Ideal gas constant (8.314 $J \cdot K^{-1} \cdot mol^{-1}$)
T: Temperature (K)
k_B: Boltzmann constant ($1.380649 \times 10^{-23}\ J \cdot K^{-1}$)
h: Plank constant ($6.62607015 \times 10^{-34}\ J \cdot Hz^{-1}$)

and rate constant (k) derived from the line width of an NMR signal according to an equation reported by Wayland *et al.*[13]

$$k = \pi(\Delta\nu^{T} - \Delta\nu^{min}) \qquad (5)$$

$\Delta\nu^{T}$: Line width of an NMR signal at half-maximum peak height at T K
$\Delta\nu^{min}$: Observed minimum line width of an NMR signal at half-maximum peak height

Singlet methylene (CH_2) signals from 4,5-dihydroimidazol groups in NHC ligands (around 3 ppm) are used for the line width analysis. We did not observe systematic increase of line width increase in temperature range between 297 and 315. We assume that slight variation of line width in this temperature region is due to NMR shimming. $\Delta\nu^{min}$ was chosen from the minimum peak width of this temperature region. The raw kinetic data and Eyring plot (ln(k/T) vs. 1/T) based on line width analysis of **2-Mes** are available in Supplementary Data File (Eyring plot data .xlsx).

6. NMR, EPR, and FT-IR spectra

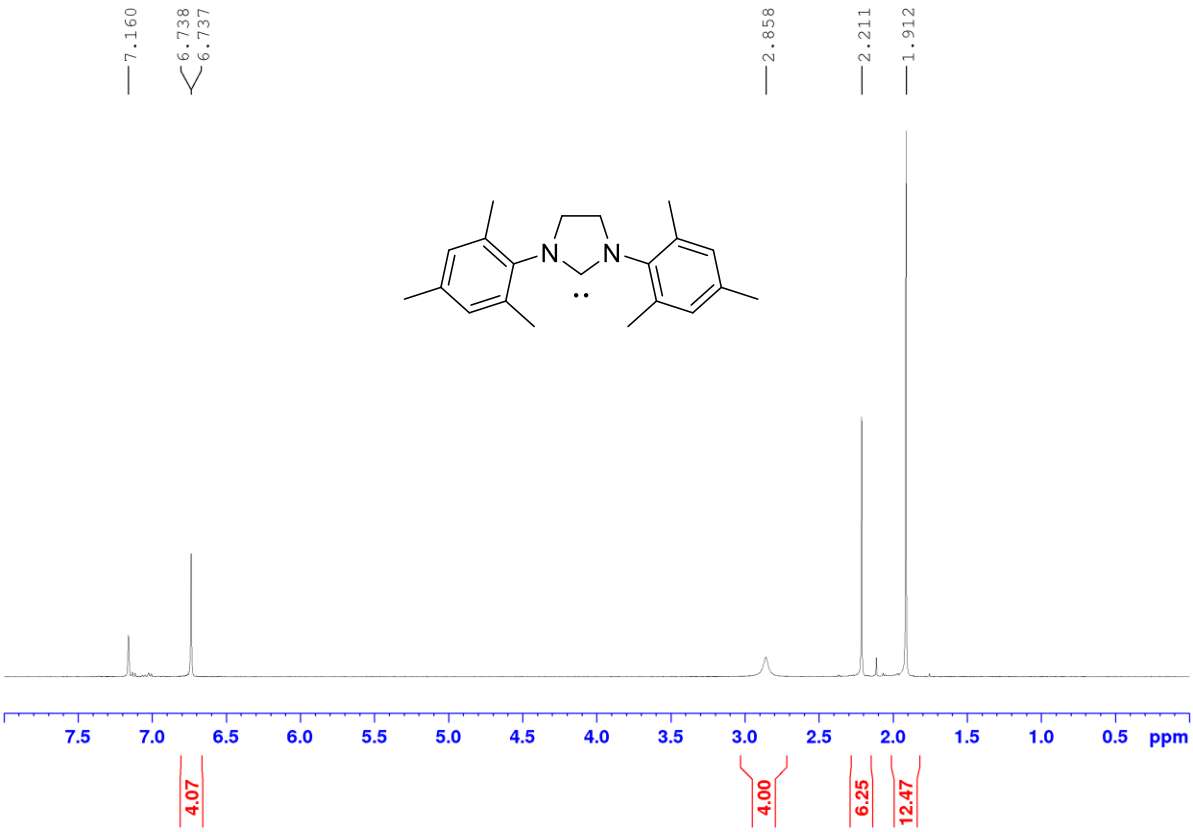

Figure S1 ^{1}H NMR spectrum (400.15 MHz, C_6D_6, 298 K) of **SIMes**.

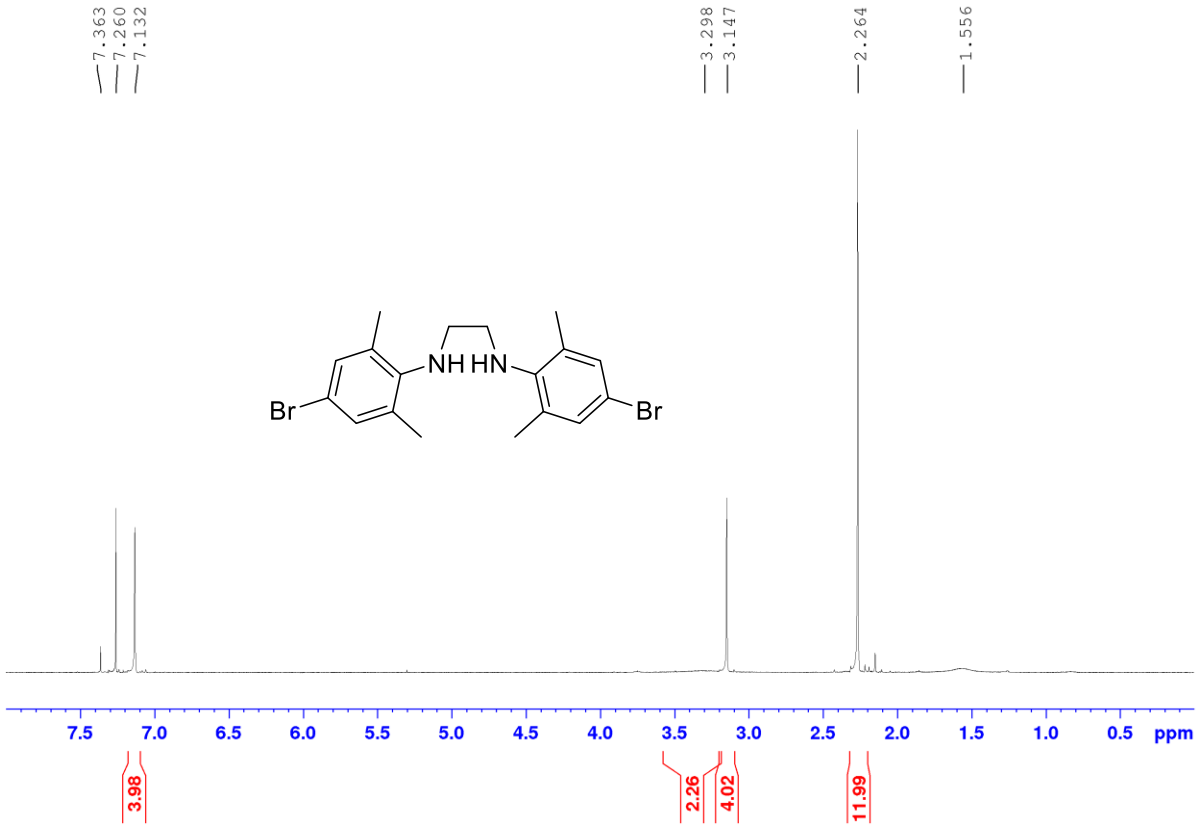

Figure S2 ^{1}H NMR spectrum (400.15 MHz, $CDCl_3$, 298 K) of **Br-diamine**.

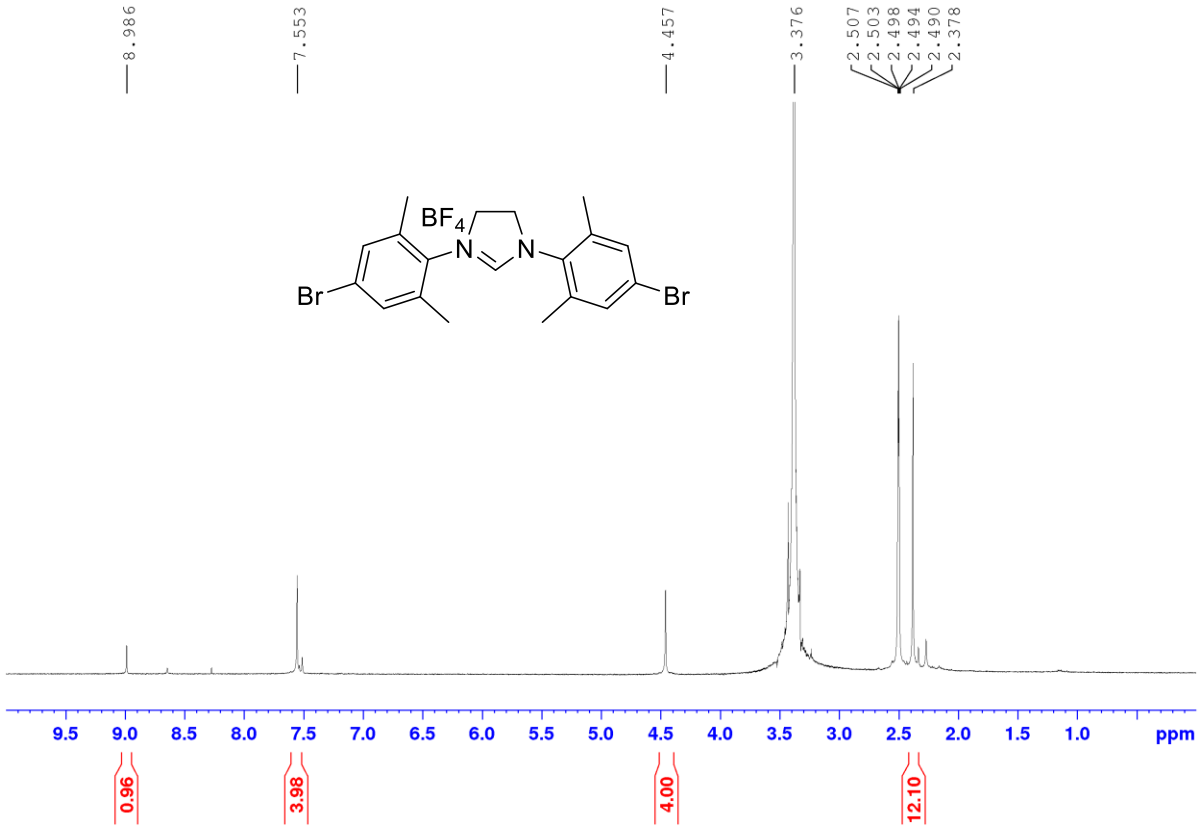

Figure S3 ^{1}H NMR spectrum (400.15 MHz, DMSO-d_6, 298 K) of **Br-SIMe-HBF$_4$**.

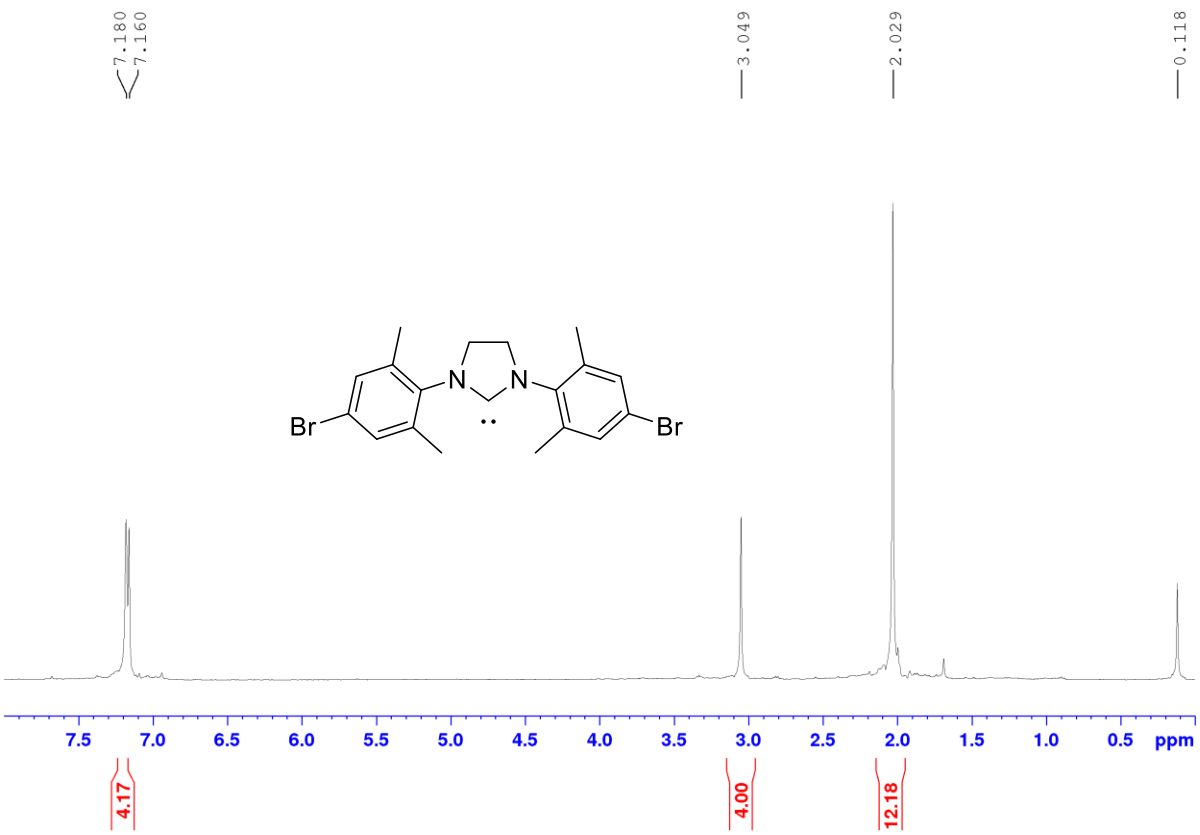

Figure S4 ^{1}H NMR spectrum (400.15 MHz, C_6D_6, 298 K) of **Br-SIMe**.

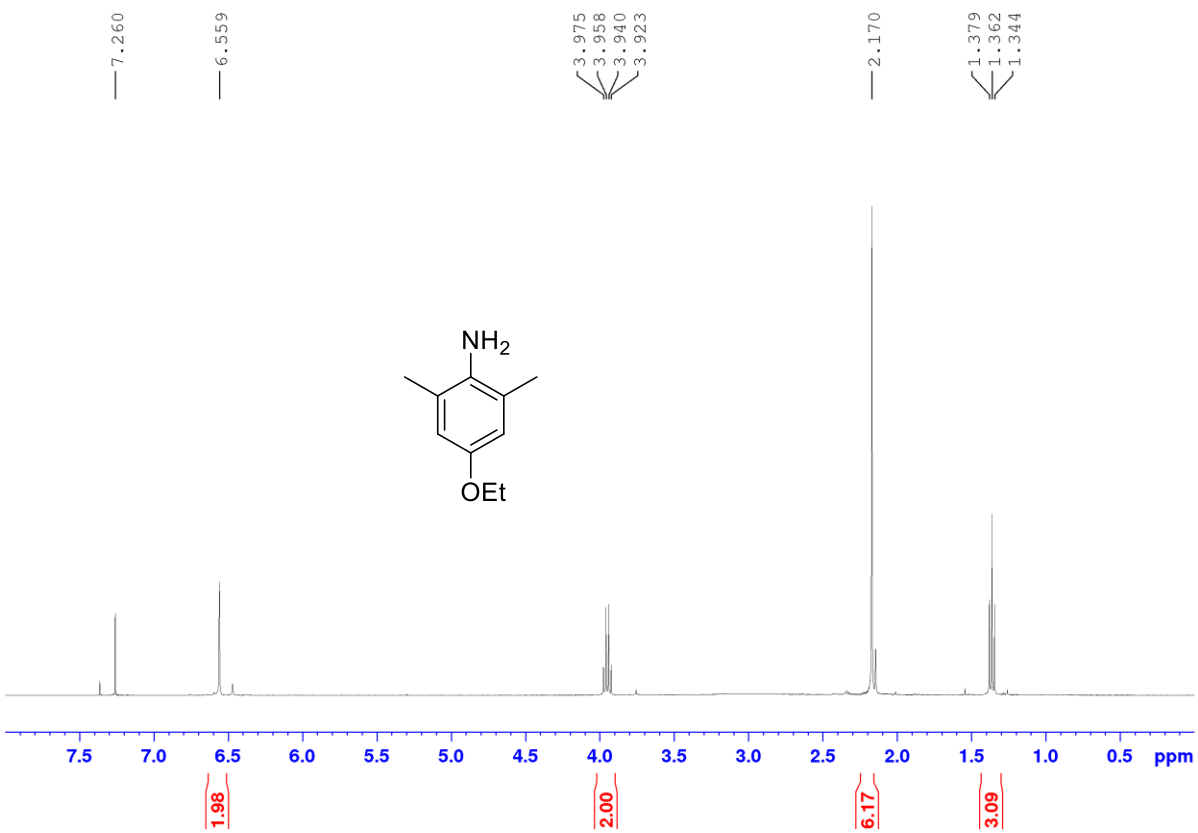

Figure S5 ^{1}H NMR spectrum (400.15 MHz, $CDCl_3$, 298 K) of 4-ethoxy-2,6-dimethylaniline.

(A)

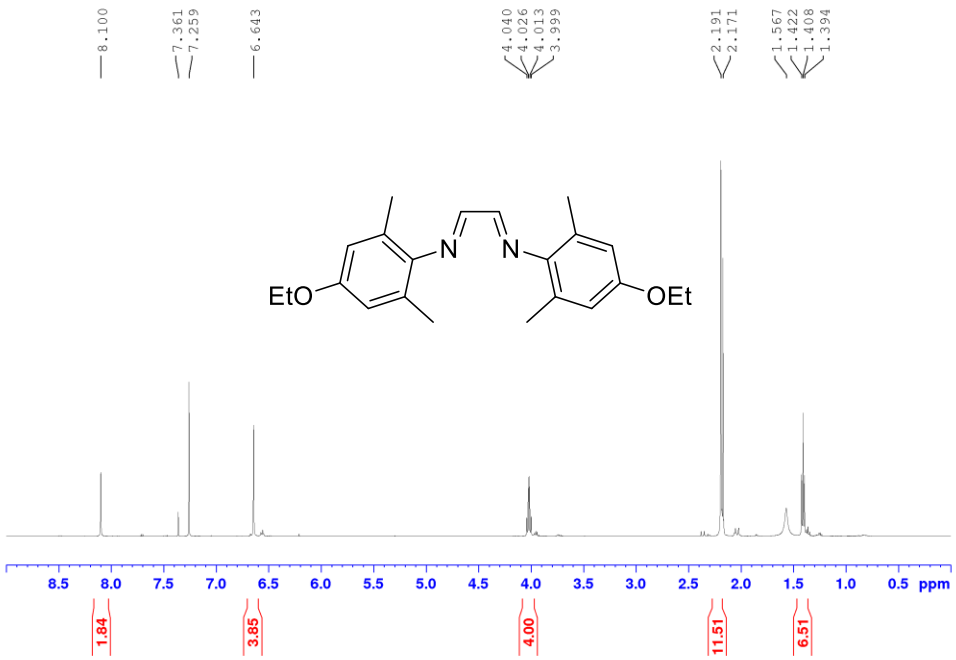

(B)

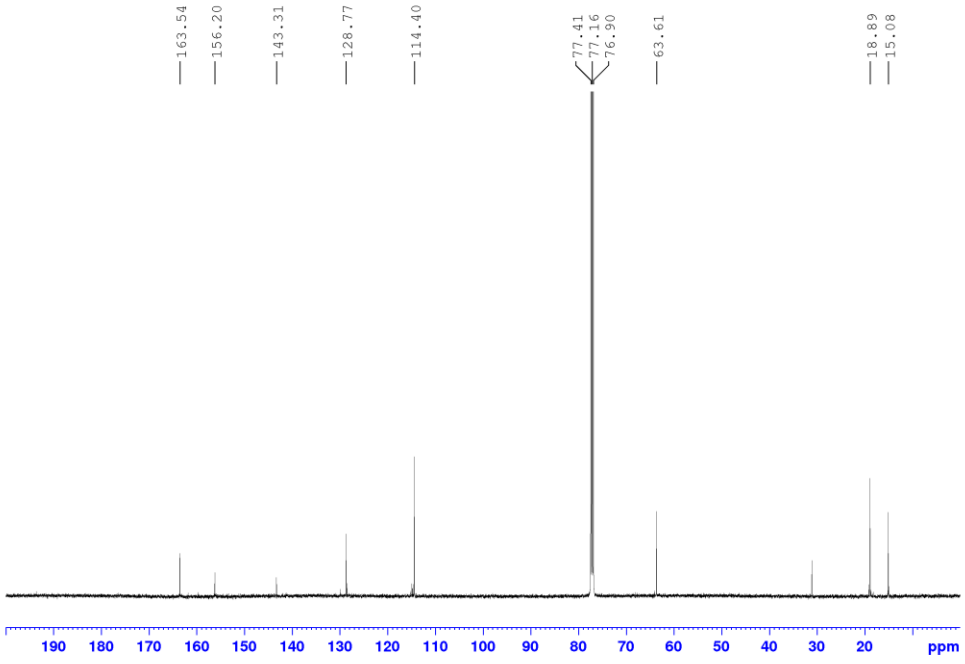

Figure S6 (A) ^{1}H NMR spectrum (500.13 MHz, $CDCl_3$, 298 K) of **EtO-diimine**. (B) $^{13}C\{^{1}H\}$ NMR spectrum (125.76 MHz, $CDCl_3$, 298 K) of **EtO-diimine**.

(A)

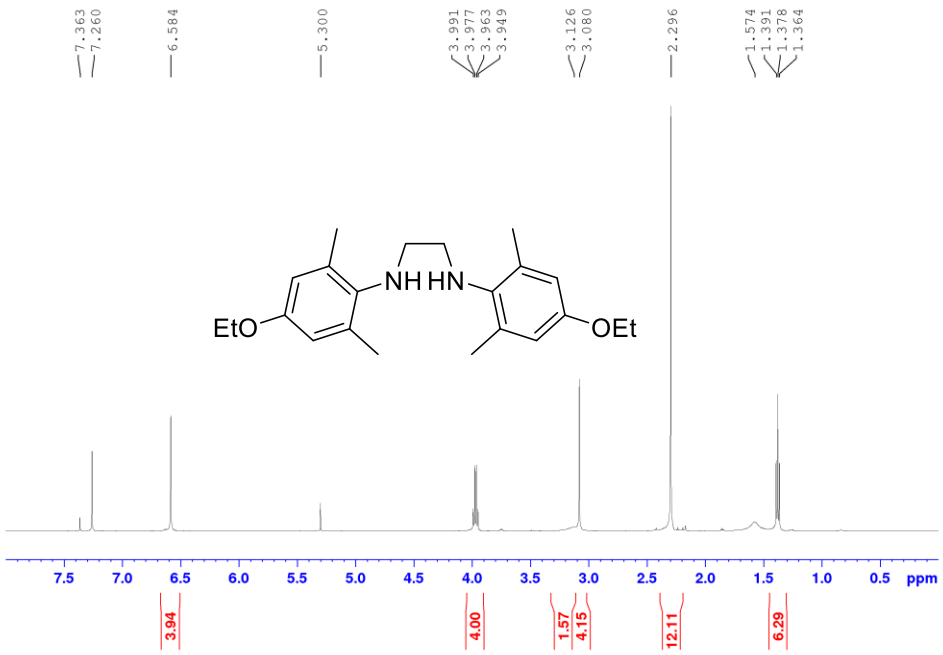

(B)

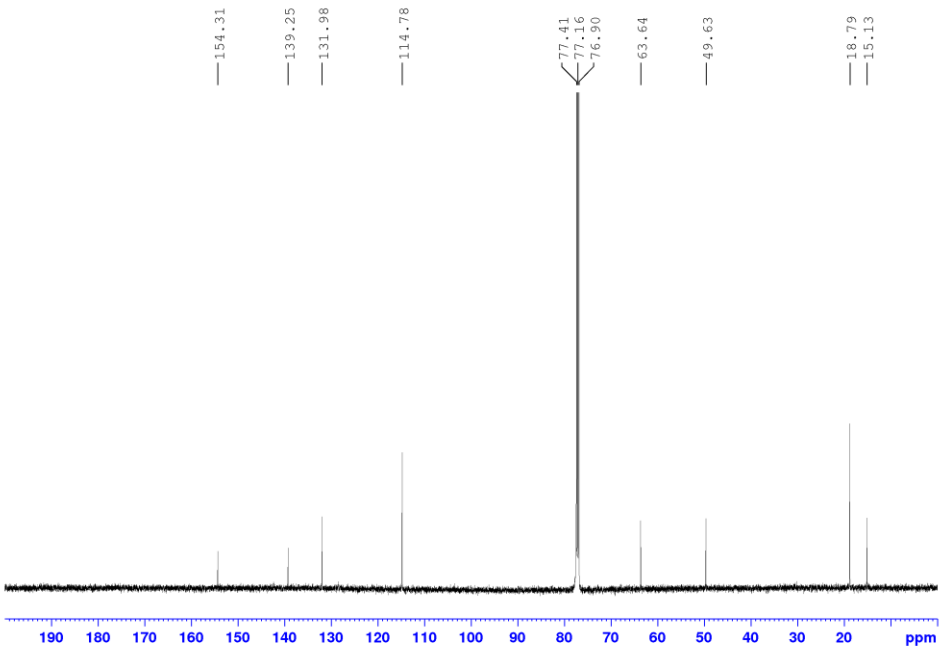

Figure S7 (A) ^{1}H NMR spectrum (500.13 MHz, $CDCl_3$, 298 K) of **EtO-diamine**. (B) $^{13}C\{^{1}H\}$ NMR spectrum (125.76 MHz, $CDCl_3$, 298 K) of **EtO-diamine**.

(A)

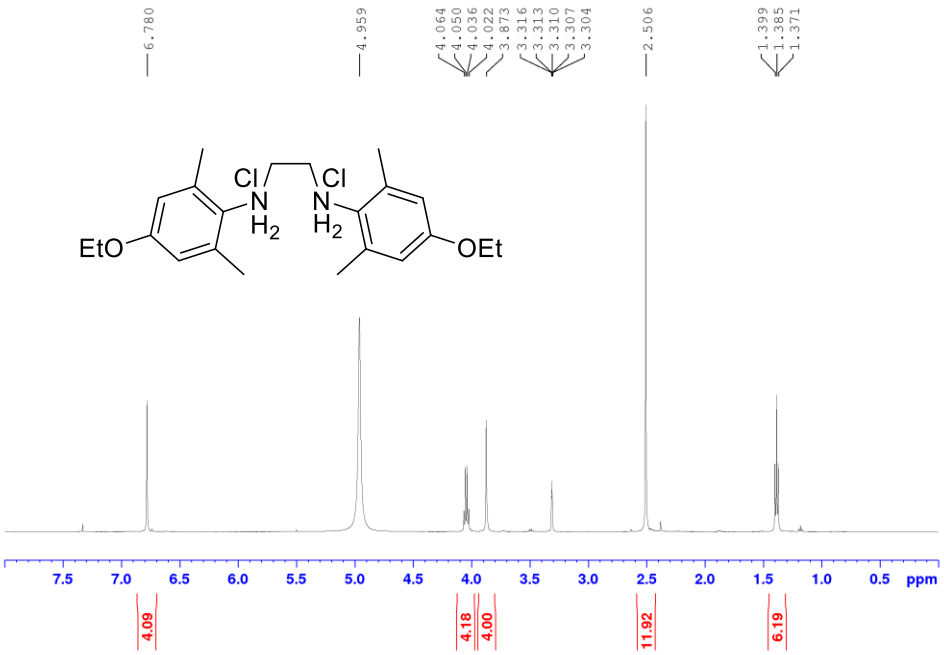

(B)

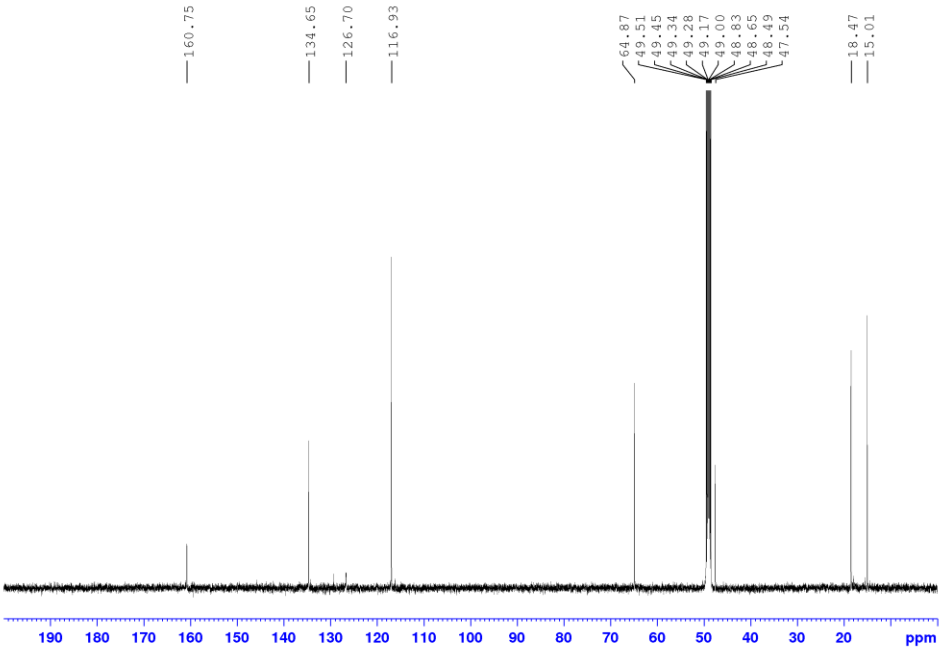

Figure S8 (A) ^{1}H NMR spectrum (500.13 MHz, methanol-d_4, 298 K) of **EtO-diamine-HCl**. (B) ^{13}C{^{1}H} NMR spectrum (125.76 MHz, methanol-d_4, 298 K) of **EtO-diamine-HCl**.

(A)

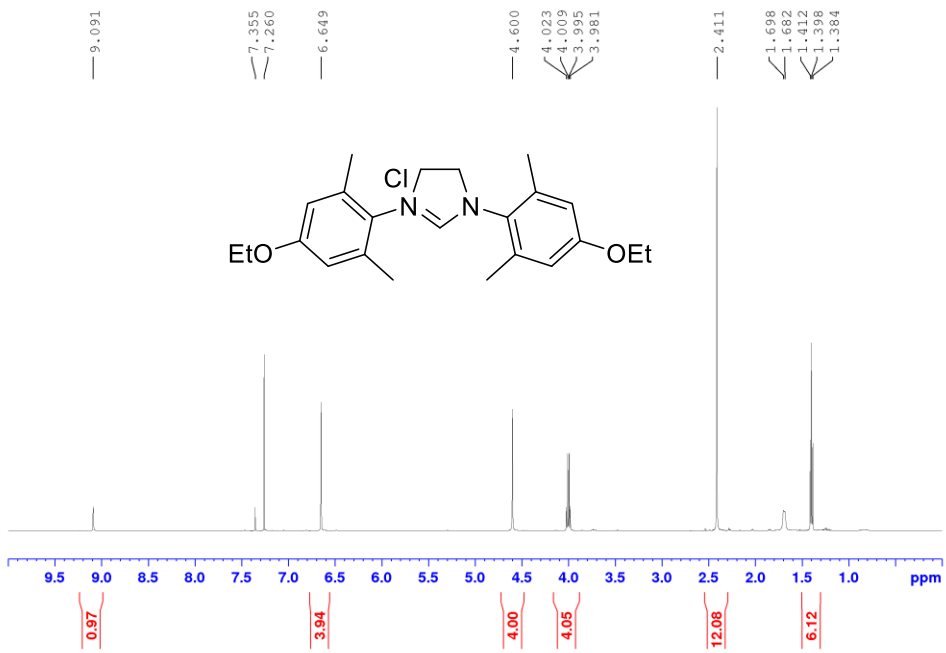

(B)

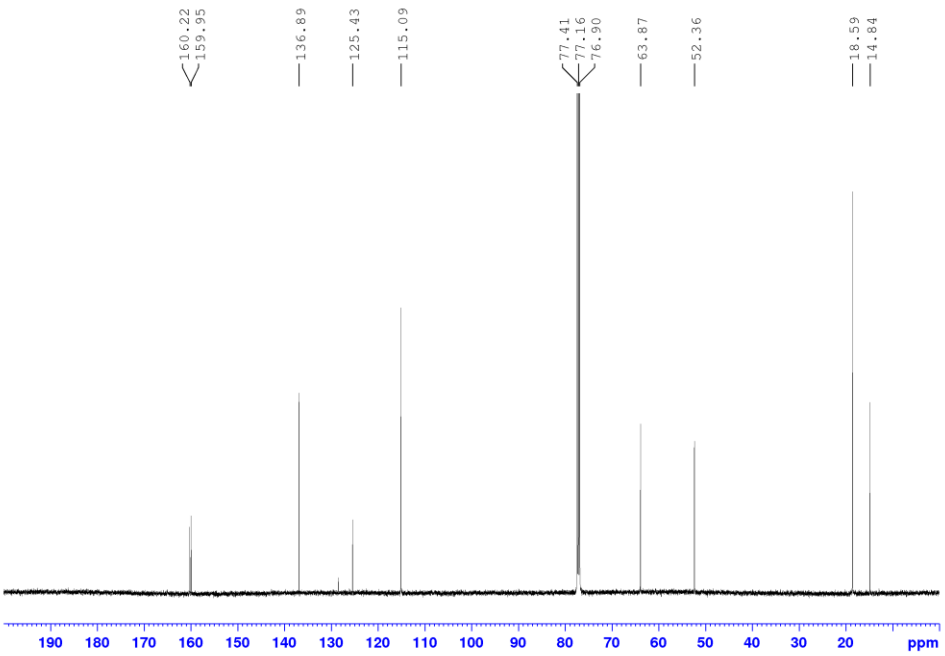

Figure S9 (A) ^{1}H NMR spectrum (500.13 MHz, $CDCl_3$, 298 K) of **EtO-SIMe-HCl**. (B) $^{13}C\{^{1}H\}$ NMR spectrum (125.76 MHz, $CDCl_3$, 298 K) of **EtO-SIMe-HCl**.

(A)

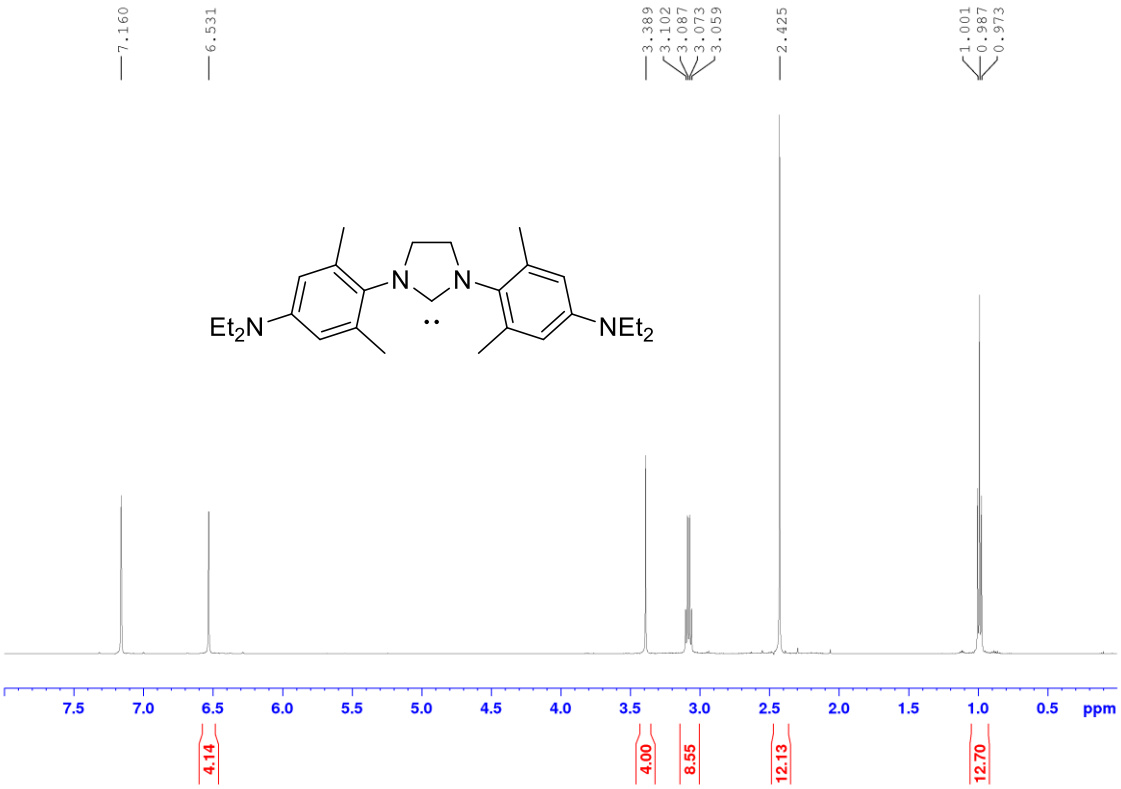

(B)

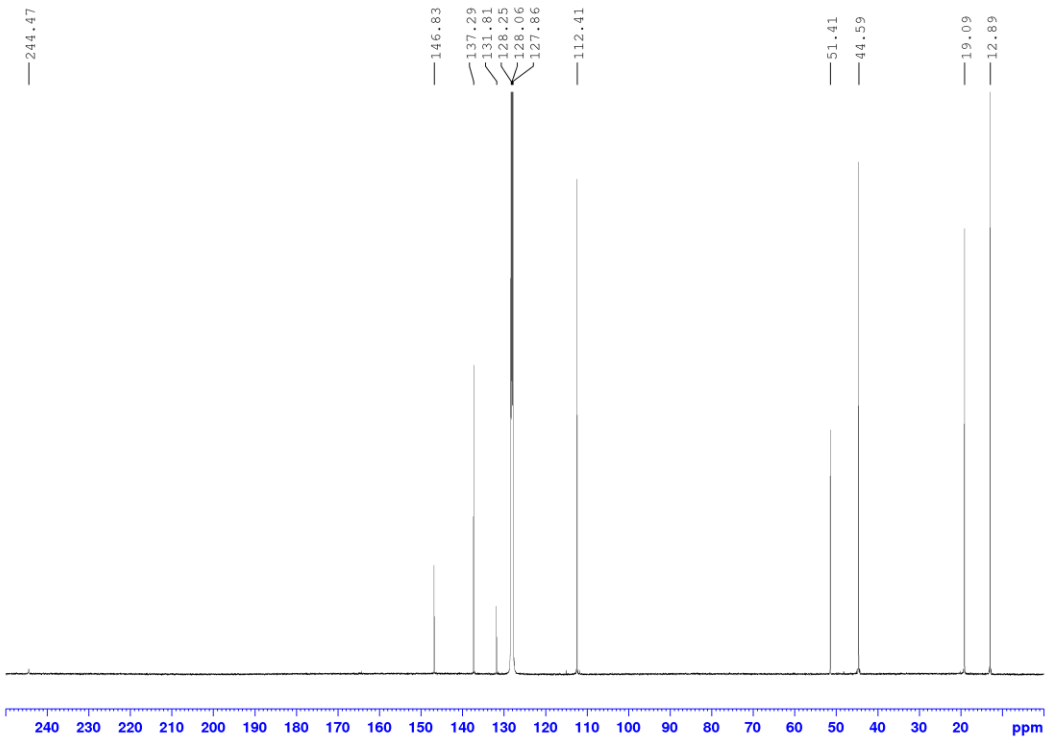

Figure S10 (A) ^{1}H NMR spectrum (500.13 MHz, $CDCl_3$, 298 K) of **NEt$_2$-SIMe**. (B) $^{13}C\{^{1}H\}$ NMR spectrum (125.76 MHz, $CDCl_3$, 298 K) of **NEt$_2$-SIMe**.

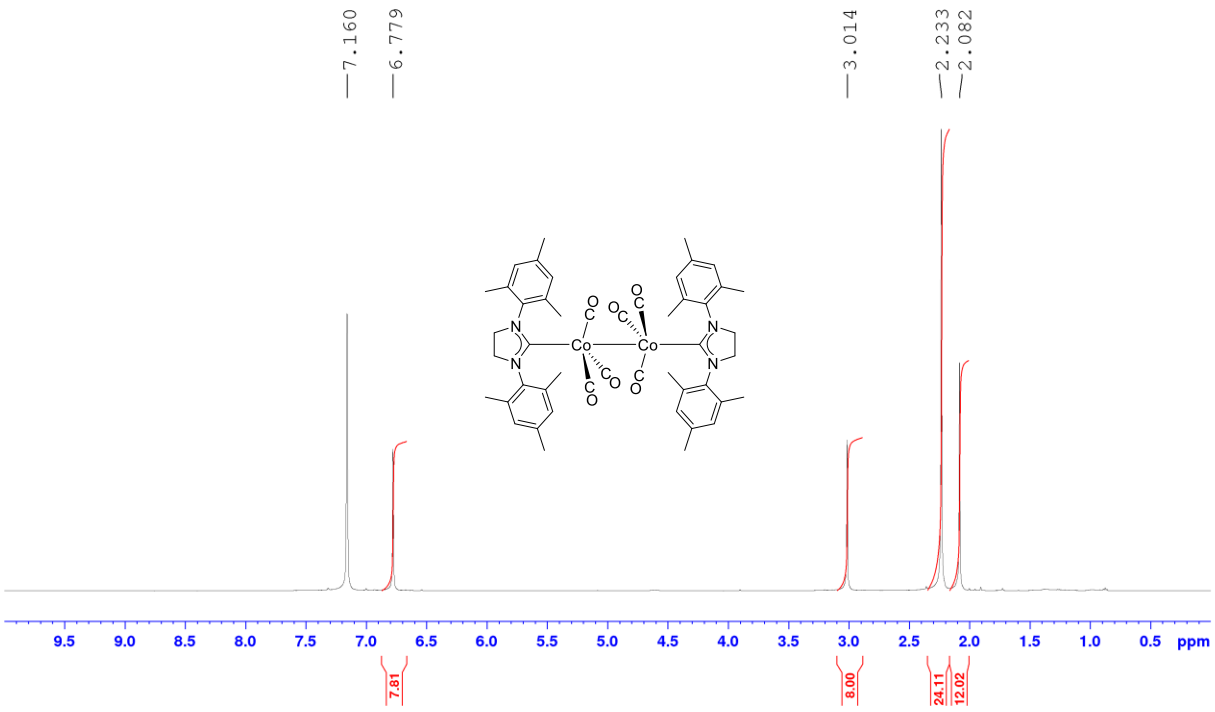

Figure S11 ^{1}H NMR spectrum (500.13 MHz, C_6D_6, 298 K) of **2-Mes**.

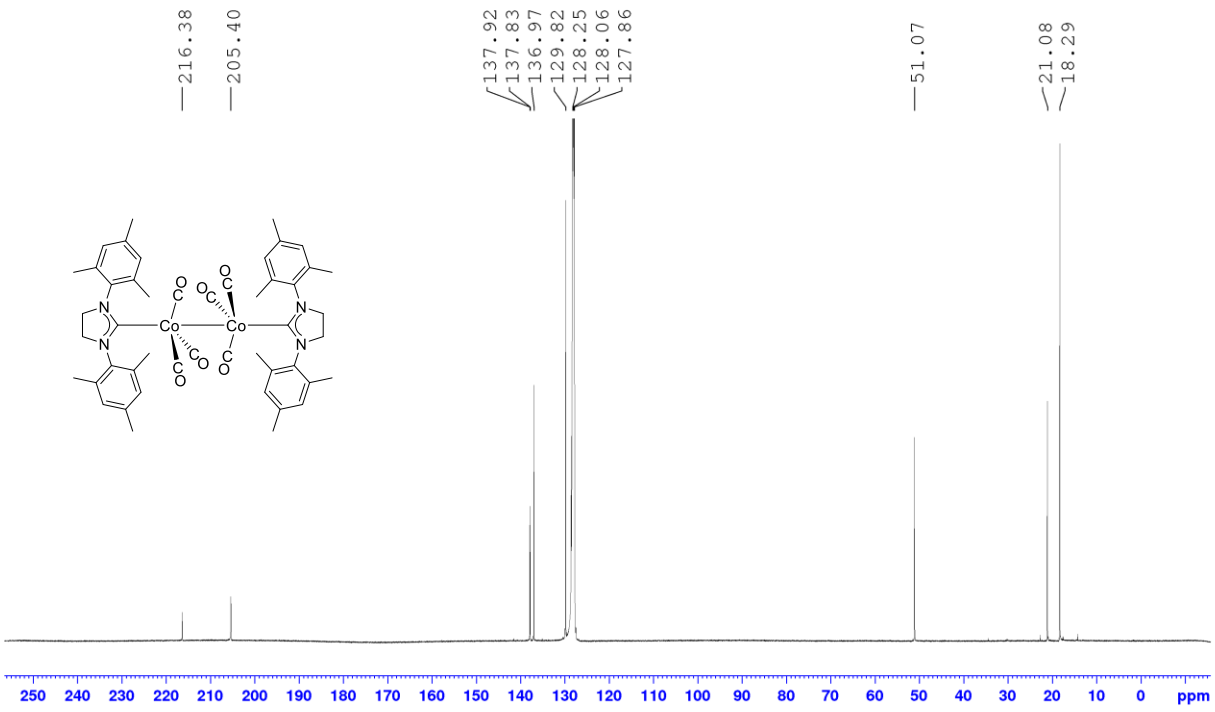

Figure S12 ^{13}C{^{1}H} NMR spectrum (125.76 MHz, C_6D_6, 298 K) of **2-Mes**.

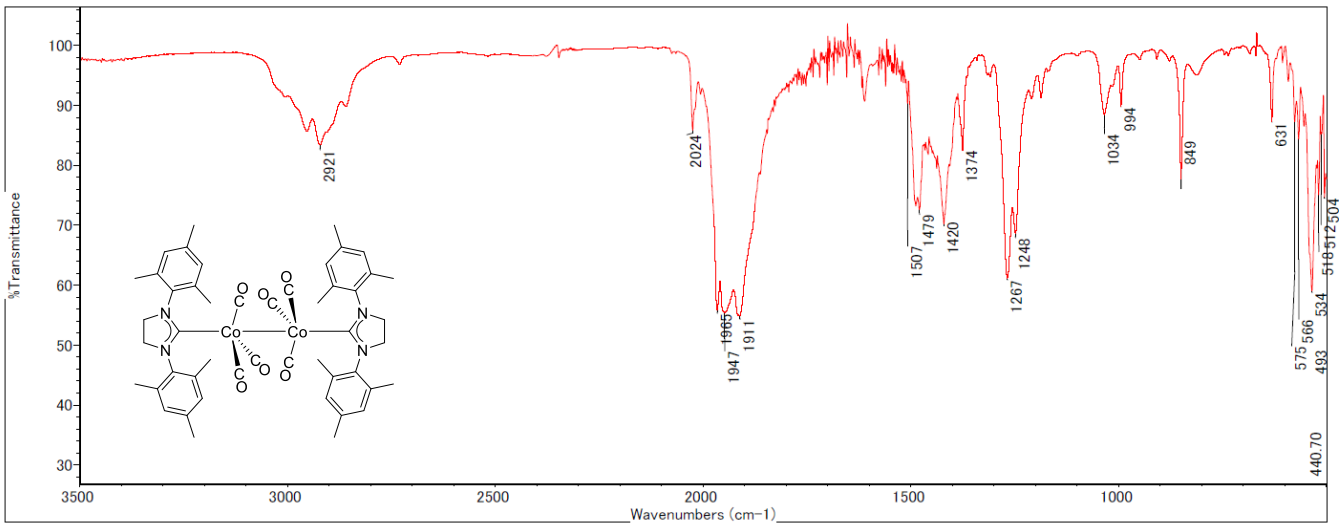

Figure S13 FTIR spectrum (KBr pellet) of **2-Mes**.

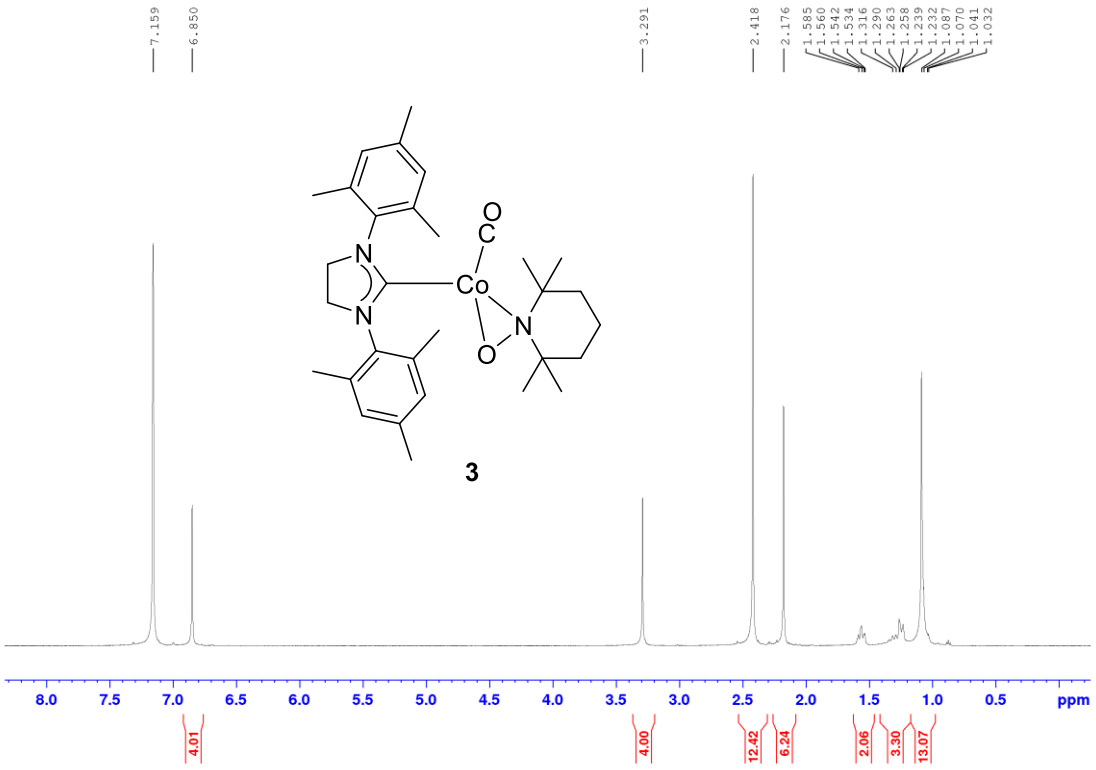

Figure S14 ^{1}H NMR spectrum (500.13 MHz, C_6D_6, 298 K) of **3**.

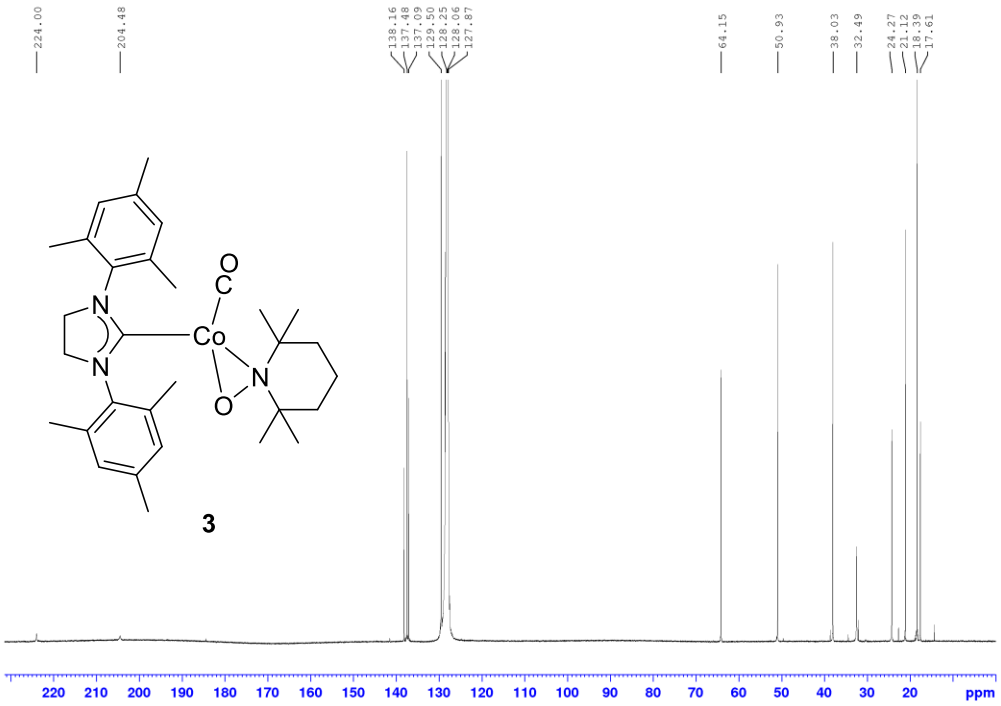

Figure S15 $^{13}C\{^{1}H\}$ NMR spectrum (125.77 MHz, C_6D_6, 298 K) of **3**.

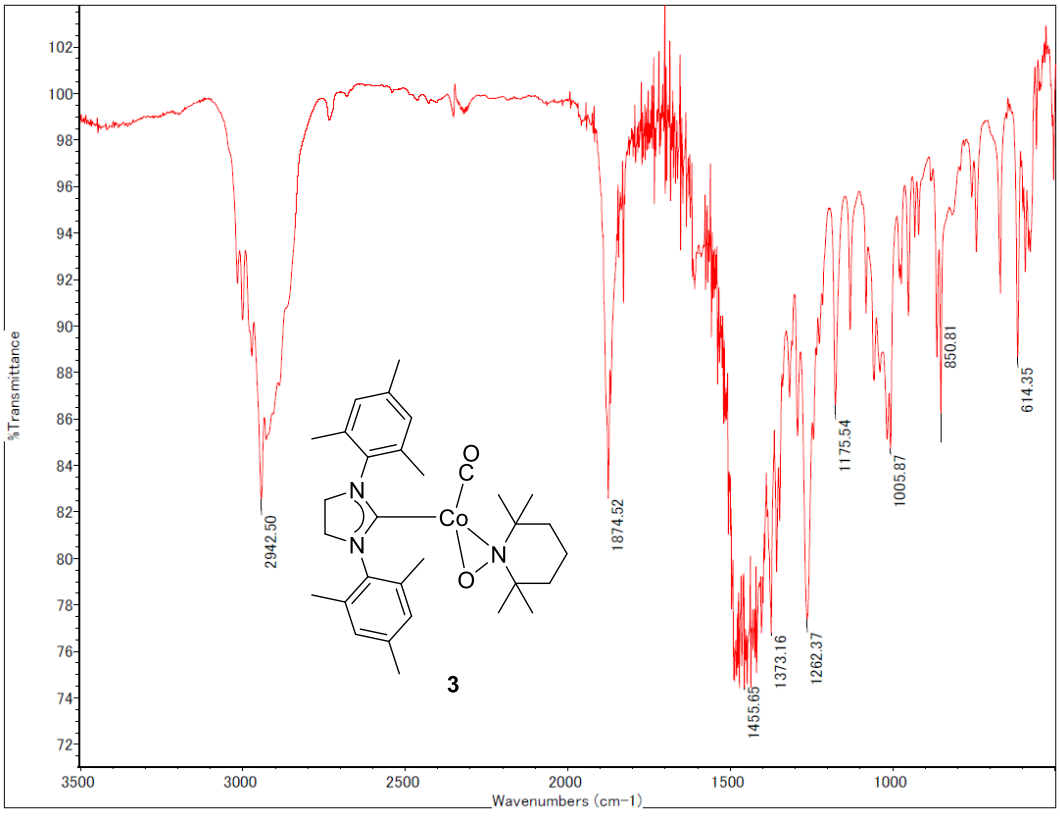

Figure S16 FTIR spectrum (thin film) of **3**.

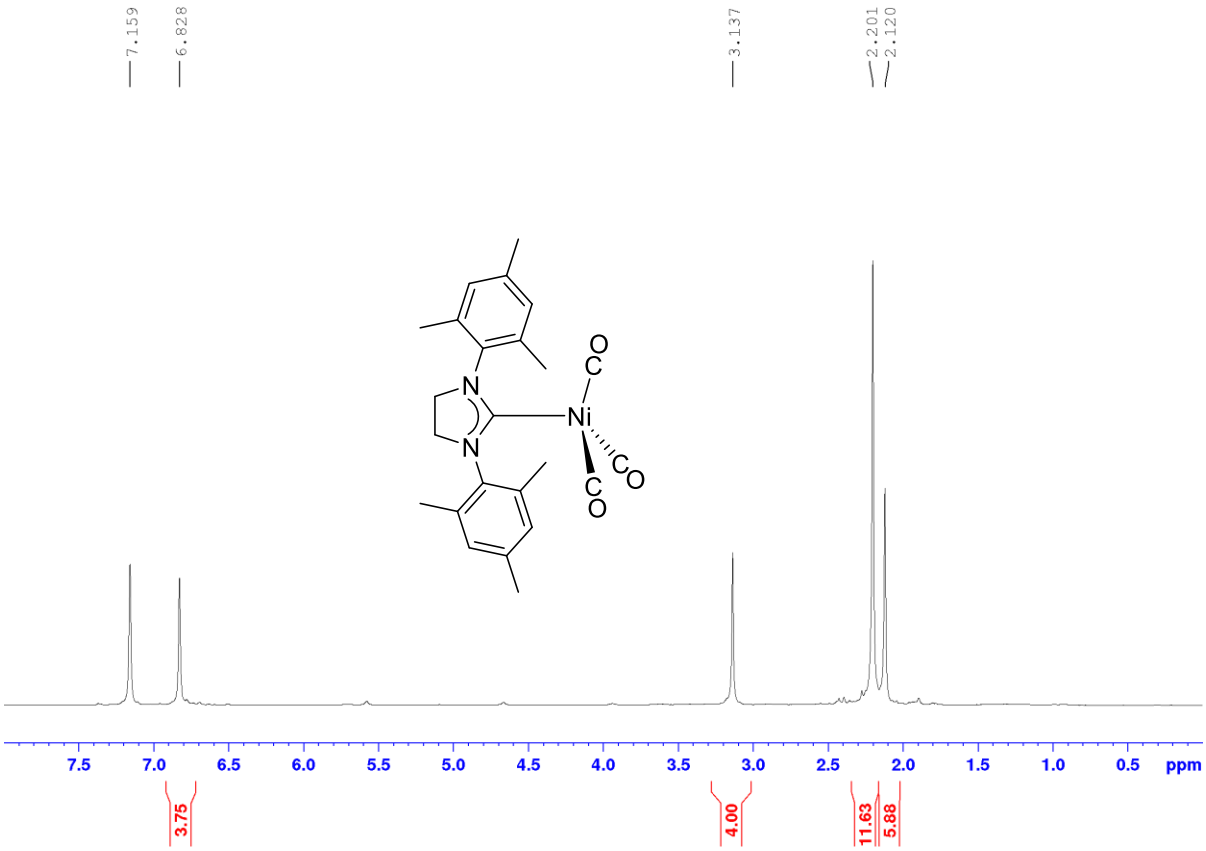

Figure S17 ^{1}H NMR spectrum (500.15 MHz, C_6D_6, 298 K) of **4**.

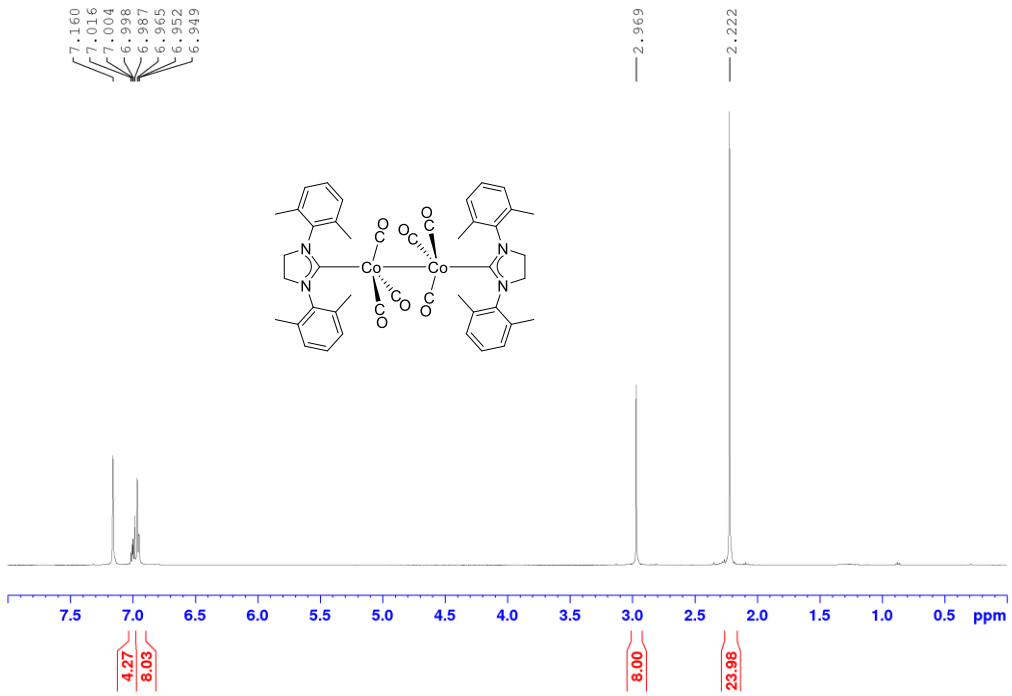

Figure S18 ^{1}H NMR spectrum (500.13 MHz, C_6D_6, 298 K) of **2-Me**.

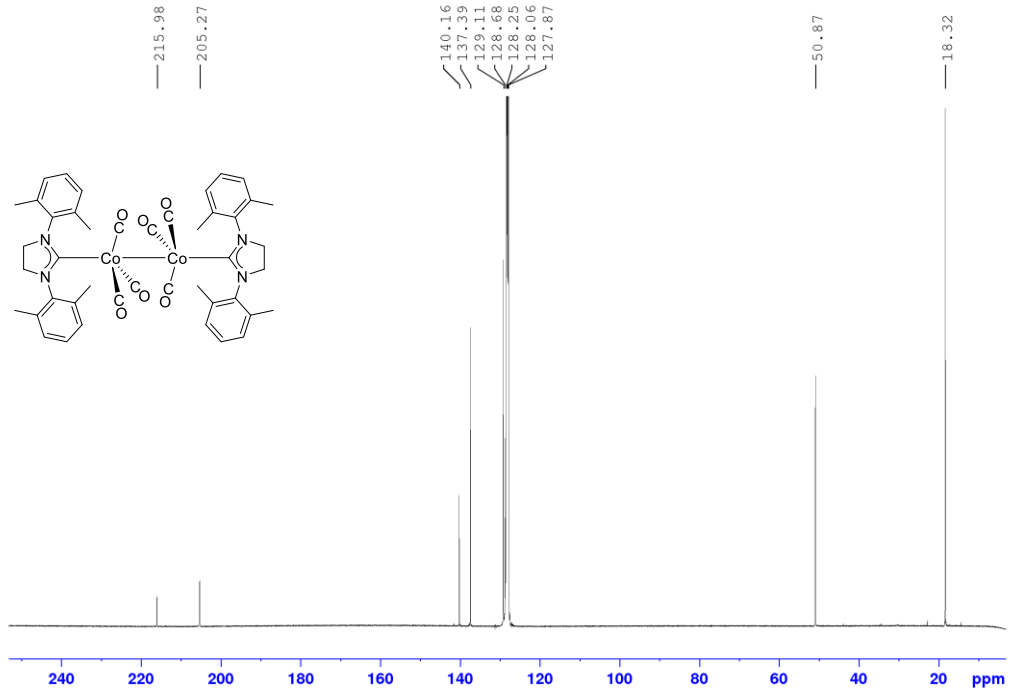

Figure S19 ^{13}C{^{1}H} NMR spectrum (125.76 MHz, C_6D_6, 298 K) of **2-Me**.

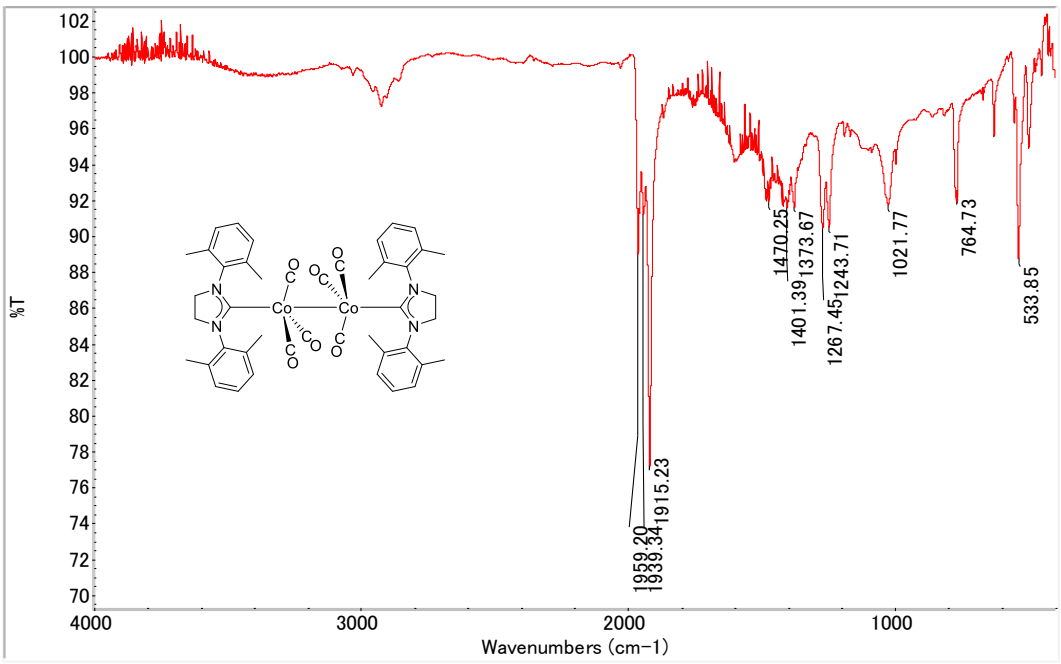

Figure S20 FTIR spectrum (thin film) of **2-Me**.

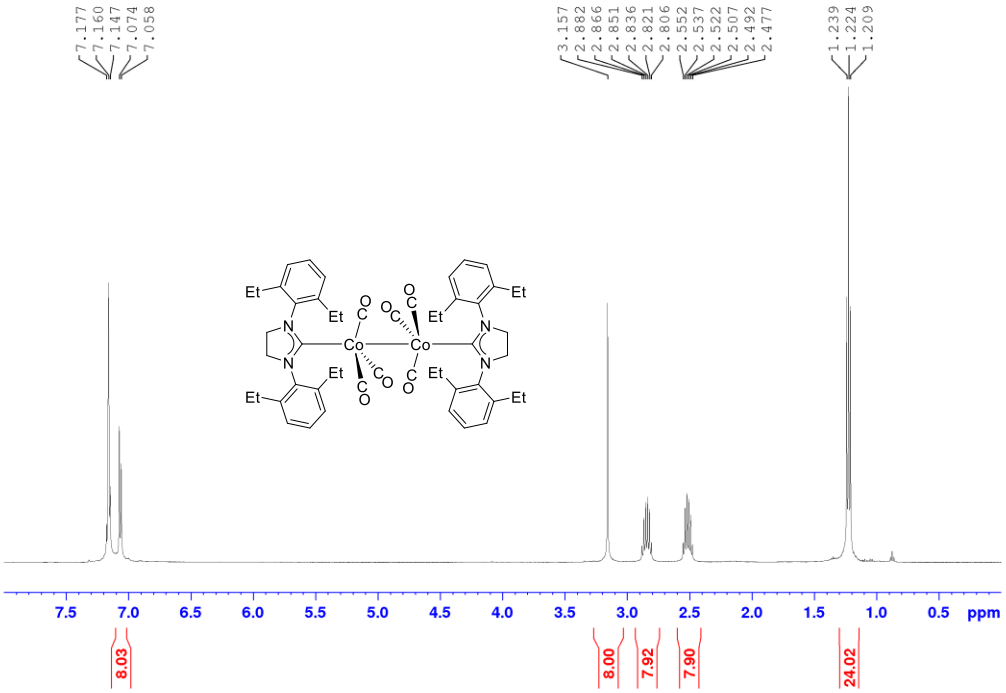

Figure S21 ^{1}H NMR spectrum (500.13 MHz, C_6D_6, 298 K) of **2-Et**.

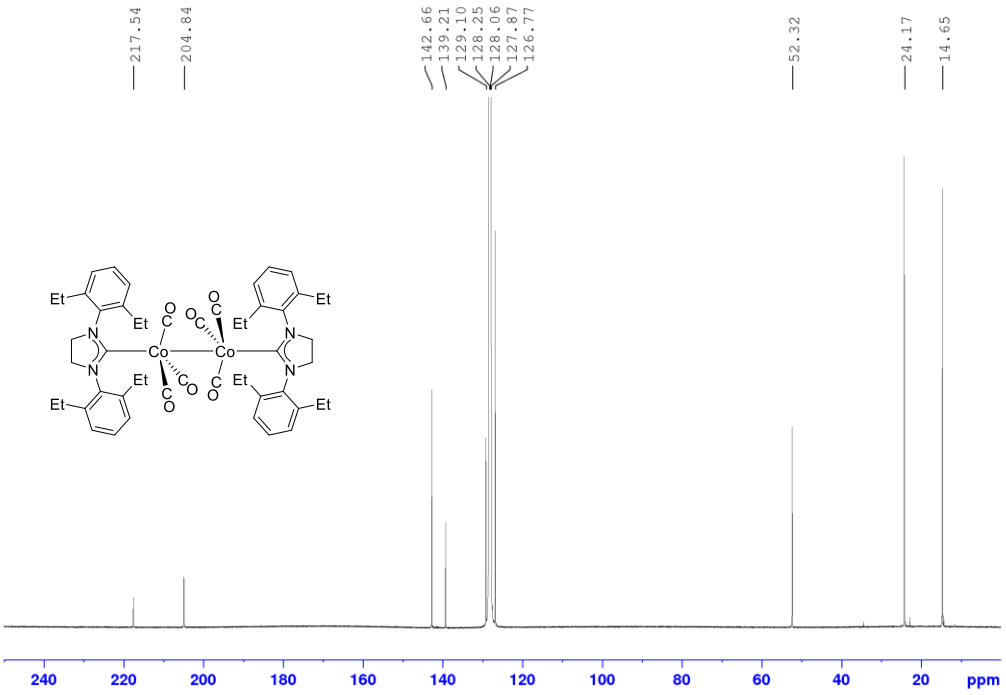

Figure S22 $^{13}C\{^{1}H\}$ NMR spectrum (125.76 MHz, C_6D_6, 298 K) of **2-Et**.

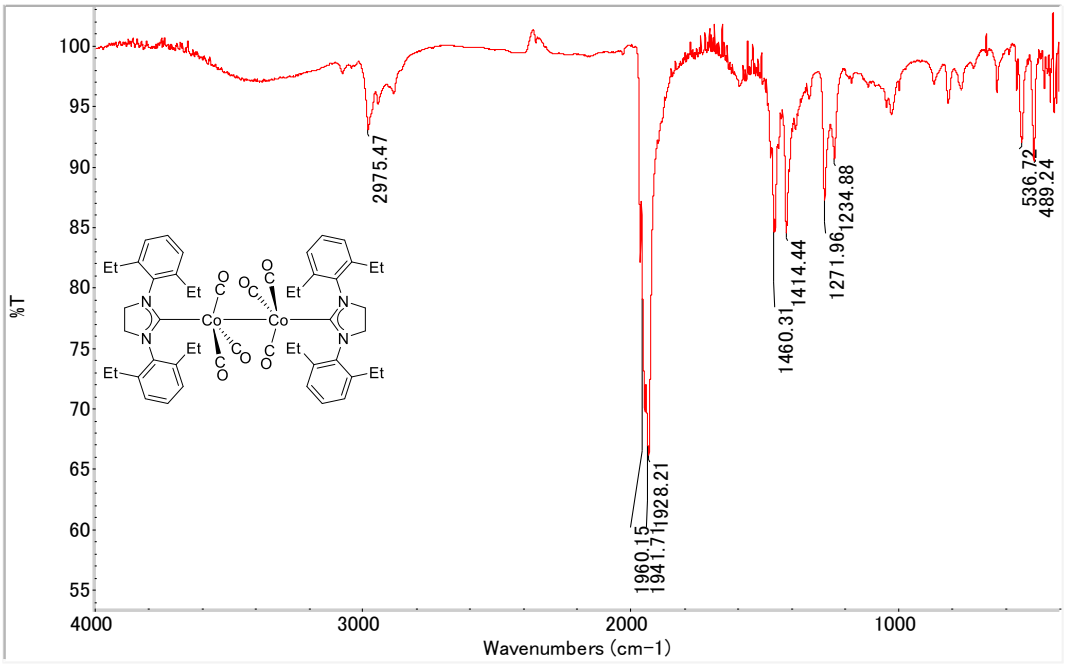

Figure S23 FTIR spectrum (thin film) of **2-Et**.

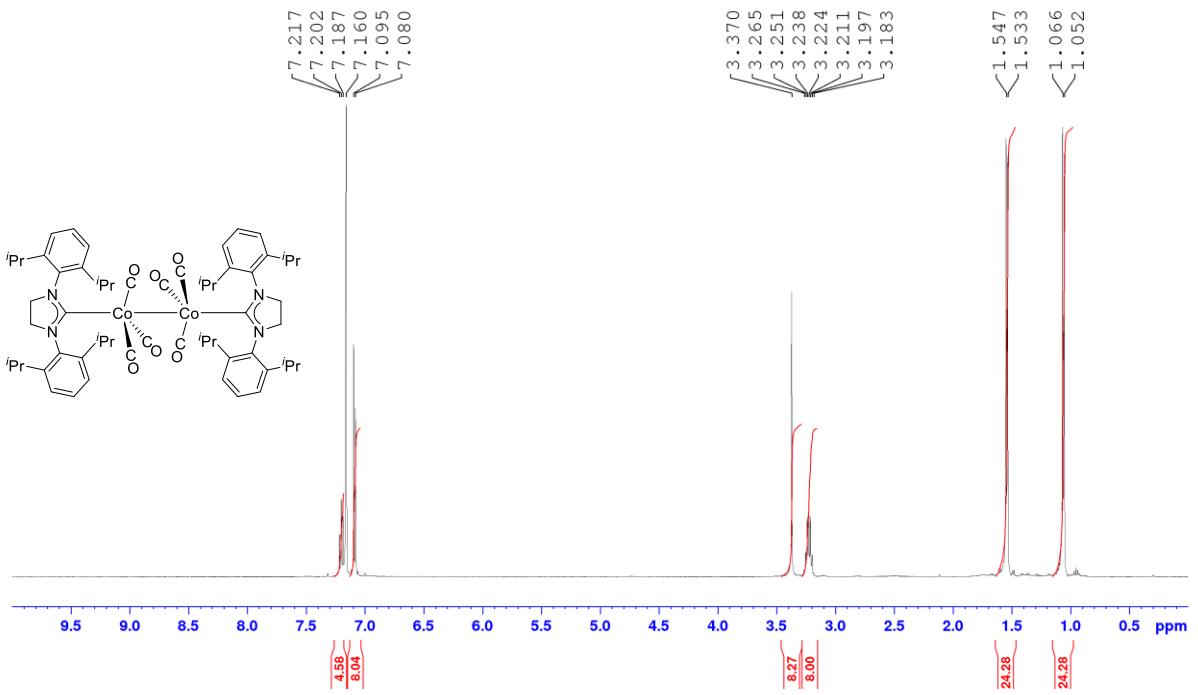

Figure S24 ^{1}H NMR spectrum (500.13 MHz, C_6D_6, 298 K) of **2-^{i}Pr**.

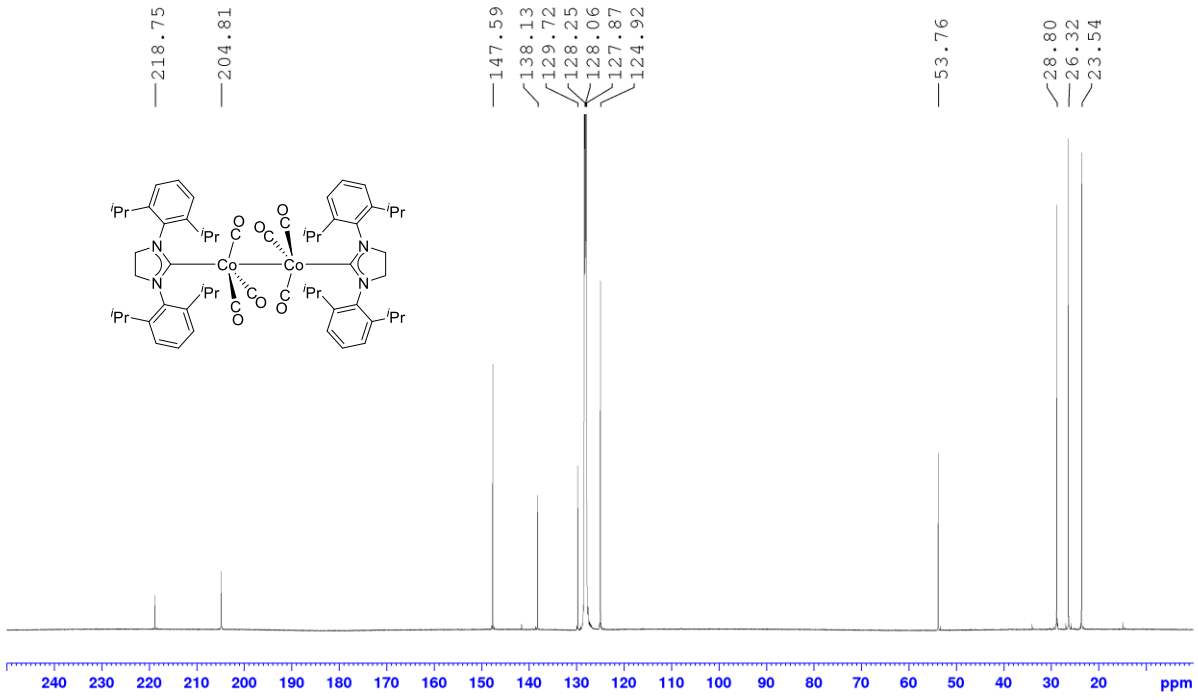

Figure S25 ^{13}C{^{1}H} NMR spectrum (125.76 MHz, C_6D_6, 298 K) of **2-^{i}Pr**.

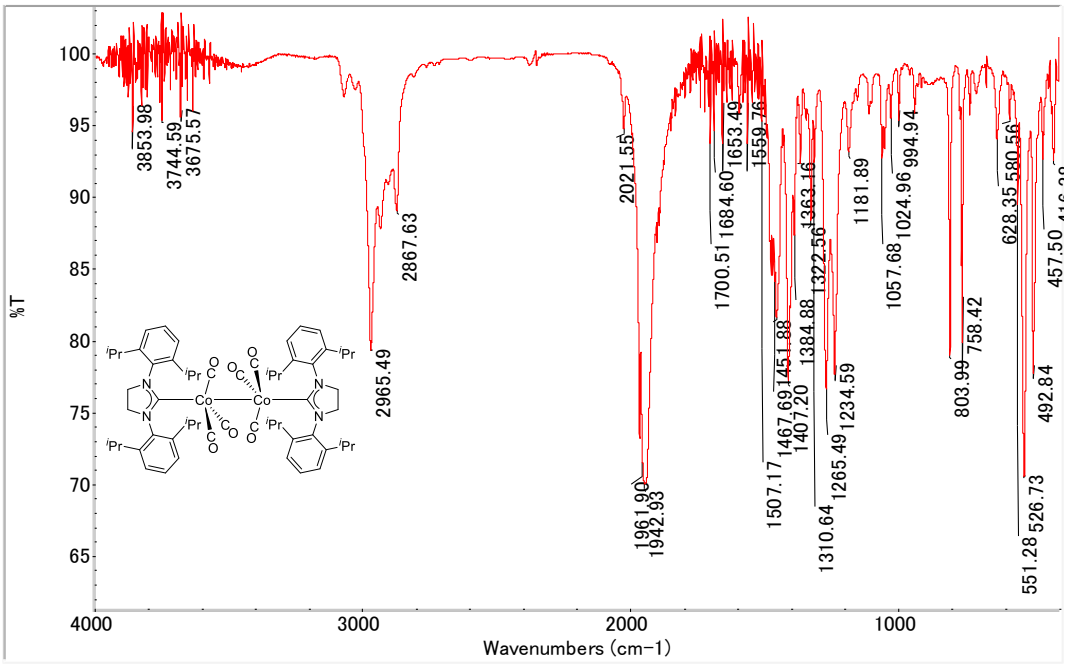

Figure S26 FTIR spectrum (thin film) of **2-^{i}Pr**.

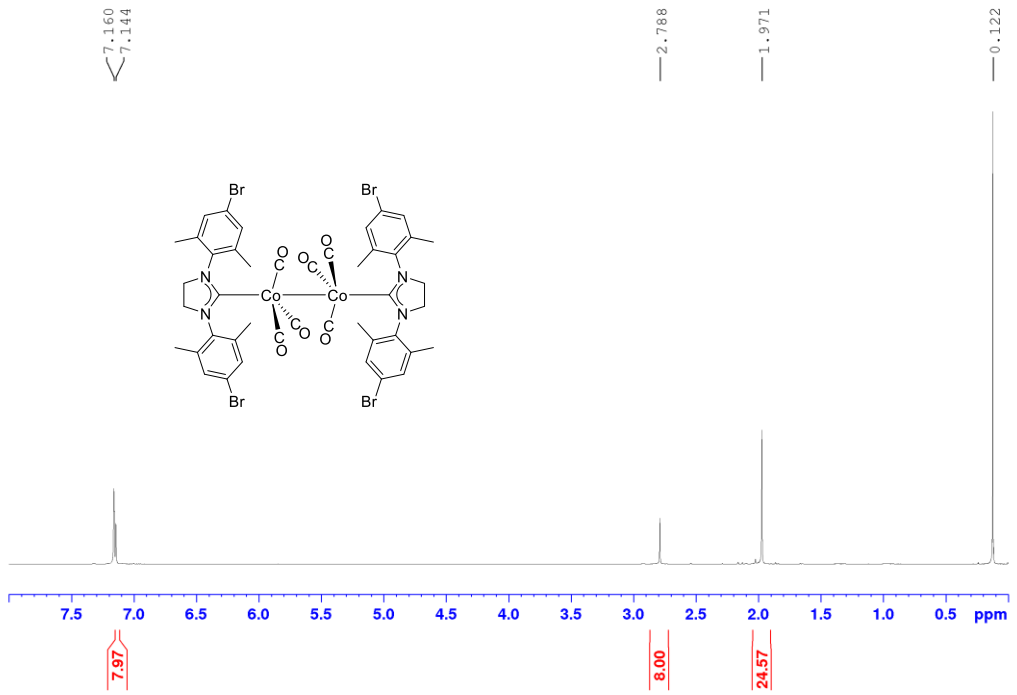

Figure S27 ^{1}H NMR spectrum (500.13 MHz, C_6D_6, 298 K) of **2-Br**.

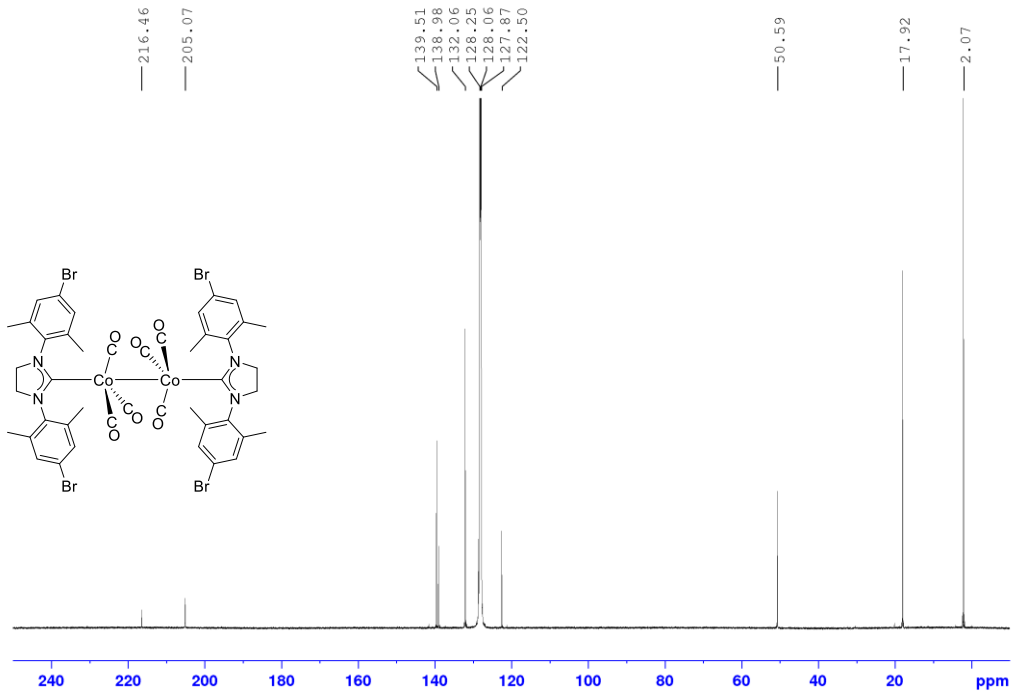

Figure S28 $^{13}C\{^{1}H\}$ NMR spectrum (125.76 MHz, C_6D_6, 298 K) of **2-Br**.

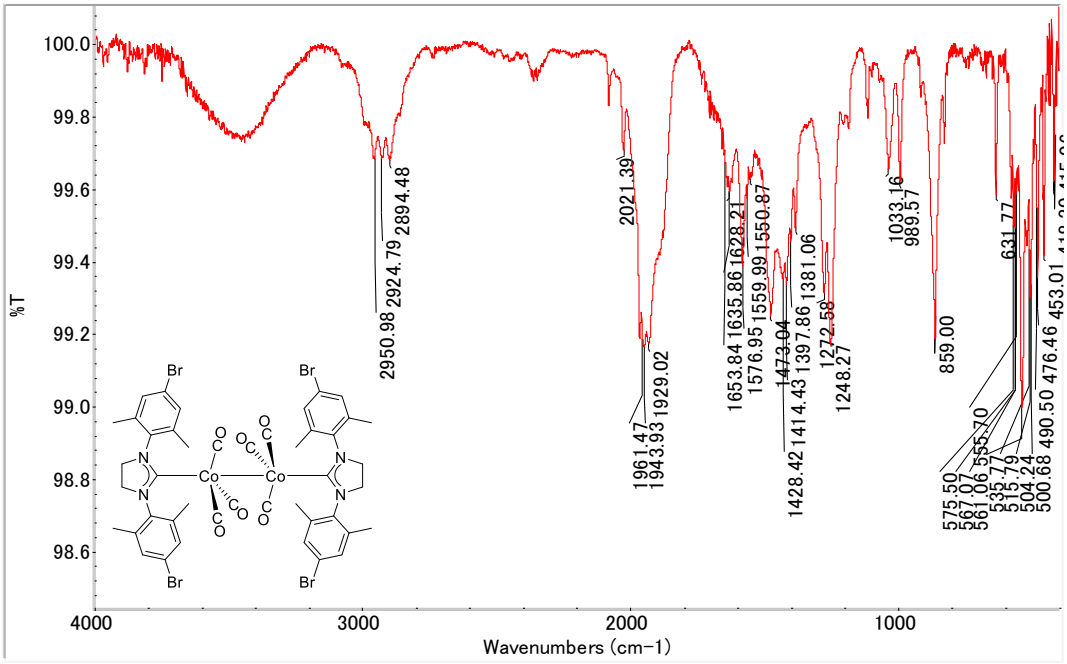

Figure S29 FTIR spectrum (thin film) of **2-Br**.

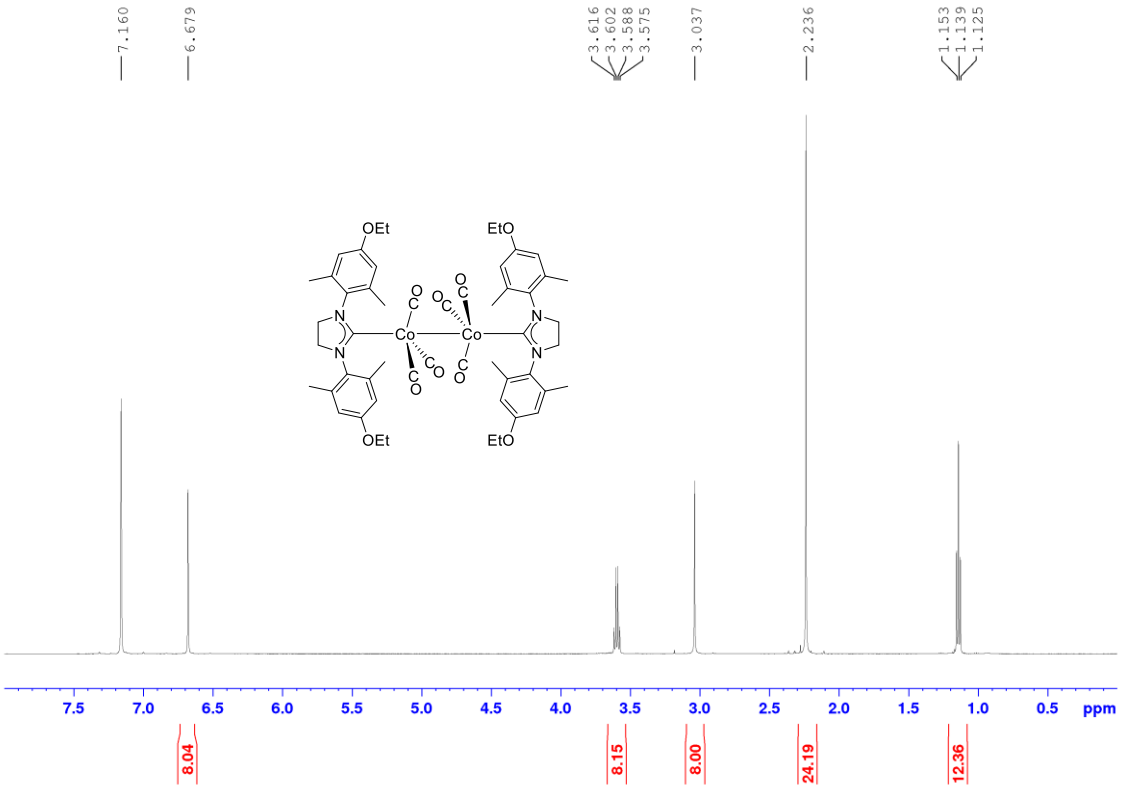

Figure S30 ^{1}H NMR spectrum (500.13 MHz, C_6D_6, 298 K) of **2-OEt**.

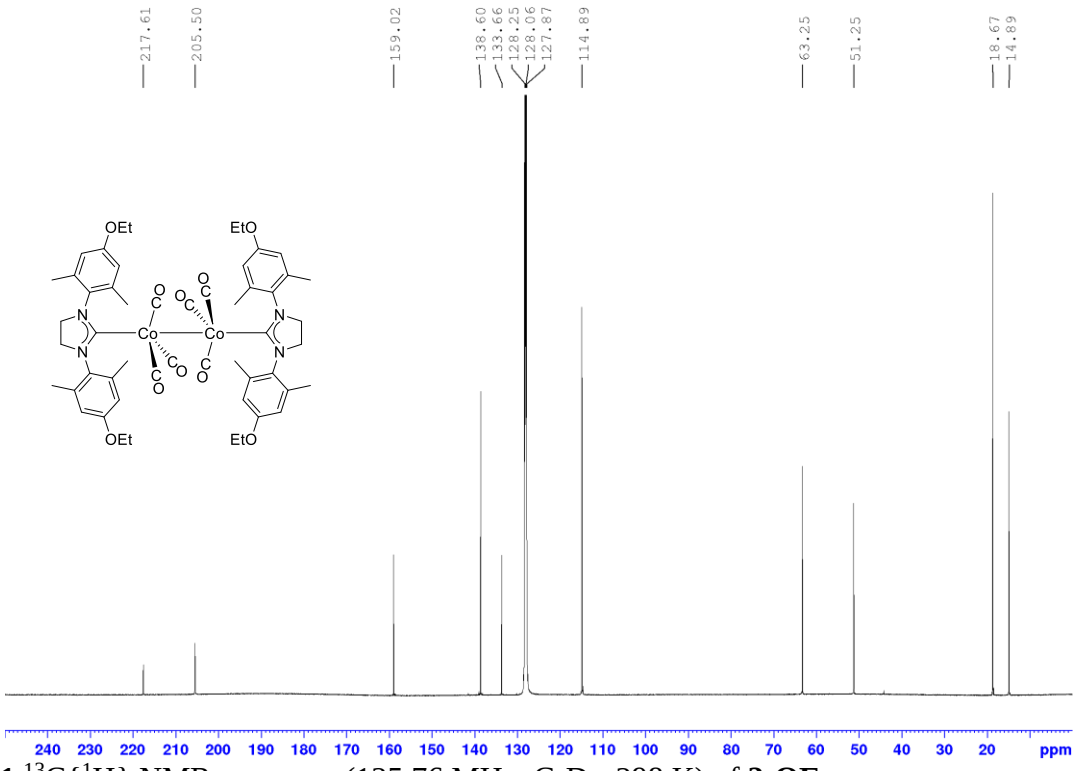

Figure S31 ^{13}C{^{1}H} NMR spectrum (125.76 MHz, C_6D_6, 298 K) of **2-OEt**.

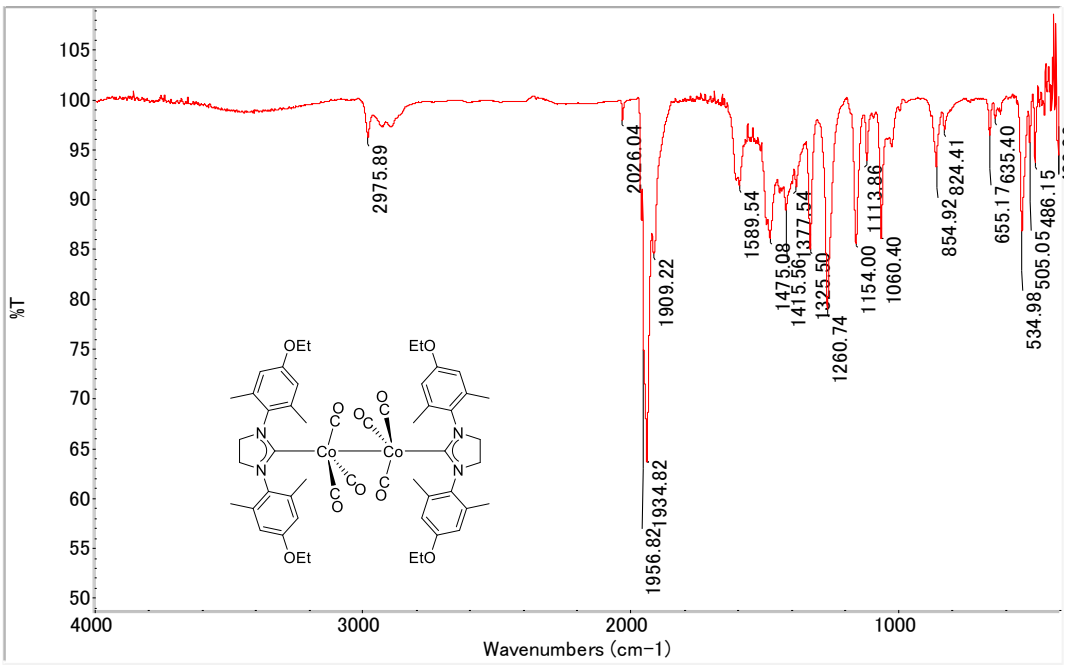

Figure S32 FTIR spectrum (thin film) of **2-OEt**.

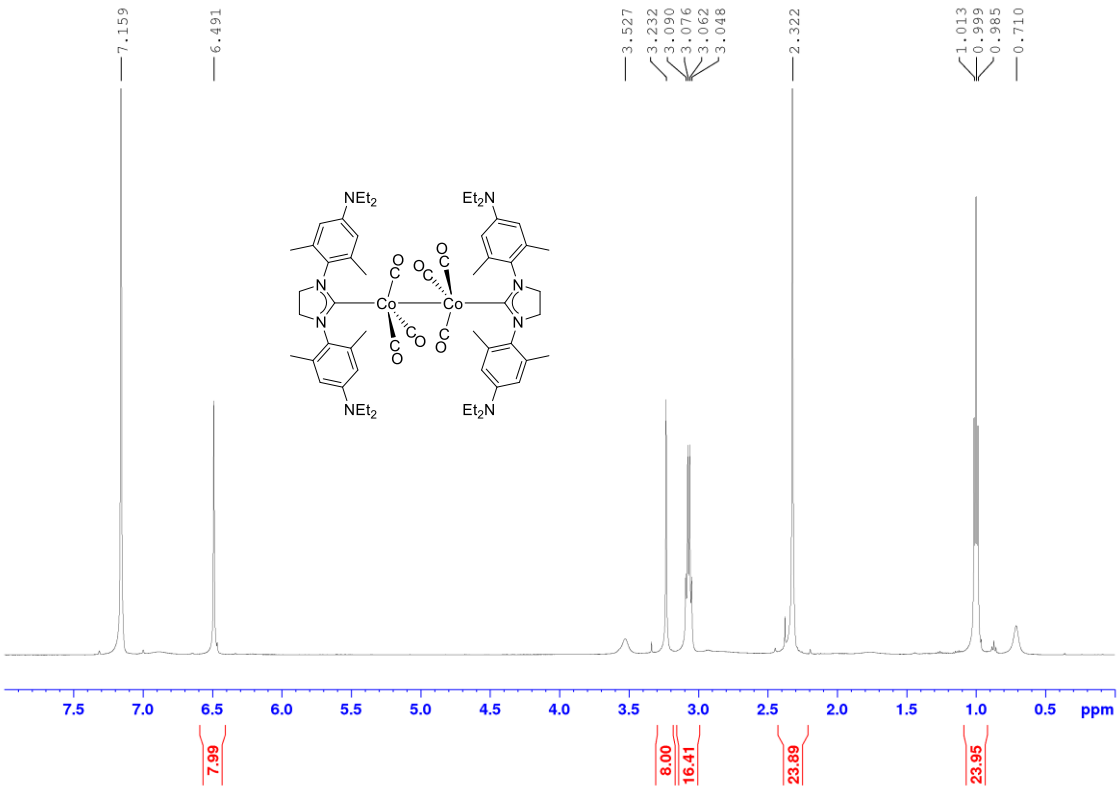

Figure S33 ^{1}H NMR spectrum (500.13 MHz, C_6D_6, 298 K) of **2-NEt2**.

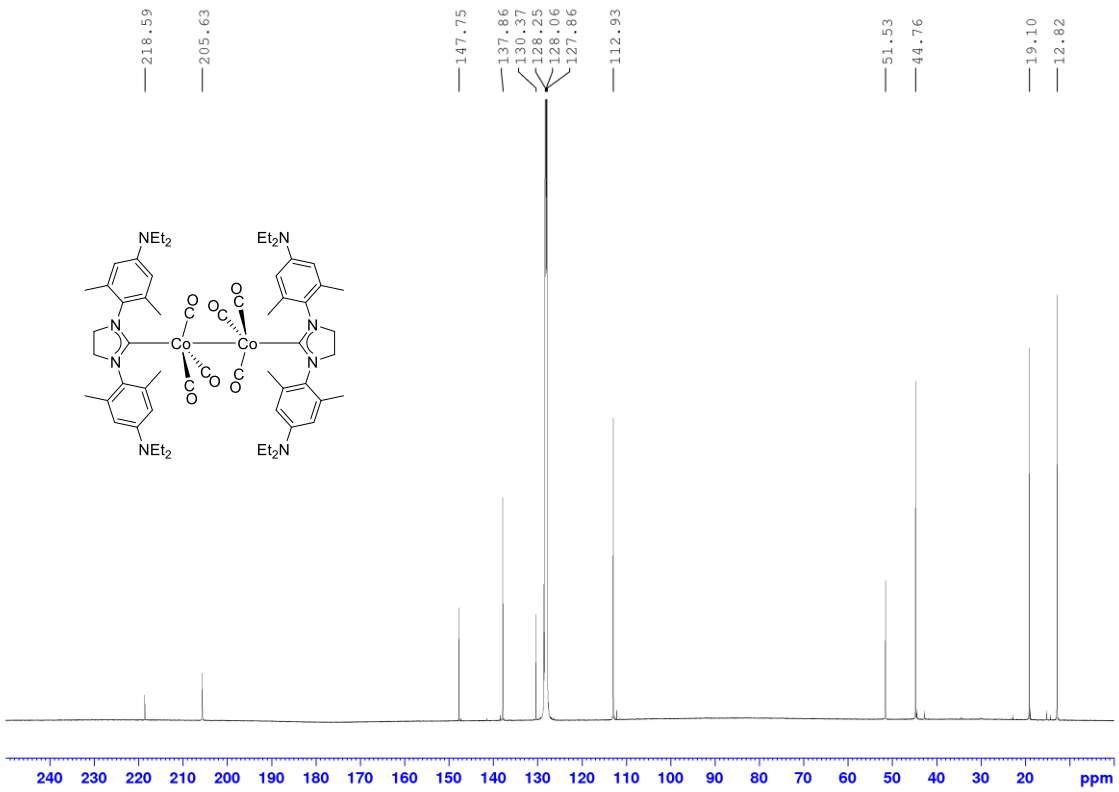

Figure S34 $^{13}C\{^{1}H\}$ NMR spectrum (125.76 MHz, C_6D_6, 298 K) of **2-NEt$_2$**.

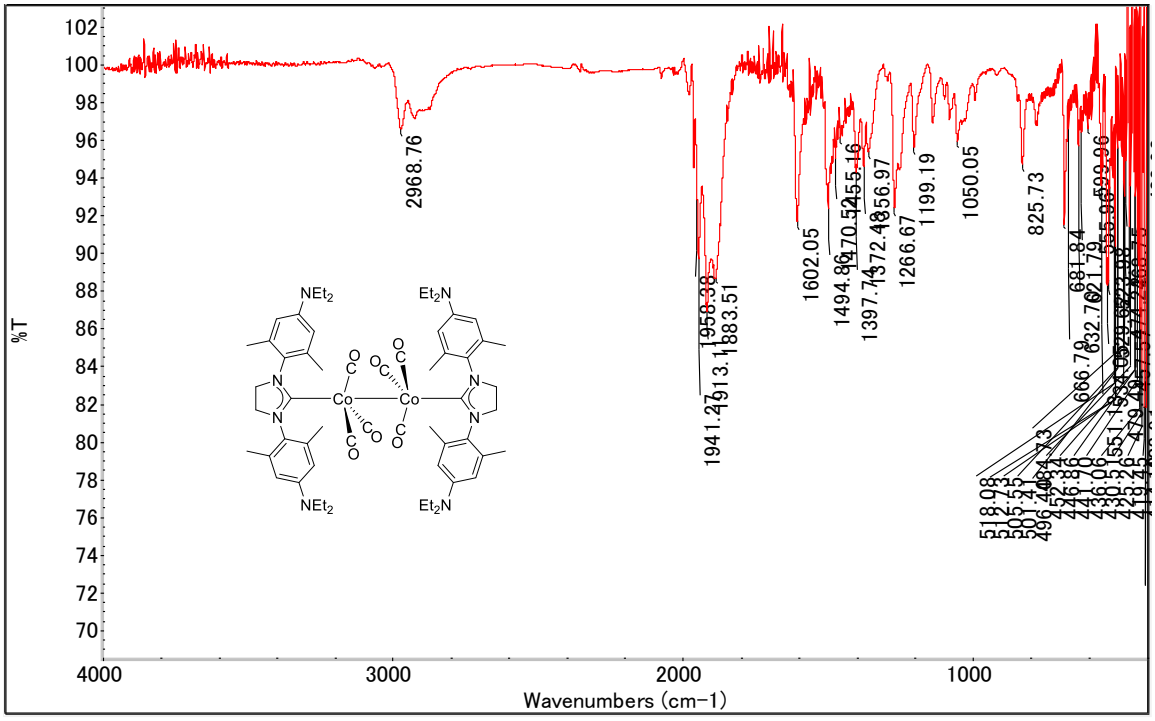

Figure S35 FTIR spectrum (thin film) of **2-NEt$_2$**.

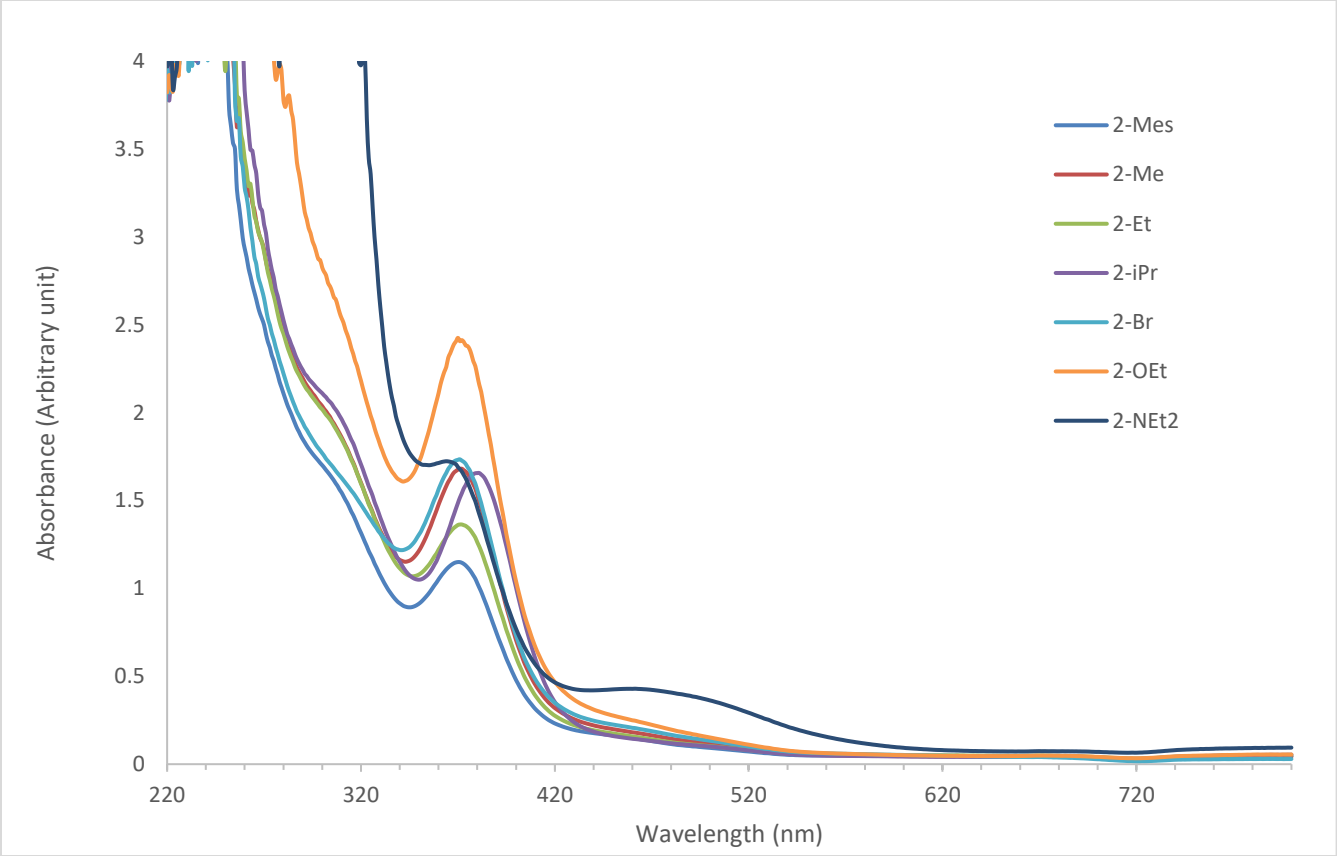

Figure S36 UV-Vis spectrum (in THF, 25 °C, 220-800 nm) of complexes **2-Mes**, **2-Me**, **2-Et**, **2-^{i}Pr**, **2-Br**, **2-OEt**, and **2-NEt$_2$**.

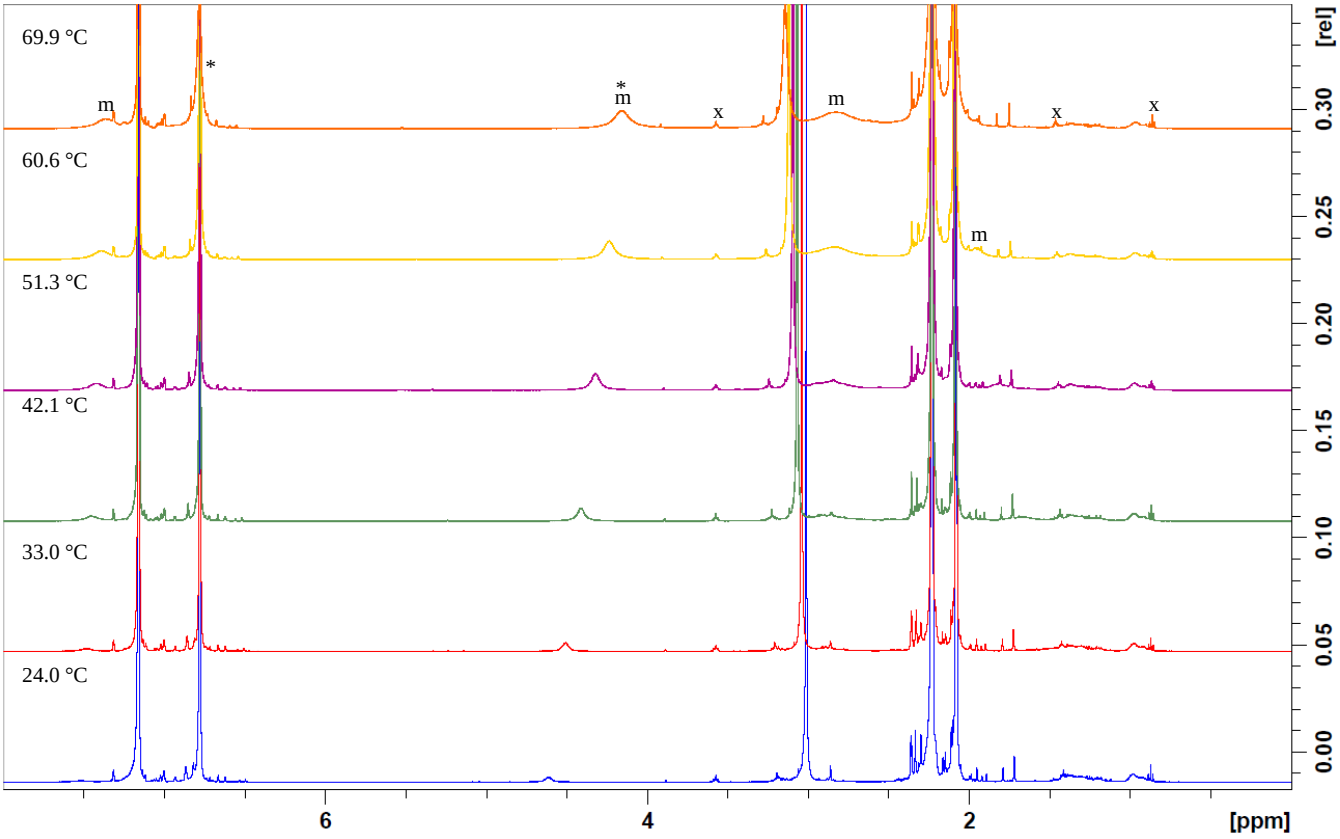

Figure S37 Variable temperature ^{1}H NMR spectra of **2-Mes** (500 MHz, in C_6D_6). Sharp signals exceeding the spectral y-axis ranges are from the dimeric form of **2-Mes** and residual C_6D_6 signal (7.16 ppm). m: signals from the monomeric form of **2-Mes**, *: signals used for integration analysis, x: signals from solvent (THF, n-pentane, and/or ether).

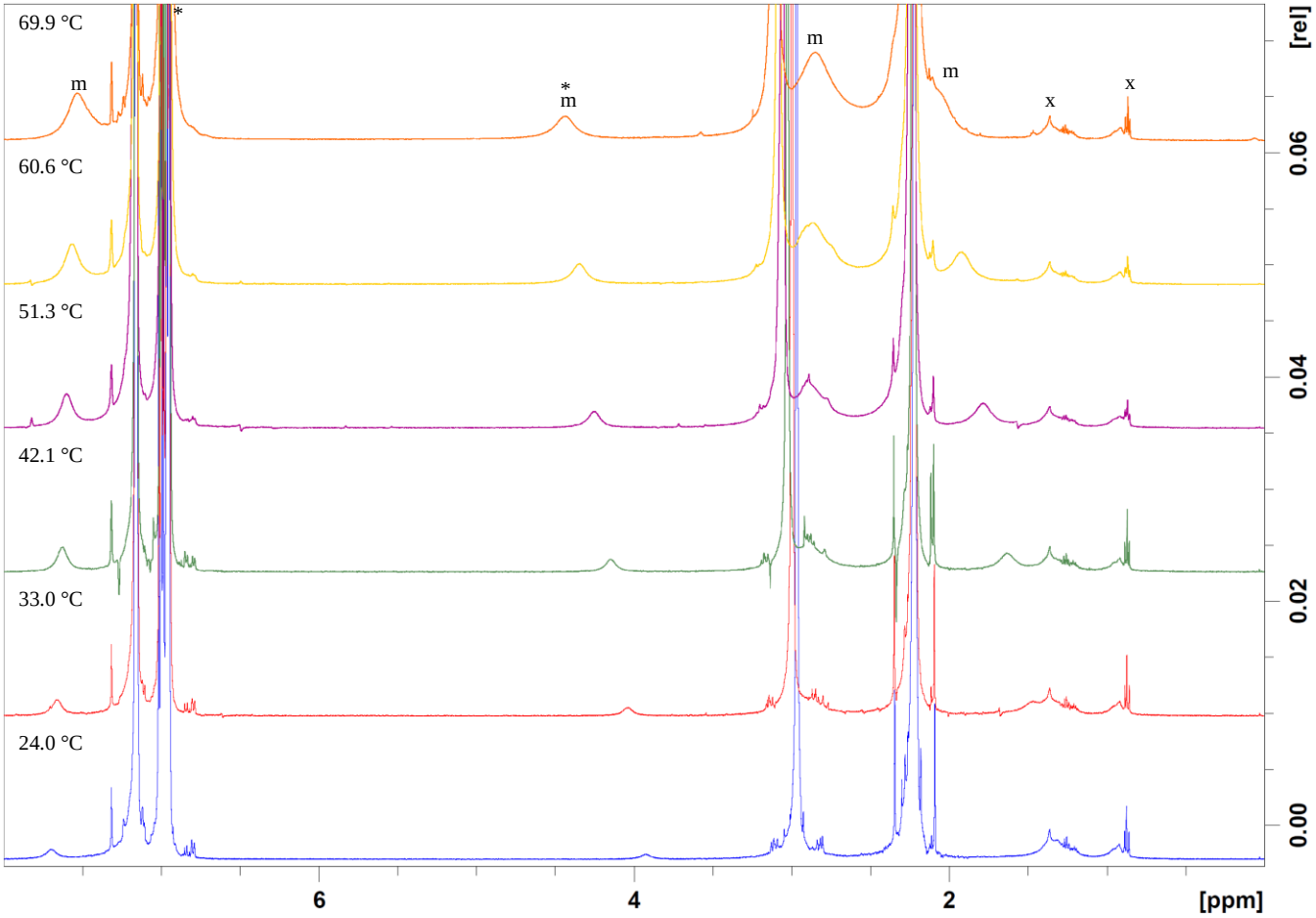

Figure S38 Variable temperature ^{1}H NMR spectra of **2-Me** (500 MHz, in C_6D_6). Sharp signals exceeding the spectral y-axis ranges are from the dimeric form of **2-Me** and residual C_6D_6 signal (7.16 ppm). m: signals from the monomeric form of **2-Me**, *: signals used for integration analysis, x: signals from solvent (THF, n-pentane, and/or ether).

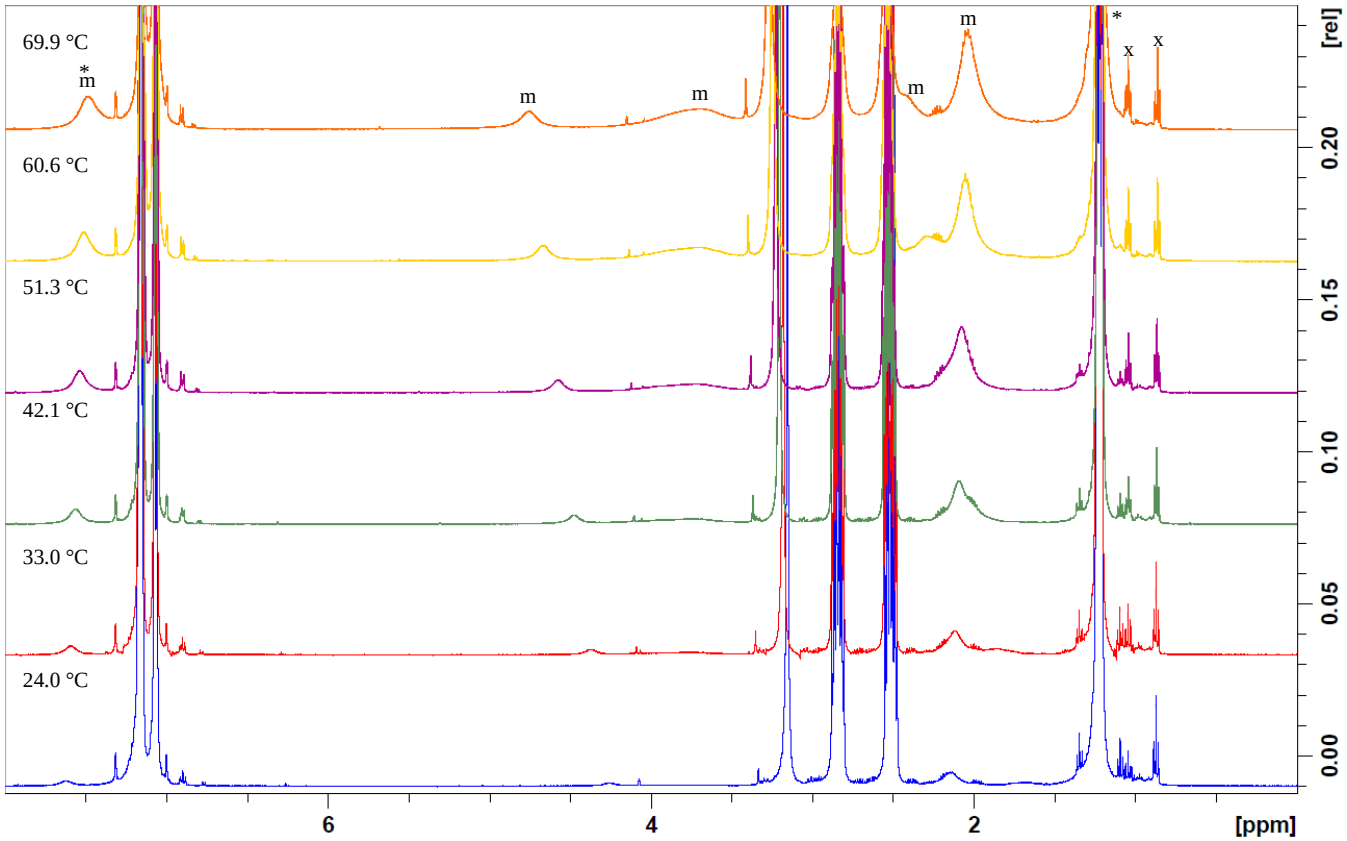

Figure S39 Variable temperature ^{1}H NMR spectra of **2-Et** (500 MHz, in C_6D_6). Sharp signals exceeding the spectral y-axis ranges are from the dimeric form of **2-Et** and residual C_6D_6 signal (7.16 ppm). m: signals from the monomeric form of **2-Et**, *: signals used for integration analysis, x: signals from residual solvent (THF, n-pentane, and/or ether).

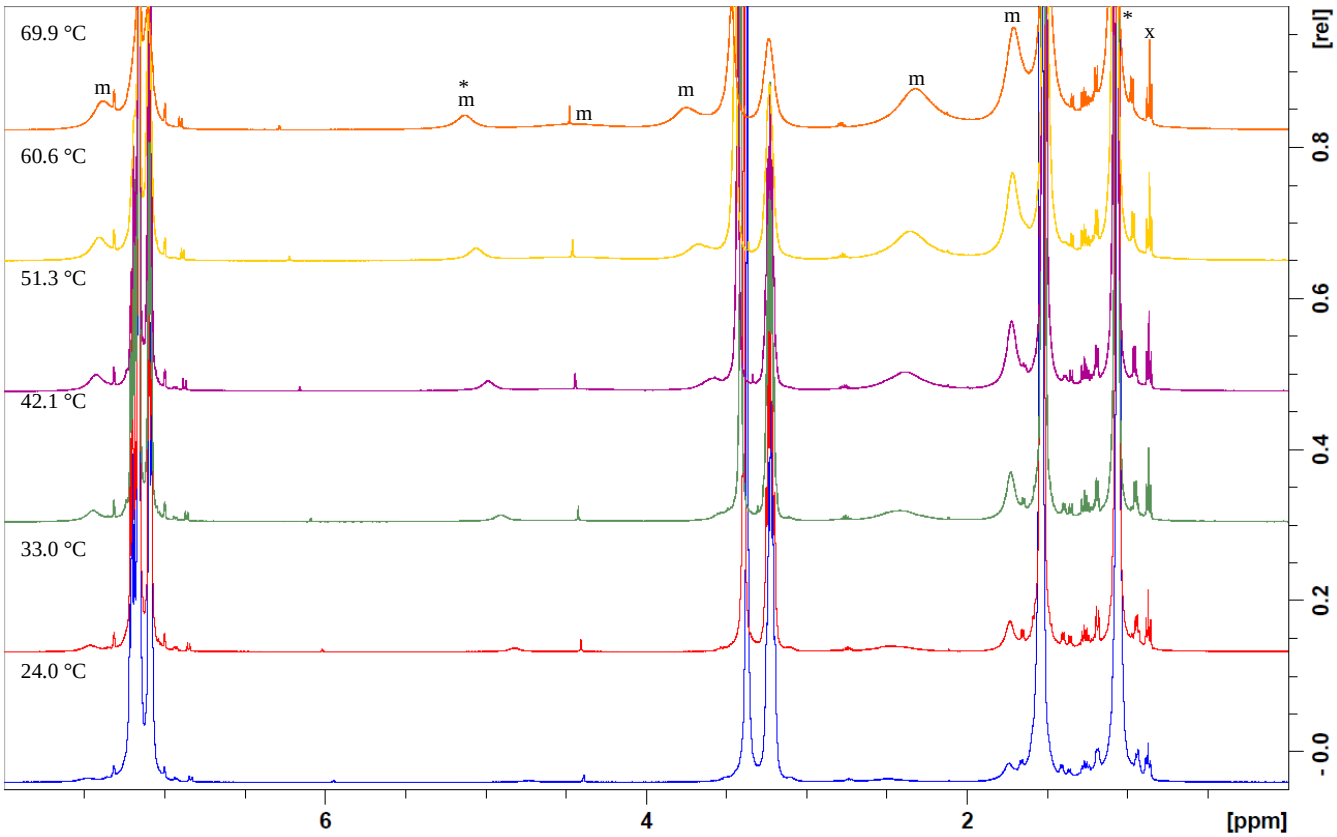

Figure S40 Variable temperature ^{1}H NMR spectra of **2-^{i}Pr** (500 MHz, in C_6D_6). Sharp signals exceeding the spectral y-axis ranges are from the dimeric form of **2-^{i}Pr** and residual C_6D_6 signal (7.16 ppm). m: signals from the monomeric form of **2-^{i}Pr**, *: signals used for integration analysis, x: signals from solvent (THF, n-pentane, and/or ether).

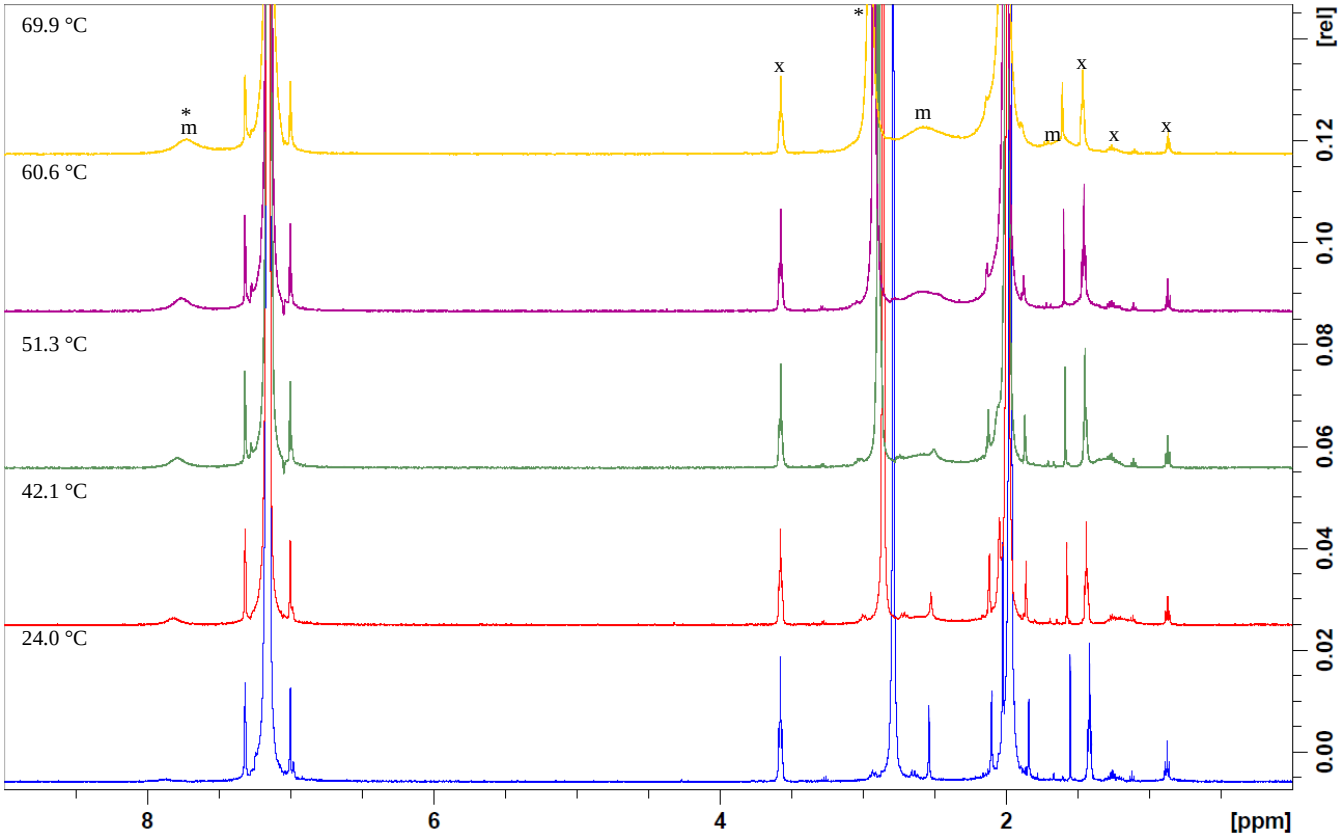

Figure S41 Variable temperature ^{1}H NMR spectra of **2-Br** (500 MHz, in C_6D_6). Sharp signals exceeding the spectral y-axis ranges are from the dimeric form of **2-Br** and residual C_6D_6 signal (7.16 ppm). m: signals from the monomeric form of **2-Br**, *: signals used for integration analysis, x: signals from solvent (THF, n-pentane, and/or ether).

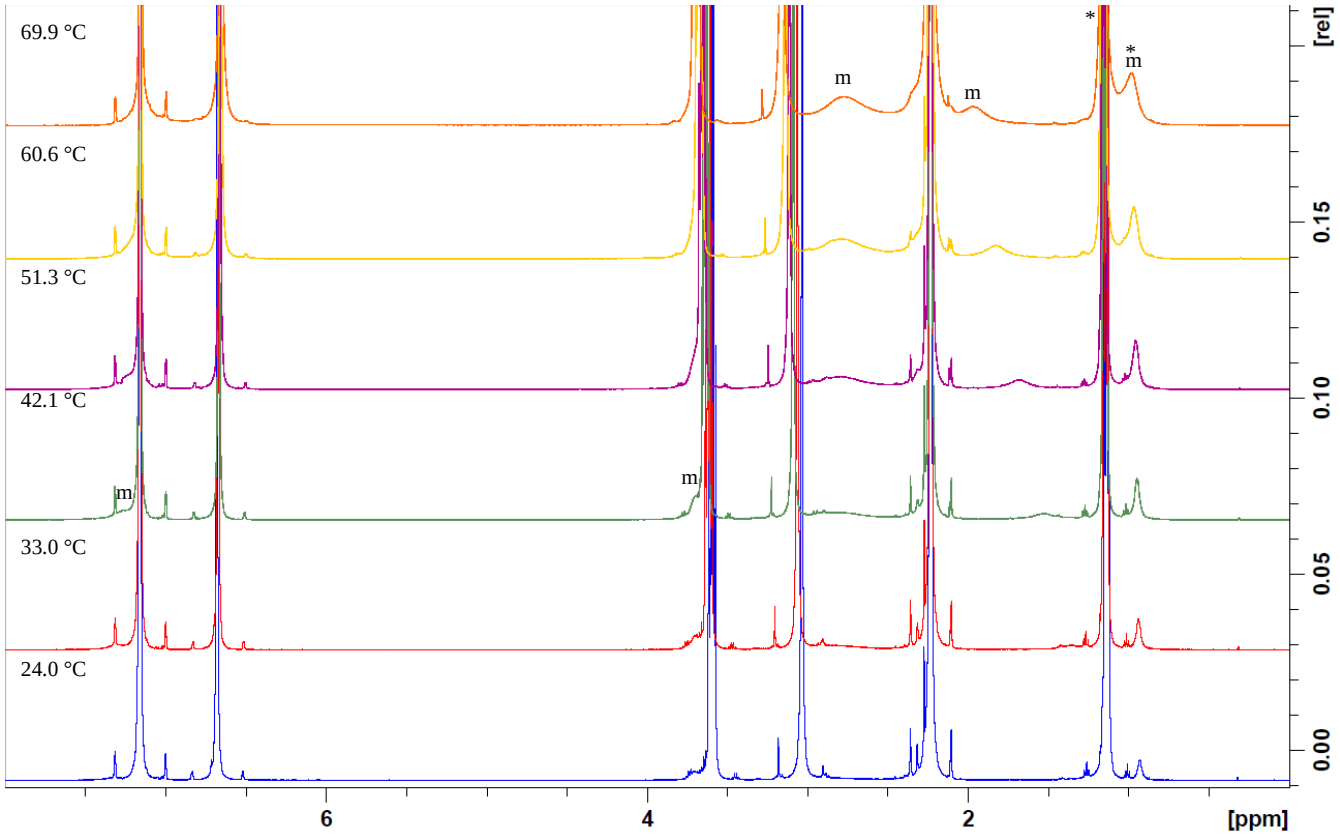

Figure S42 Variable temperature ^{1}H NMR spectra of **2-OEt** (500 MHz, in C_6D_6). Sharp signals exceeding the spectral y-axis ranges are from the dimeric form of **2-OEt** and residual C_6D_6 signal (7.16 ppm). m: signals from the monomeric form of **2-OEt**, *: signals used for integration analysis.

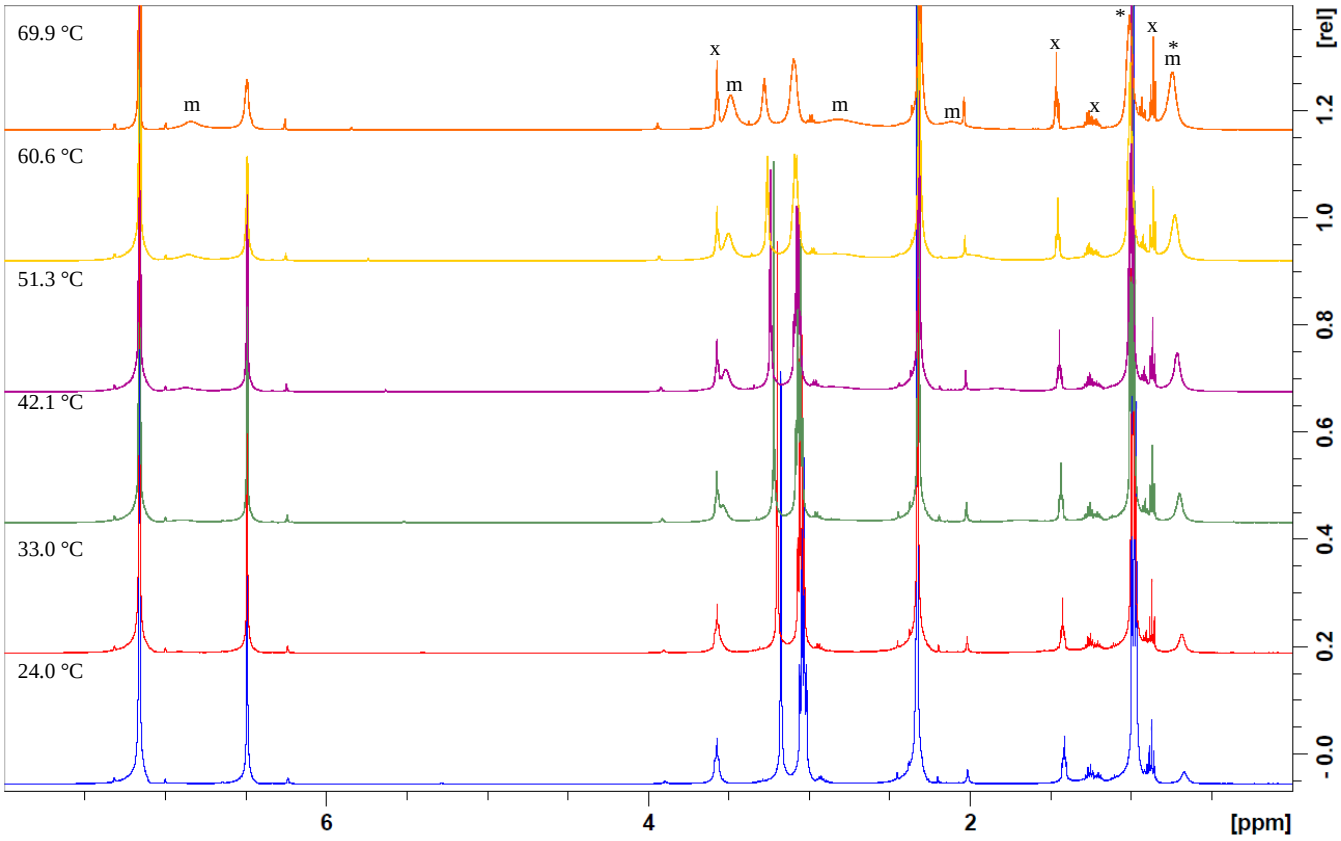

Figure S43 Variable temperature ^{1}H NMR spectra of **2-NEt$_2$** (500 MHz, in C_6D_6). Sharp signals exceeding the spectral y-axis ranges are from the dimeric form of **2-NEt$_2$** and residual C_6D_6 signal (7.16 ppm). m: signals from the monomeric form of **2-NEt$_2$**, *: signals used for integration analysis, x: signals from solvent (THF, n-pentane, and/or ether).

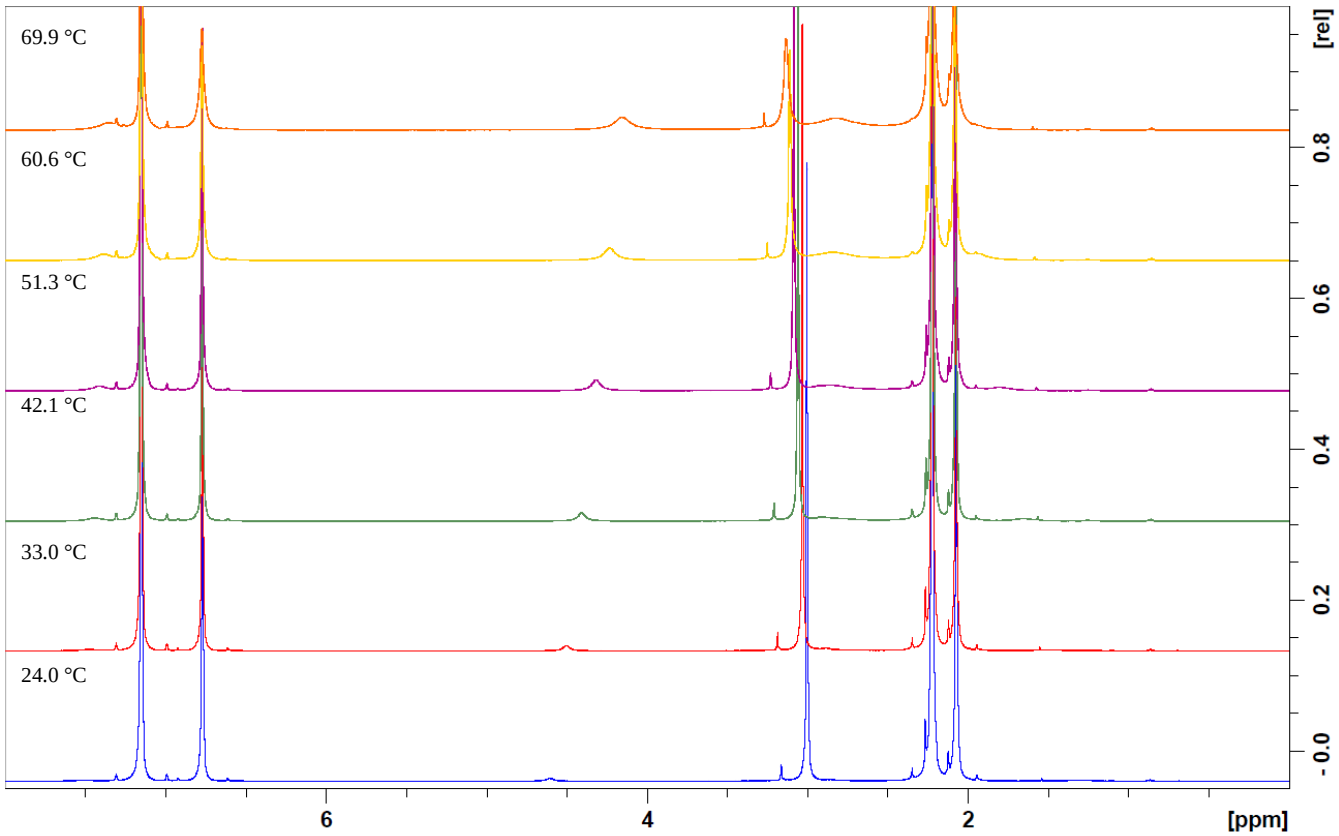

Figure S44 Variable temperature ^{1}H NMR spectra of **2-Mes** under 3 bar CO (500 MHz, in C_6D_6).

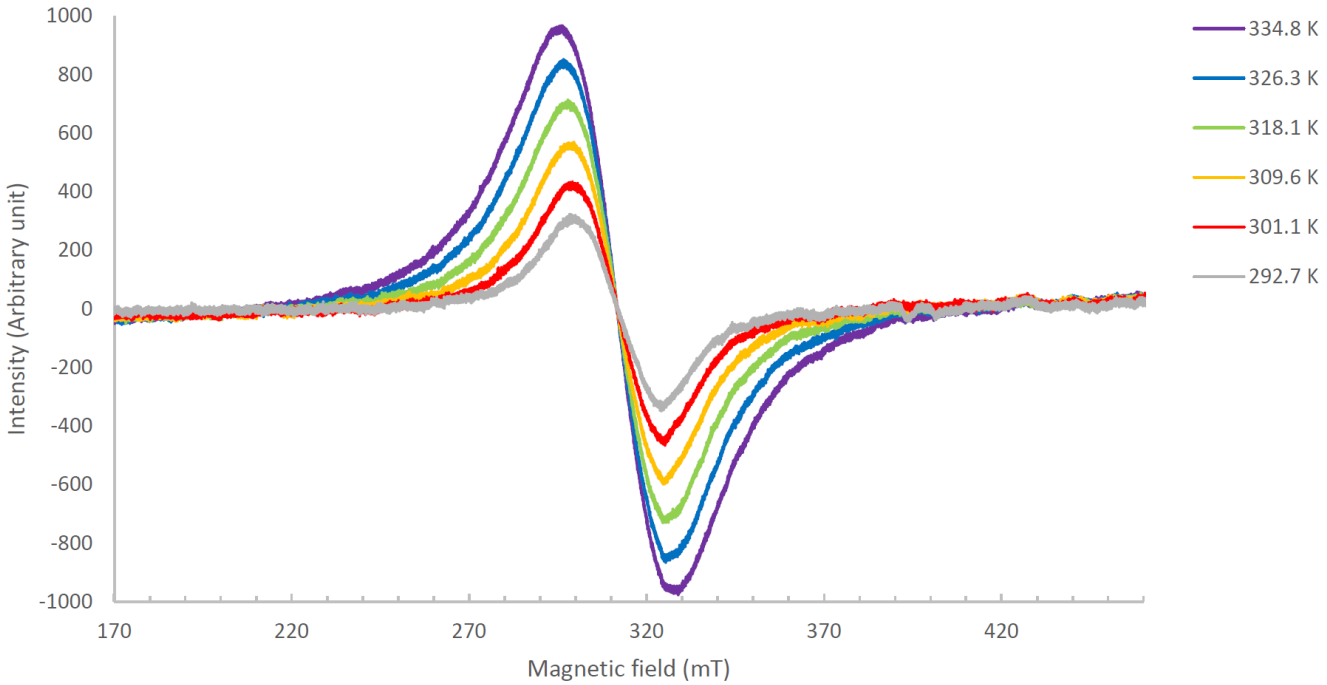

Figure S45 Variable temperature EPR spectra of **2-Mes**.

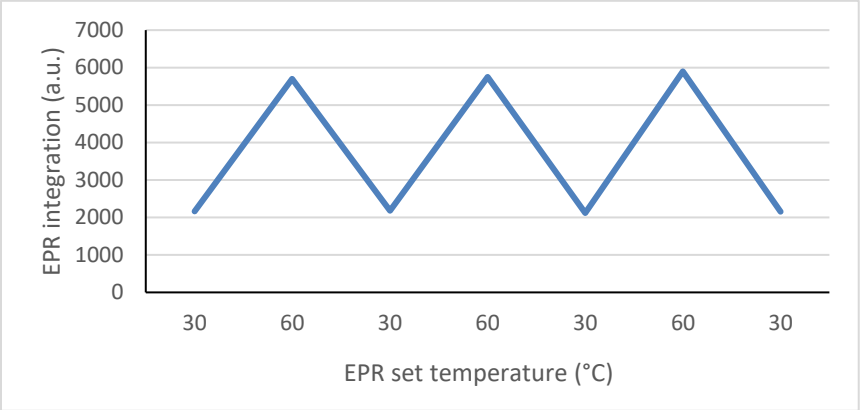

Figure S46 Temperature-dependent reversible formation of **2-Mes*** detected as a change of EPR double integration values.

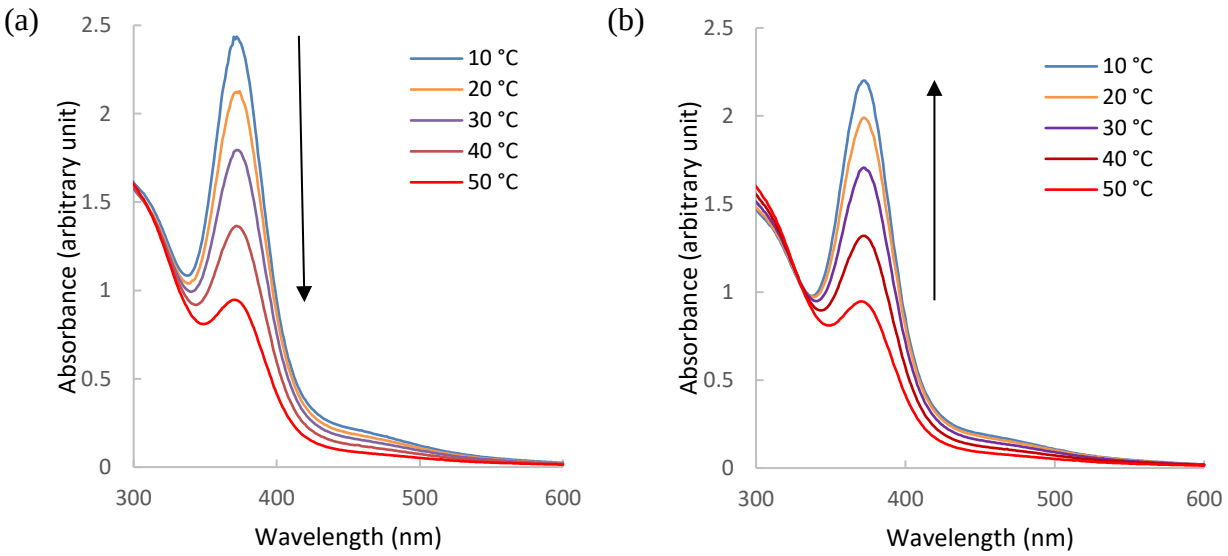

Figure S47 Change of UV-Vis spectra of **2-Mes** in benzene (a) on heating and (b) on cooling.

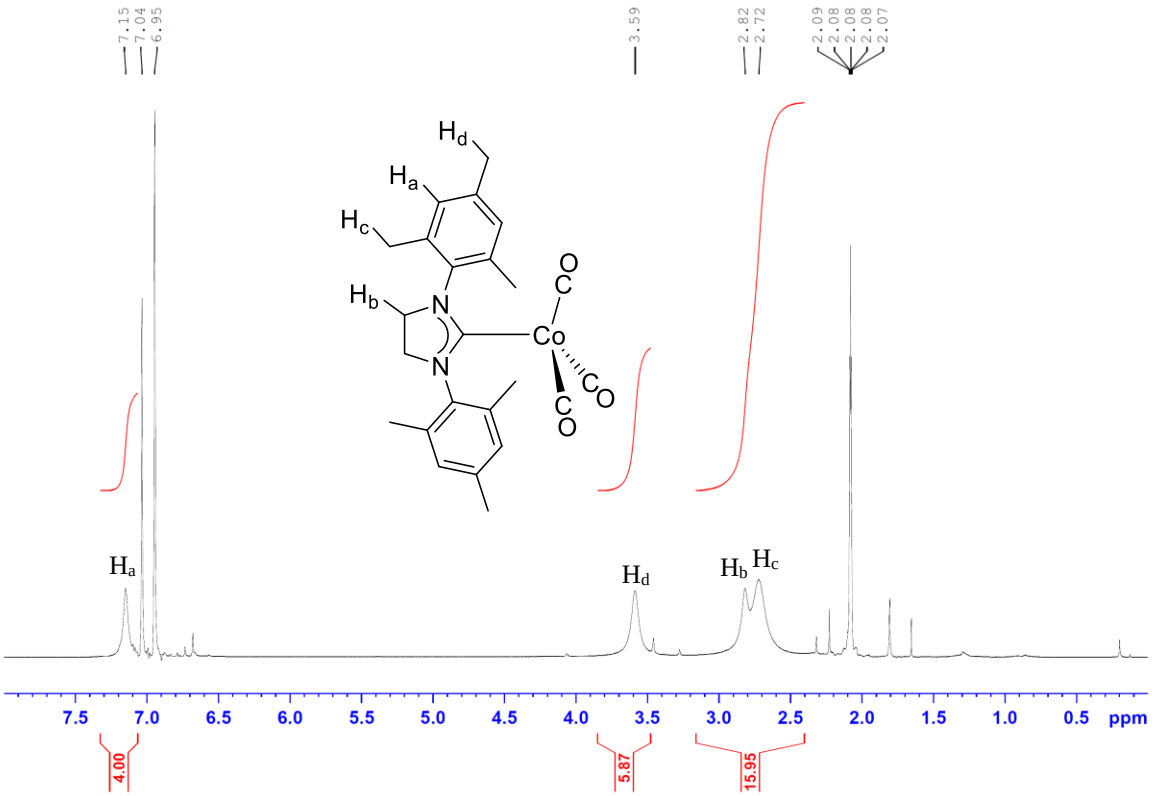

Figure S48 ^{1}H NMR spectra of **2-Mes*** recorded at 137.3 °C (500 MHz, in toluene-d_8 under 5 bar N_2).

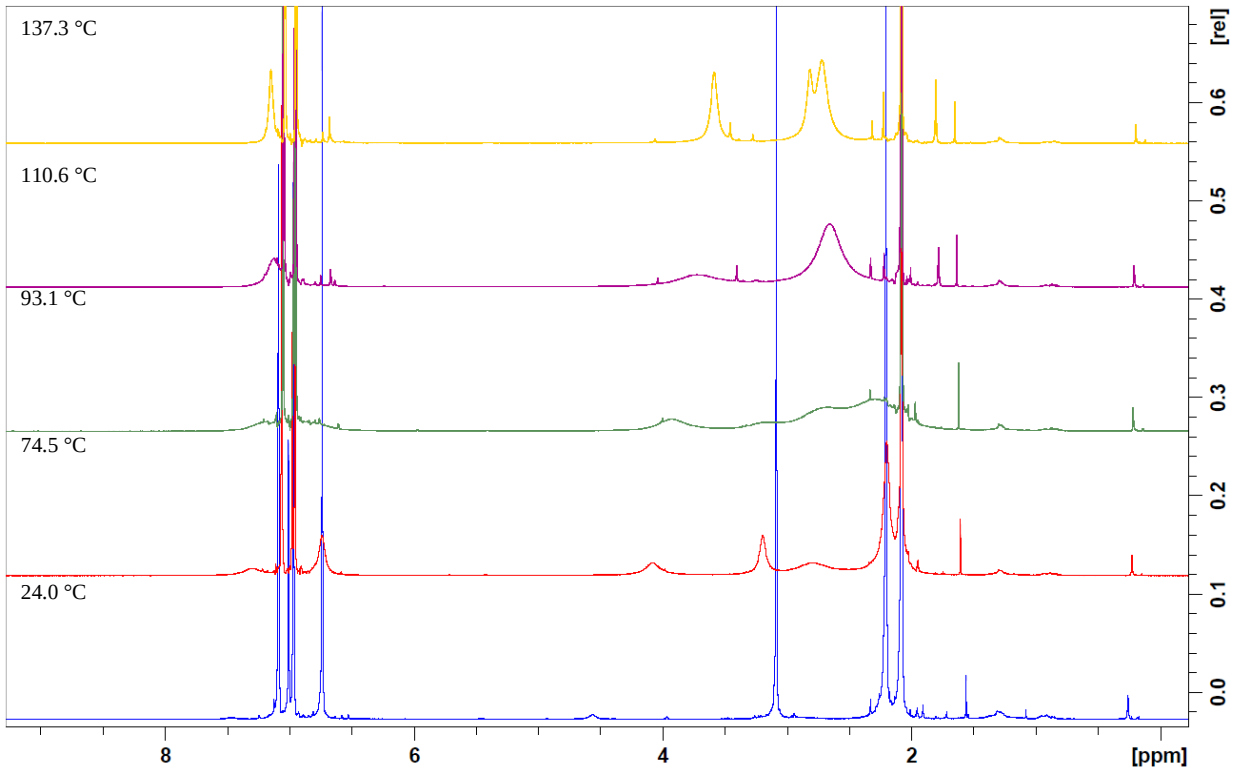

Figure S49 ^{1}H NMR spectra of **2-Mes** recorded at 24.0-137.3 °C (500 MHz, in toluene-d_8 under 5 bar N_2).

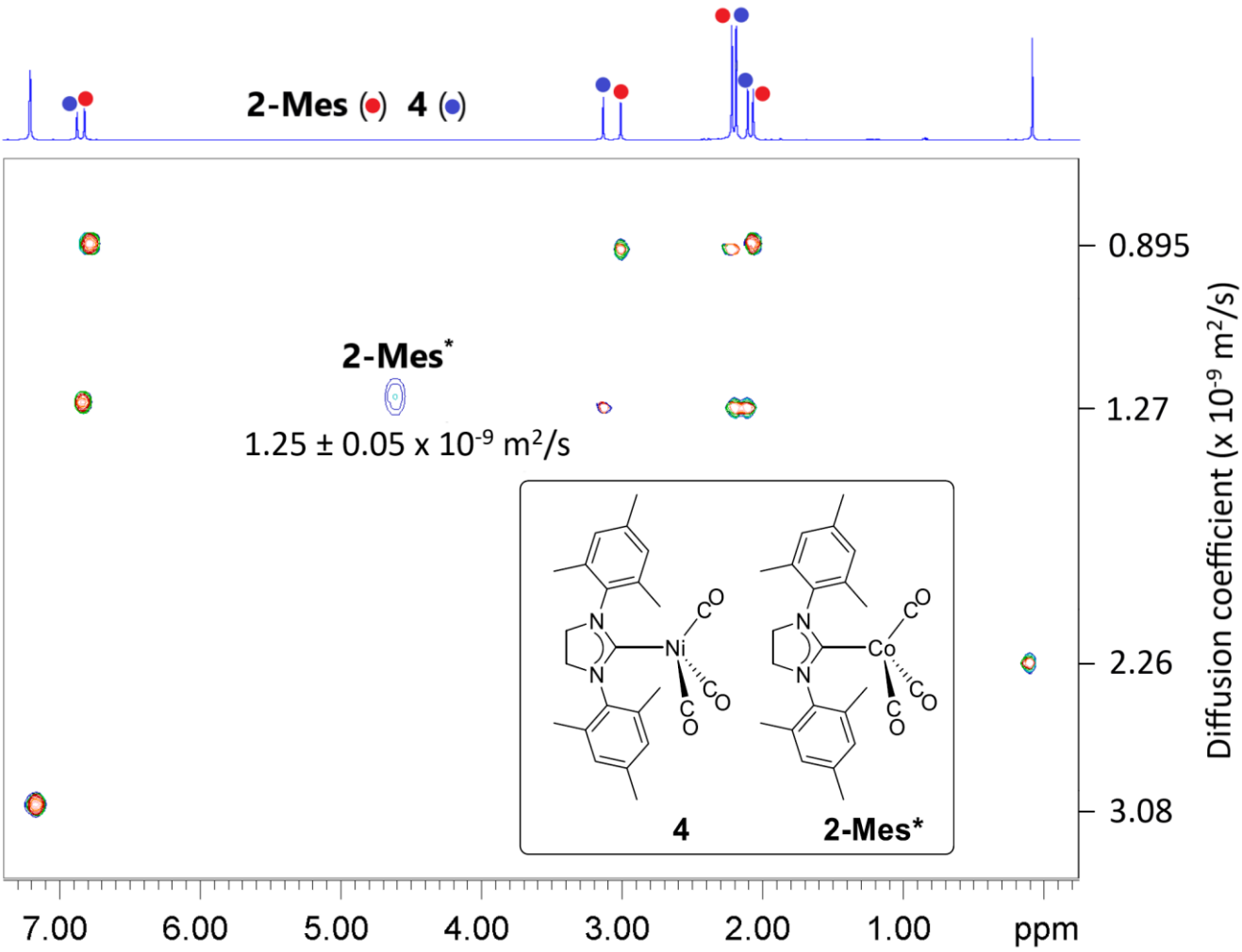

Figure S50 2D DOSY NMR spectrum (500 MHz, in C_6D_6, 24.0 °C) of **2-Mes** and **2-Mes*** in the presence of **4** and $Me_3SiOSiMe_3$ as internal standards.

```
Current Data Parameters
NAME      ST1522 DOSY of [Co(sIMes)(CO)3]2 + Ni(sIMes)(CO)3
EXPNO                 5
PROCNO                1

F2 - Acquisition Parameters
Date_           20210325
Time              15.49 h
INSTRUM           Avance
PROBHD   Z167889_0002 (
PULPROG       ledbpgp2s
TD                16384
SOLVENT            C6D6
NS                   64
DS                    4
SWH             5882.353 Hz
FIDRES          0.718061 Hz
AQ             1.3926400 sec
RG               19.7269
DW                85.000 usec
DE                13.42 usec
TE                298.1 K
D1            3.00000000 sec
D16           0.00020000 sec
D20           0.03000000 sec
D21           0.00500000 sec
TDav                  1
SFO1         500.1325006 MHz
NUC1                 1H
P1                12.30 usec
P2                24.60 usec
PLW1          7.80000019 W
GPNAM[6]        Difftrap
GPZ6              100.00 %
GPNAM[7]     SMSQ10.100
GPZ7              -17.13 %
GPNAM[8]     SMSQ10.100
GPZ8              -13.17 %
P19               600.00 usec
P30              1000.00 usec

F1 - Acquisition parameters
TD                   16
SFO1            500.1325 MHz
FIDRES        625.000000 Hz
SW                 9.997 ppm
FnMODE               QF

F2 - Processing parameters
SI                 8192
SF          500.1300000 MHz
WDW                  EM
SSB                   0
LB                 1.00 Hz
GB                    0
PC                 1.00

F1 - Processing parameters
SI                   16
MC2                  QF
SF          500.1300000 MHz
WDW                  no
SSB                   0
LB                    0 Hz
GB                    0
```

Figure S51 2D DOSY NMR acquisition parameters.

Fitted function:	f (x) = Io * exp (-D * x^2 * gamma^2 * littleDelta^2 (bigDelta-littleDelta/3)* 10^4
used gamma:	26752 rad/(s*Gauss)
used little delta:	0.0020000 s
used big delta:	0.029900 s
used gradient strength:	variable
Random error estimation of data:	RMS per spectrum (or trace/plane)
Systematic error estimation of data:	worst case per peak scenario
Fit parameter Error estimation method:	from fit using arbitray y uncertainties
Confidence level:	95%
Used peaks:	peaks from Z:/nmrsu/.topspin-NMR-DATA/NMRData/OIST/STG/data/ST/nmr/ST1522 DOSY of [Co(sIMes)(CO)3]2 + Ni(sIMes)(CO)3/5/pdata/1/peaklist1D.xml
Used integrals:	peak intensities
Used Gradient strength:	all values (including replicates) used

Peak name	F2 [ppm]	Io	error	D [m2/s]	error	fitInfo
1	7.150	6.38e+07	2.734e+05	3.08e-09	3.121e-11	Done
2	6.820	7.13e+07	2.721e+05	1.27e-09	1.159e-11	Done
3	6.768	9.09e+07	3.165e+05	8.90e-10	7.903e-12	Done
4	4.606	2.02e+05	3678	1.25e-09	5.455e-11	Done
5	3.126	1.29e+08	2.265e+05	1.28e-09	5.408e-12	Done
6	3.004	1.09e+08	2.595e+05	8.93e-10	5.439e-12	Done
7	2.223	3.45e+08	5.764e+05	8.97e-10	3.815e-12	Done
8	2.192	3.34e+08	7.398e+05	1.27e-09	6.748e-12	Done
9	2.112	1.60e+08	3.650e+05	1.27e-09	6.962e-12	Done
10	2.072	1.61e+08	4.695e+05	8.90e-10	6.630e-12	Done
11	0.113	1.55e+08	3.582e+05	2.26e-09	1.230e-11	Done

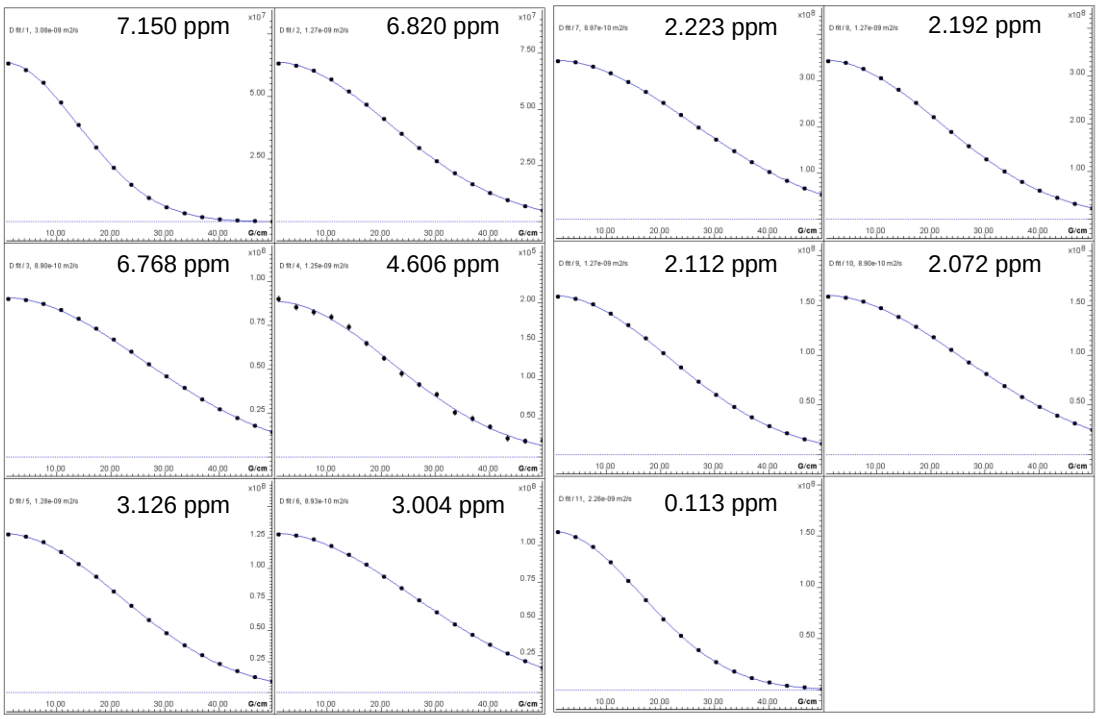

Figure S52 2D DOSY NMR data fitting parameters, non-linear fitting curves, and diffusion coefficient (D) for 11 peaks in Figure S50.

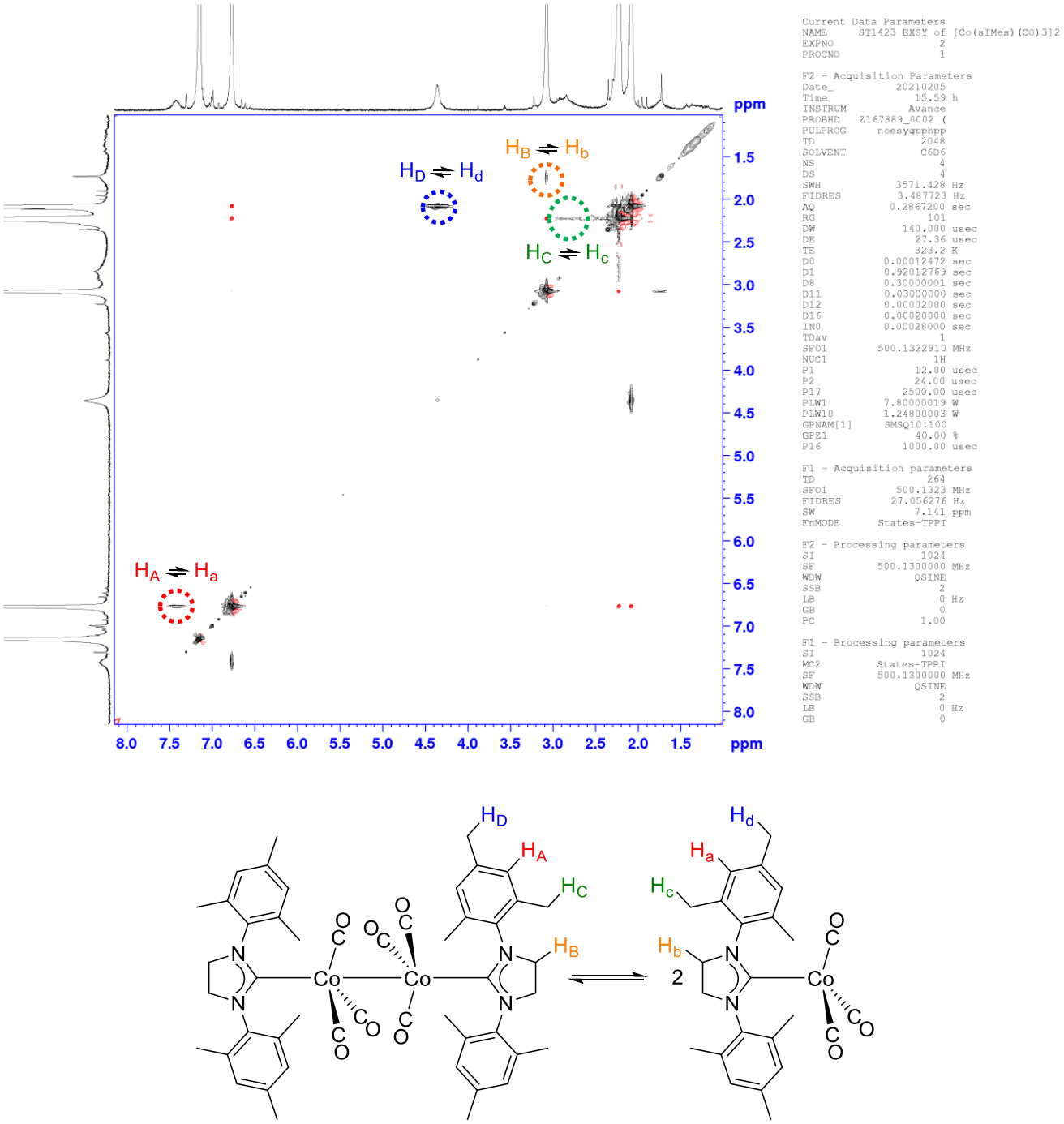

Figure S53 2D EXSY NMR spectra of **2-Mes** (500 MHz, in C_6D_6, 323 K). Red contours: NOE signals, black contour: exchange signals.

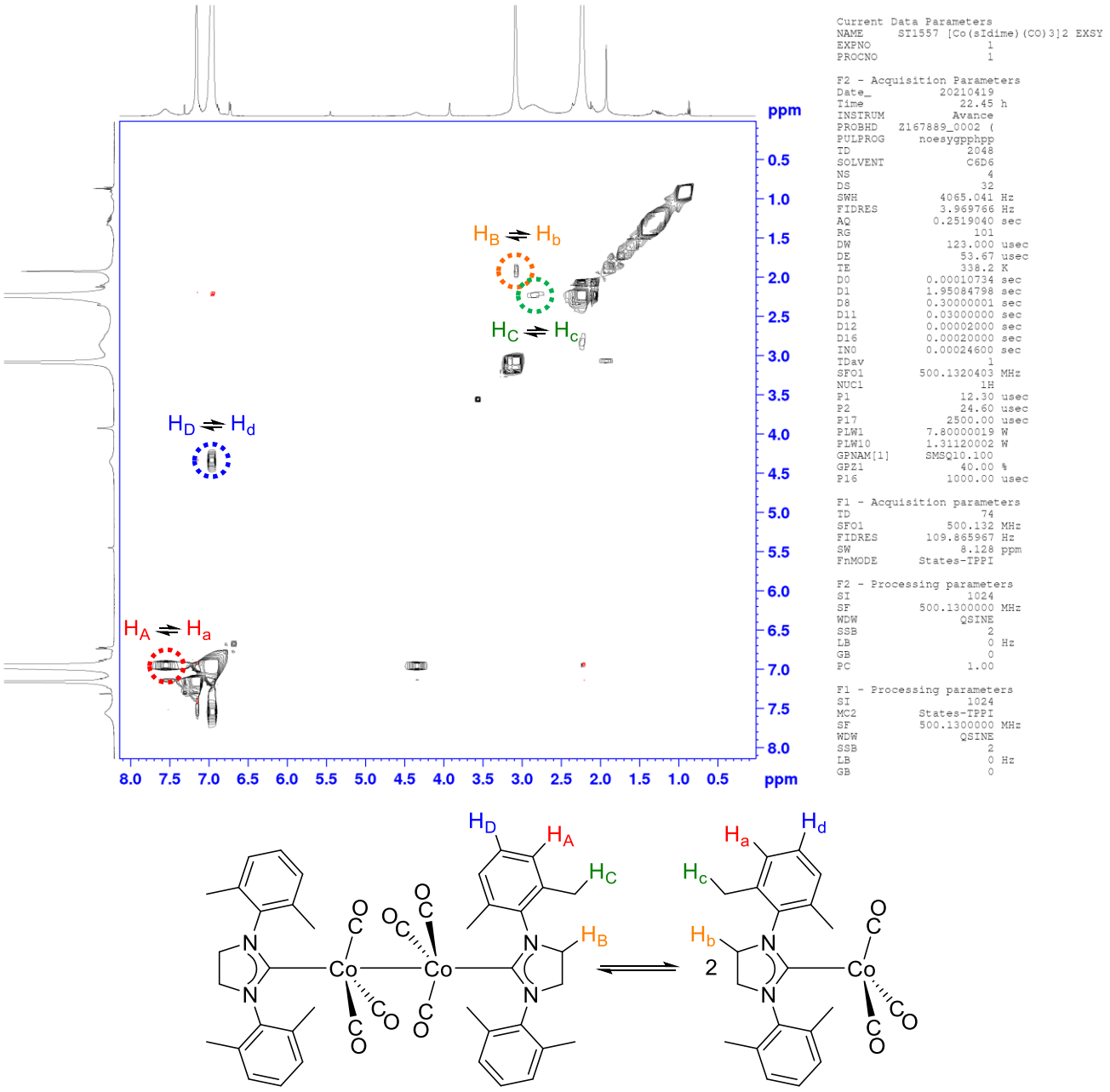


```
Current Data Parameters
NAME      ST1557 [Co(sIdime)(CO)3]2 EXSY
EXPNO                 1
PROCNO                1

F2 - Acquisition Parameters
Date_          20210419
Time              22.45 h
INSTRUM           Avance
PROBHD    Z167889_0002 (
PULPROG     noesygpphpp
TD                 2048
SOLVENT            C6D6
NS                    4
DS                   32
SWH           4065.041 Hz
FIDRES        3.969766 Hz
AQ            0.2519040 sec
RG                  101
DW              123.000 usec
DE               53.67 usec
TE               338.2 K
D0            0.00010734 sec
D1            1.95084798 sec
D8            0.30000001 sec
D11           0.03000000 sec
D12           0.00002000 sec
D16           0.00020000 sec
IN0           0.00024600 sec
TDav                  1
SFO1         500.1320403 MHz
NUC1                 1H
P1                12.30 usec
P2                24.60 usec
P17            2500.00 usec
PLW1          7.80000019 W
PLW10         1.31120002 W
GPNAM[1]      SMSQ10.100
GPZ1             40.00 %
P16            1000.00 usec

F1 - Acquisition parameters
TD                   74
SFO1            500.132 MHz
FIDRES        109.865967 Hz
SW                8.128 ppm
FnMODE       States-TPPI

F2 - Processing parameters
SI                 1024
SF           500.1300000 MHz
WDW                QSINE
SSB                   2
LB                    0 Hz
GB                    0
PC                 1.00

F1 - Processing parameters
SI                 1024
MC2          States-TPPI
SF           500.1300000 MHz
WDW                QSINE
SSB                   2
LB                    0 Hz
GB                    0
```

Figure S54 2D EXSY NMR spectra of **2-Me** (500 MHz, in C_6D_6, 338 K). Red contours: NOE signals, black contour: exchange signals.

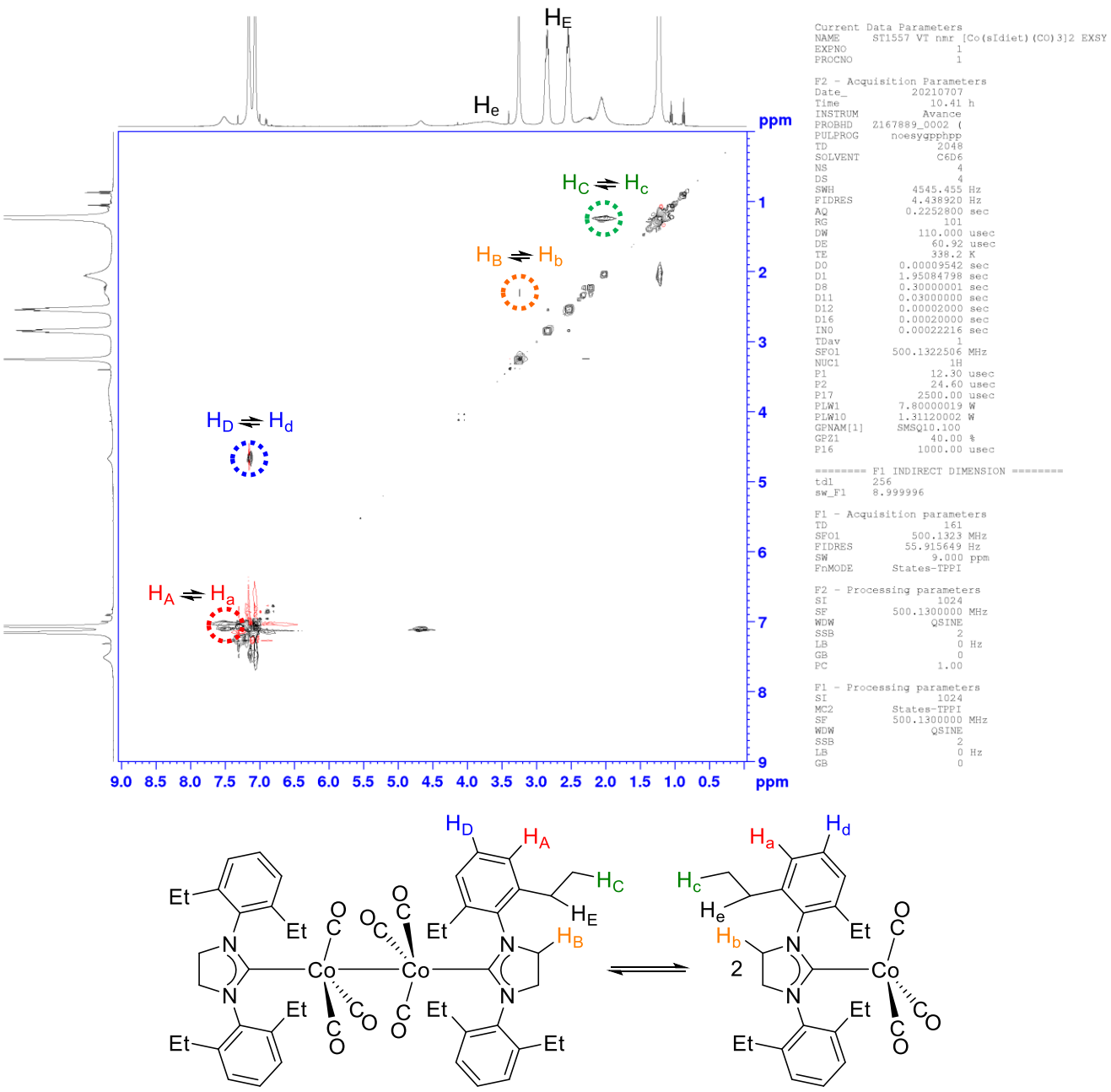

Figure S55 2D EXSY NMR spectra of **2-Et** (500 MHz, in C_6D_6, 338 K). Red contours: NOE signals, black contour: exchange signals. The exchange between H_E and H_e was not detectable due to the broadening of H_e.

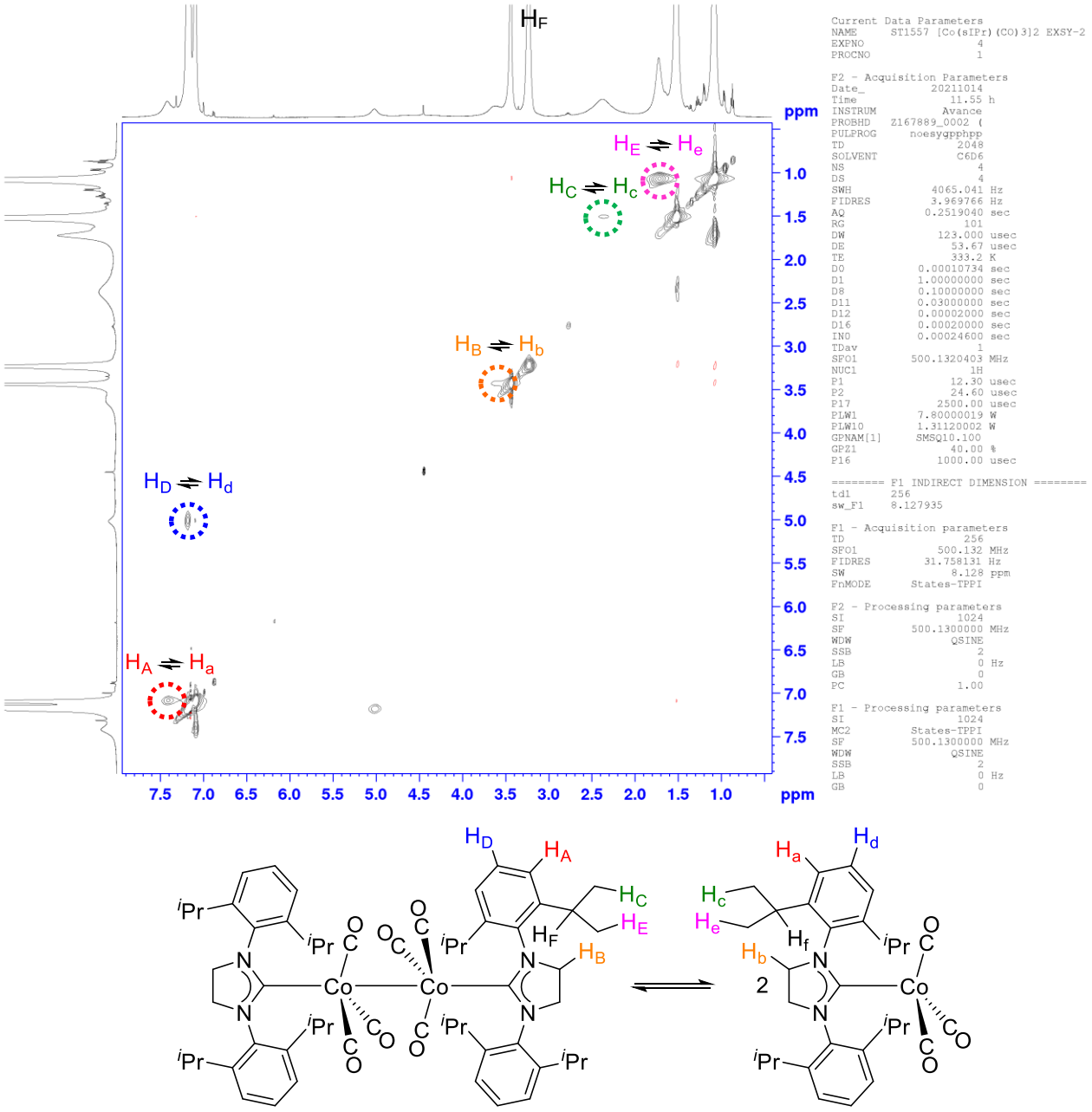

Figure S56 2D EXSY NMR spectra of **2-^{i}Pr** (500 MHz, in C_6D_6, 333 K). Red contours: NOE signals, black contour: exchange signals. H_f was not detectable due to its proximity to the paramagnetic Co center.

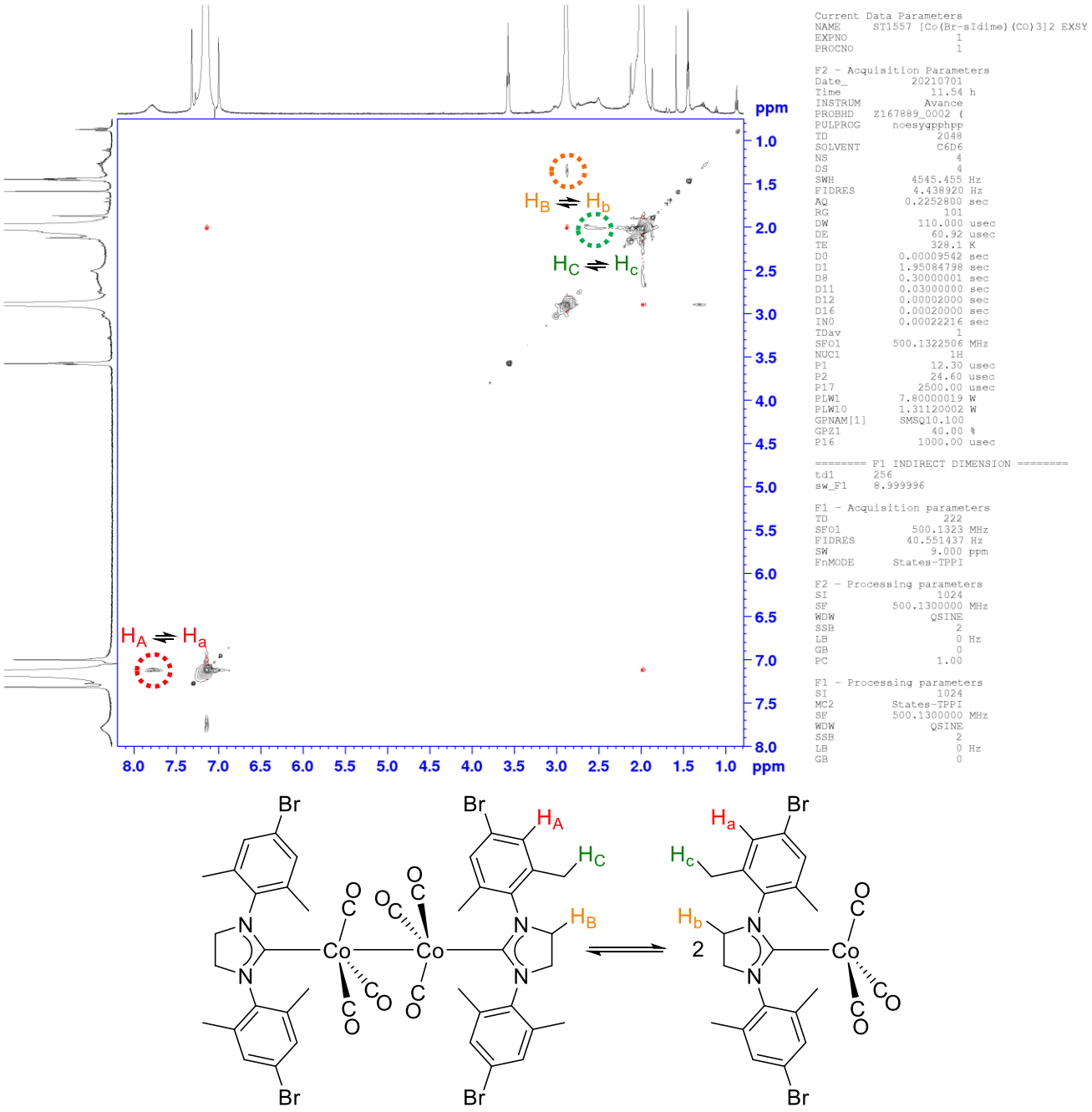

Figure S57 2D EXSY NMR spectra of **2-Br** (500 MHz, in C_6D_6, 328 K). Red contours: NOE signals, black contour: exchange signals.

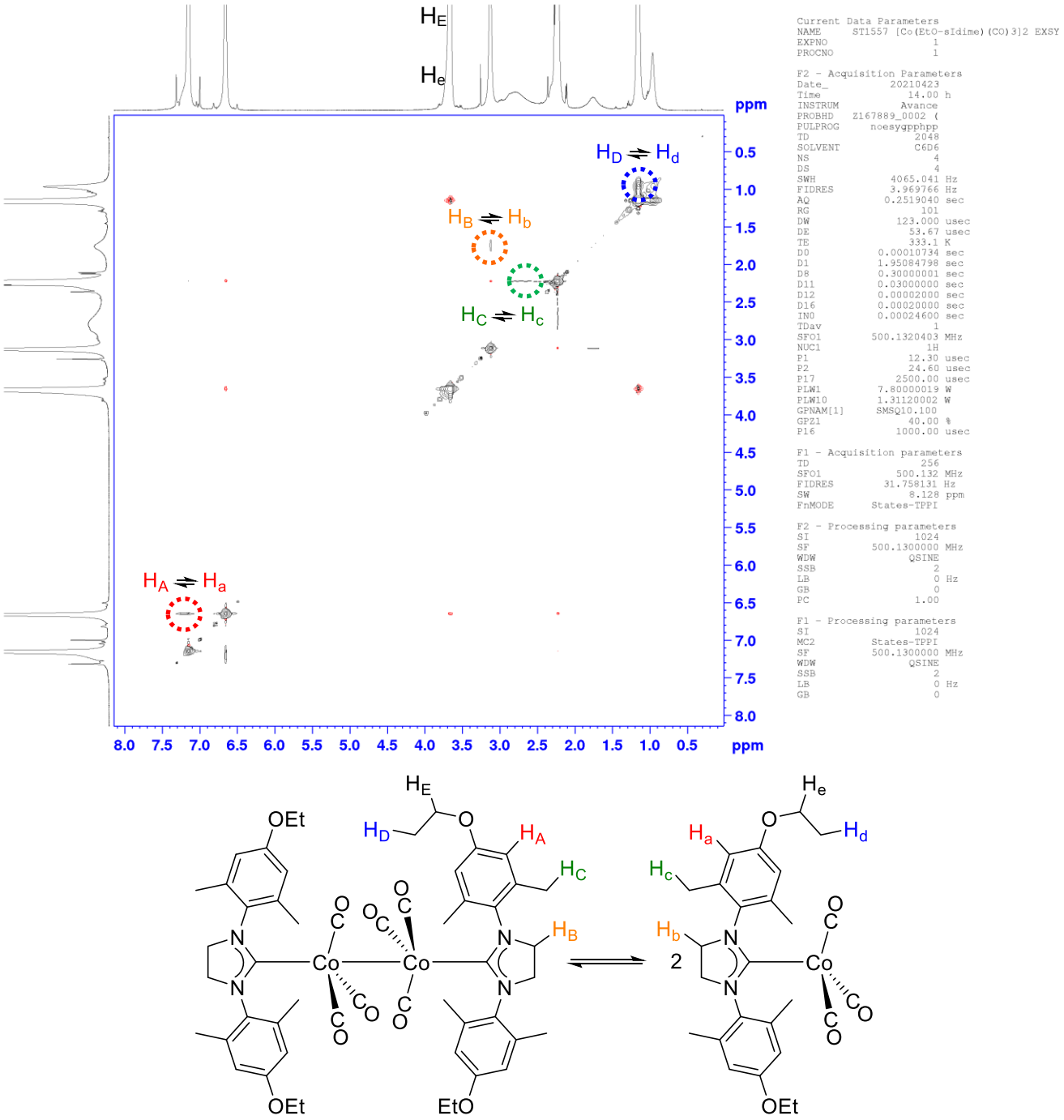

Figure S58 2D EXSY NMR spectra of **2-OEt** (500 MHz, in C_6D_6, 333 K). Red contours: NOE signals, black contour: exchange signals. The exchange between H_E and H_e was not detectable due to the overlapping of ^{1}H NMR signals from H_E and H_e at 333K.

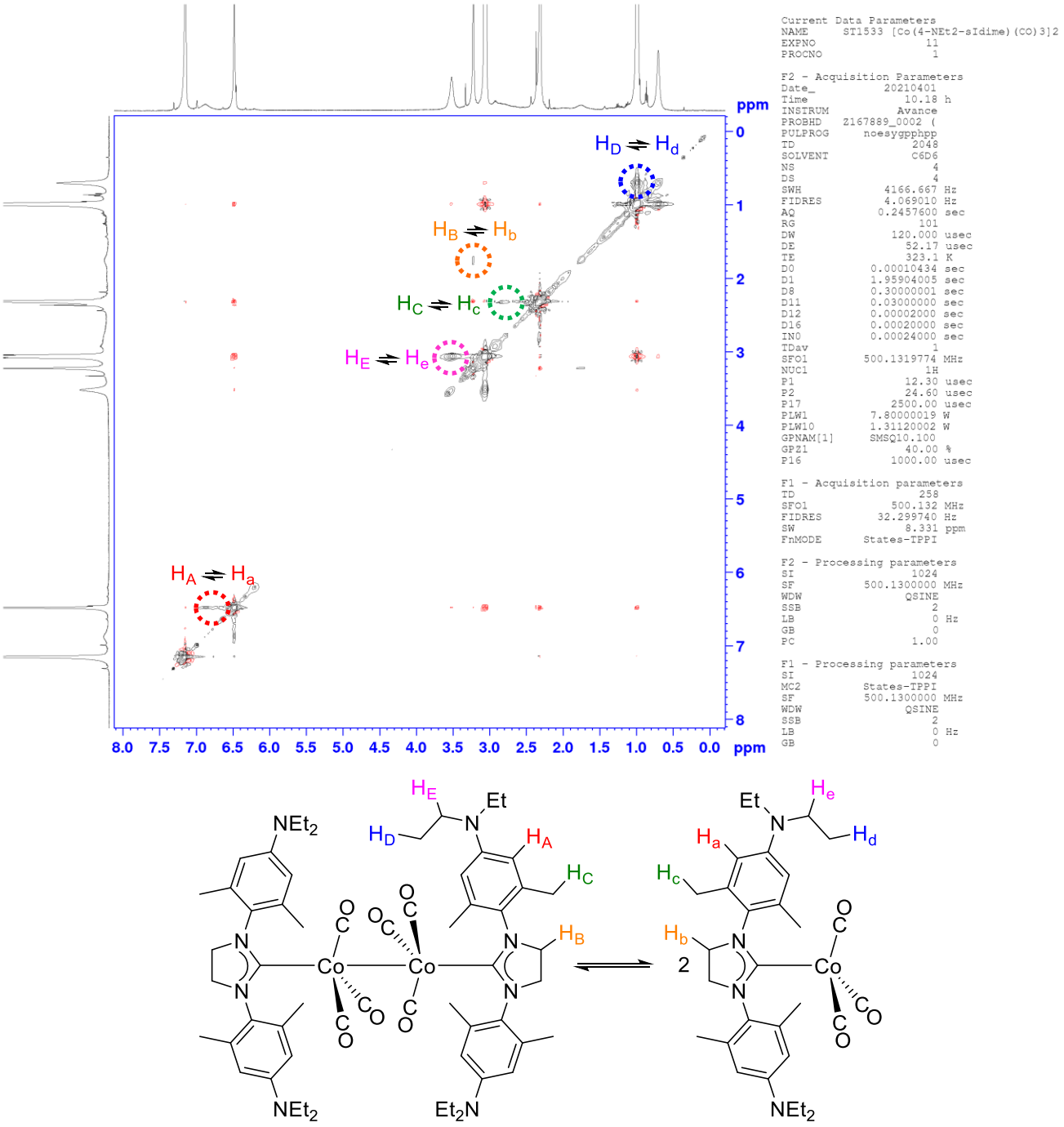

Figure S59 2D EXSY NMR spectra of **2-NEt$_2$** (500 MHz, in C_6D_6, 323 K). Red contours: NOE signals, black contour: exchange signals. The exchange between H_E and H_e was not detectable due to the overlapping of ^{1}H NMR signals from H_E and H_e at 333K.

7. Single-crystal XRD studies

The X-ray diffraction experiments for **2-Br**, **2-Et**, **2-^{i}Pr**, **2-Me**, **2-Mes**, **2-NEt$_2$**, and **2-OEt** were performed on a Bruker D8 Venture diffractometer equipped with a PHOTON II CPAD detector, an IμS 3.0 microfocus X-ray source (Mo *K*α radiation), and an Oxford Cryostream LT device. The data were collected according to recommended strategies in a φ/ω-scan mode at 100(2) K. Final cell constants were determined by the global refinement of reflections from the complete data set. Images were indexed and integrated using the *APEX*3 data reduction package. Data were corrected for systematic errors and absorption by means of SADABS-2016/2: Numerical absorption correction based on a multifaceted crystal model and empirical absorption correction based on spherical harmonics according to the point group symmetry using equivalent reflections. *XPREP*-2014/2 and the *ASSIGN SPACEGROUP* routine of the *WinGX* suite were used for the analysis of systematic absences and space-group determination.

The X-ray diffraction data for the single crystal **3** were collected on a Rigaku XtaLab PRO instrument in an ω-scan mode with a PILATUS3 R 200K hybrid pixel array detector and MicroMax^{TM}-003 microfocus X-ray tubes using a Cu Kα radiation at 93(2) K. Images were indexed and integrated using the *CrysAlis*^{Pro} data reduction package. Data were corrected for systematic errors and absorption using the *ABSPACK* module: Numerical absorption correction based on Gaussian integration over a multifaceted crystal model and empirical absorption correction based on spherical harmonics according to the point group symmetry using equivalent reflections. The *GRAL* module and the ASSIGN SPACEGROUP routine of the *WinGX* suite were used for the analysis of systematic absences and space-group determination.

All structures were solved by intrinsic phasing approach using *SHELXT*-2018/2[14] and refined by the full-matrix least-squares on F^2 using *SHELXL*-2018/3.[15] Calculations were mainly performed using the *WinGX*-2020.3 suite of programs[16]. Non-hydrogen atoms were refined anisotropically. The positions of the hydrogen atoms of methyl groups were found using rotating group refinement with idealized tetrahedral angles. The other hydrogen atoms were inserted at the calculated positions and refined as riding atoms. The disorder, if present, was resolved using free variables and reasonable restraints on geometry and anisotropic displacement parameters.

Deposition Numbers 2165654-2165661 contain the supplementary crystallographic data for this paper. These data are provided free of charge by the joint Cambridge Crystallographic Data Centre and Fachinformationszentrum Karlsruhe Access Structures service www.ccdc.cam.ac.uk/structures.

Table S3. Methods used to prepare crystals for SC-XRD study

Complex	Method
2-Br	Diffusion of pentane to a benzene/THF solution
2-Et	Diffusion of pentane to a benzene solution
2-^{i}Pr	Slow cooling of hot benzene solution to room temperature
2-Me	Diffusion of pentane to a benzene solution
2-Mes	Slow cooling of hot benzene solution to room temperature
2-NEt$_2$	Diffusion of pentane to a benzene solution
2-OEt	Diffusion of pentane to a benzene solution
3	Cooling of concentrated pentane solution to –35 °C

Crystallographic data for **2-Br**.

$C_{44}H_{40}Br_4Co_2N_4O_6$, brown prism (0.359 × 0.257 × 0.170 mm^3), formula weight 1158.30 g mol^{-1}; triclinic, $P\overline{1}$ (No. 2), a = 9.4017(4) Å, b = 10.5681(5) Å, c = 12.6960(6) Å, α = 66.4289(10)°, β = 77.1738(11)°, γ = 84.9305(11)°, V = 1127.35(9) Å^3, Z = 1, Z' = 0.5, T = 100(2) K, d_{calc} = 1.706 g cm^{-3}, μ(Mo Kα) = 4.331 mm^{-1}, F(000) = 574; $T_{max/min}$ = 0.2168/0.1074; 73279 reflections were collected (2.551° ≤ θ ≤ 36.751°, index ranges: –15 ≤ h ≤ 15, –17 ≤ k ≤ 17, –21 ≤ l ≤ 21), 10272 of which were unique, R_{int} = 0.0283, $R_σ$ = 0.0192; completeness to θ of 36.751° 91.1 %. The refinement of 275 parameters with no restraints converged to R1 = 0.0291 and wR2 = 0.0718 for 9006 reflections with $I > 2σ(I)$ and R1 = 0.0357 and wR2 = 0.0749 for all data with goodness-of-fit S = 1.030 and residual electron density; $ρ_{max/min}$ = 1.746 and –1.223 e Å^{-3}, rms 0.079; max shift/e.s.d. in the last cycle 0.002.

Crystallographic data for **2-Et**.

$C_{52}H_{60}Co_2N_4O_6$, orange prism (0.147 × 0.109 × 0.057 mm^3), formula weight 954.90 g mol^{-1}; triclinic, $P\overline{1}$ (No. 2), a = 11.1341(4) Å, b = 13.1609(4) Å, c = 17.4589(6) Å, α = 81.6740(9)°, β = 71.6133(9)°, γ = 84.1723(9)°, V = 2397.89(14) Å^3, Z = 2, Z' = 0.5 + 0.5, T = 100(2) K, d_{calc} = 1.323 g cm^{-3}, μ(Mo Kα) = 0.745 mm^{-1}, F(000) = 1004; $T_{max/min}$ = 0.9315/0.8357; 157918 reflections were collected (1.567° ≤ θ ≤ 28.280°, index ranges: –14 ≤ h ≤ 14, –17 ≤ k ≤ 17, –23 ≤ l ≤ 23), 11897 of which were unique, R_{int} = 0.0497, $R_σ$ = 0.0225; completeness to θ of 28.280° 99.9 %. The refinement of 585 parameters with no restraints converged to R1 = 0.0340 and wR2 = 0.0749 for 9098 reflections with $I > 2σ(I)$ and R1 = 0.0536 and wR2 = 0.0863 for all data with goodness-of-fit S = 1.046 and residual electron density; $ρ_{max/min}$ = 0.454 and –0.329 e Å^{-3}, rms 0.058; max shift/e.s.d. in the last cycle 0.002.

Crystallographic data for **2-^{i}Pr**.

$C_{60}H_{76}Co_2N_4O_6 \times 4(C_6H_6)$, dark orange prism (0.534 × 0.312 × 0.150 mm^3), formula weight 1379.53 g mol^{-1}; triclinic, $P\overline{1}$ (No. 2), a = 11.1838(5) Å, b = 12.1674(6) Å, c = 15.6011(8) Å, α = 72.164(2)°, β =

70.4512(18)°, γ = 89.2308(19)°, V = 1895.03(16) Å^3, Z = 1, Z' = 0.5, T = 100(2) K, d_{calc} = 1.209 g cm^{-3}, μ(Mo $K\alpha$) = 0.492 mm^{-1}, F(000) = 734; $T_{max/min}$ = 0.9000/0.7307; 144988 reflections were collected (2.467° ≤ θ ≤ 31.521°, index ranges: –16 ≤ h ≤ 16, –17 ≤ k ≤ 17, –22 ≤ l ≤ 22), 12609 of which were unique, R_{int} = 0.0626, R_σ = 0.0291; completeness to θ of 31.521° 99.8 %. The refinement of 551 parameters with 444 restraints converged to $R1$ = 0.0321 and $wR2$ = 0.0751 for 10784 reflections with $I > 2\sigma(I)$ and $R1$ = 0.0417 and $wR2$ = 0.0798 for all data with goodness-of-fit S = 1.031 and residual electron density; $\rho_{max/min}$ = 0.518 and –0.463 e Å^{-3}, rms 0.057; max shift/e.s.d. in the last cycle 0.003.

Crystallographic data for **2-Me**.

$C_{44}H_{44}Co_2N_4O_6 \times 4(C_6H_6)$, brown prism (0.279 × 0.194 × 0.064 mm^3), formula weight 1155.12 g mol^{-1}; orthorhombic, *Pbca* (No. 61), a = 10.9817(4) Å, b = 17.1391(6) Å, c = 31.4588(11) Å, V = 5921.1(4) Å^3, Z = 4, Z' = 0.5, T = 100(2) K, d_{calc} = 1.296 g cm^{-3}, μ(Mo $K\alpha$) = 0.616 mm^{-1}, F(000) = 2424; $T_{max/min}$ = 0.9434/0.7757; 89048 reflections were collected (2.262° ≤ θ ≤ 27.103°, index ranges: –14 ≤ h ≤ 14, –21 ≤ k ≤ 21, –40 ≤ l ≤ 40), 6516 of which were unique, R_{int} = 0.0541, R_σ = 0.0246; completeness to θ of 27.103° 99.9 %. The refinement of 420 parameters with 222 restraints converged to $R1$ = 0.0431 and $wR2$ = 0.1051 for 5371 reflections with $I > 2\sigma(I)$ and $R1$ = 0.0564 and $wR2$ = 0.1125 for all data with goodness-of-fit S = 1.109 and residual electron density; $\rho_{max/min}$ = 0.548 and –0.453 e Å^{-3}, rms 0.065; max shift/e.s.d. in the last cycle 0.002.

Crystallographic data for **2-Mes**.

$C_{48}H_{52}Co_2N_4O_6 \times C_6H_6$, dark orange prism (0.189 × 0.131 × 0.129 mm^3), formula weight 976.90 g mol^{-1}; monoclinic, $P2_1/c$ (No. 14), a = 13.5589(3) Å, b = 35.2233(10) Å, c = 16.1183(5) Å, β = 105.0699(10)°, V = 7433.2(4) Å^3, Z = 6, Z' = 1.5, T = 100(2) K, d_{calc} = 1.309 g cm^{-3}, μ(Mo $K\alpha$) = 0.722 mm^{-1}, F(000) = 3072; $T_{max/min}$ = 0.8827/0.7889; 477535 reflections were collected (2.313° ≤ θ ≤ 34.370°, index ranges: –21 ≤ h ≤ 17, –55 ≤ k ≤ 55, –25 ≤ l ≤ 25), 31156 of which were unique, R_{int} = 0.0475, R_σ = 0.0201; completeness to θ of 34.370° 99.8 %. The refinement of 910 parameters with no restraints converged to $R1$ = 0.0326 and $wR2$ = 0.0831 for 25404 reflections with $I > 2\sigma(I)$ and $R1$ = 0.0460 and $wR2$ = 0.0914 for all data with goodness-of-fit S = 1.057 and residual electron density; $\rho_{max/min}$ = 0.693 and –0.566 e Å^{-3}, rms 0.062; max shift/e.s.d. in the last cycle 0.004.

Crystallographic data for **2-NEt$_2$**.

$C_{60}H_{80}Co_2N_8O_6$, dark orange prism (0.330 × 0.284 × 0.128 mm^3), formula weight 1127.18 g mol^{-1}; triclinic, $P\bar{1}$ (No. 2), a = 13.2692(3) Å, b = 15.2605(4) Å, c = 16.5352(4) Å, α = 77.6834(4)°, β =

76.0242(5)°, γ = 66.2040(4)°, V = 2947.53(12) Å^3, Z = 2, Z' = 1, T = 100(2) K, d_{calc} = 1.270 g cm^{-3}, μ(Mo Kα) = 0.618 mm^{-1}, F(000) = 1196; $T_{max/min}$ = 0.8890/0.7584; 383090 reflections were collected (1.945° ≤ θ ≤ 37.035°, index ranges: –22 ≤ h ≤ 22, –25 ≤ k ≤ 25, –27 ≤ l ≤ 28), 29806 of which were unique, R_{int} = 0.0439, $R_σ$ = 0.0259; completeness to θ of 37.035° 99.1 %. The refinement of 822 parameters with 747 restraints converged to R1 = 0.0433 and wR2 = 0.1086 for 25212 reflections with I > 2σ(I) and R1 = 0.0528 and wR2 = 0.1133 for all data with goodness-of-fit S = 1.080 and residual electron density; $ρ_{max/min}$ = 0.996 and –0.911 e Å^{-3}, rms 0.079; max shift/e.s.d. in the last cycle 0.002.

Crystallographic data for **2-OEt**.

$C_{52}H_{60}Co_2N_4O_{10}$ × C_5H_{12}, dark orange prism (0.290 × 0.276 × 0.228 mm^3), formula weight 1091.04 g mol^{-1}; monoclinic, $P2_1/c$ (No. 14), a = 14.3182(3) Å, b = 12.0109(3) Å, c = 15.9104(4) Å, β = 97.5070(7)°, V = 2712.73(11) Å^3, Z = 2, Z' = 0.5, T = 100(2) K, d_{calc} = 1.336 g cm^{-3}, μ(Mo Kα) = 0.673 mm^{-1}, F(000) = 1152; $T_{max/min}$ = 0.7922/0.6658; 134219 reflections were collected (2.131° ≤ θ ≤ 34.337°, index ranges: –20 ≤ h ≤ 22, –18 ≤ k ≤ 19, –24 ≤ l ≤ 25), 11333 of which were unique, R_{int} = 0.0455, $R_σ$ = 0.0231; completeness to θ of 34.337° 99.8 %. The refinement of 360 parameters with 59 restraints converged to R1 = 0.0501 and wR2 = 0.1358 for 9676 reflections with I > 2σ(I) and R1 = 0.0581 and wR2 = 0.1419 for all data with goodness-of-fit S = 1.070 and residual electron density; $ρ_{max/min}$ = 2.175 and –0.747 e Å^{-3}, rms 0.109; max shift/e.s.d. in the last cycle 0.002.

Crystallographic data for **3**.

$C_{31}H_{44}CoN_3O_2$, dark red prism (0.185 × 0.157 × 0.044 mm^3), formula weight 549.62 g mol^{-1}; monoclinic, $P2_1/c$ (No. 14), a = 11.59303(7) Å, b = 11.77994(6) Å, c = 21.25835(12) Å, β = 91.1883(5)°, V = 2902.53(3) Å^3, Z = 4, Z' = 1, T = 93(2) K, d_{calc} = 1.258 g cm^{-3}, μ(Cu Kα) = 4.871 mm^{-1}, F(000) = 1176; $T_{max/min}$ = 1.000/0.370; 58408 reflections were collected (3.814° ≤ θ ≤ 75.900°, index ranges: –14 ≤ h ≤ 14, –14 ≤ k ≤ 14, –26 ≤ l ≤ 26), 6029 of which were unique, R_{int} = 0.0489, $R_σ$ = 0.0232; completeness to θ of 75.900° 99.6 %. The refinement of 344 parameters with no restraints converged to R1 = 0.0307 and wR2 = 0.0855 for 5773 reflections with I > 2σ(I) and R1 = 0.0319 and wR2 = 0.0863 for all data with goodness-of-fit S = 1.085 and residual electron density; $ρ_{max/min}$ = 0.296 and –0.400 e Å^{-3}, rms 0.045; max shift/e.s.d. in the last cycle 0.002.

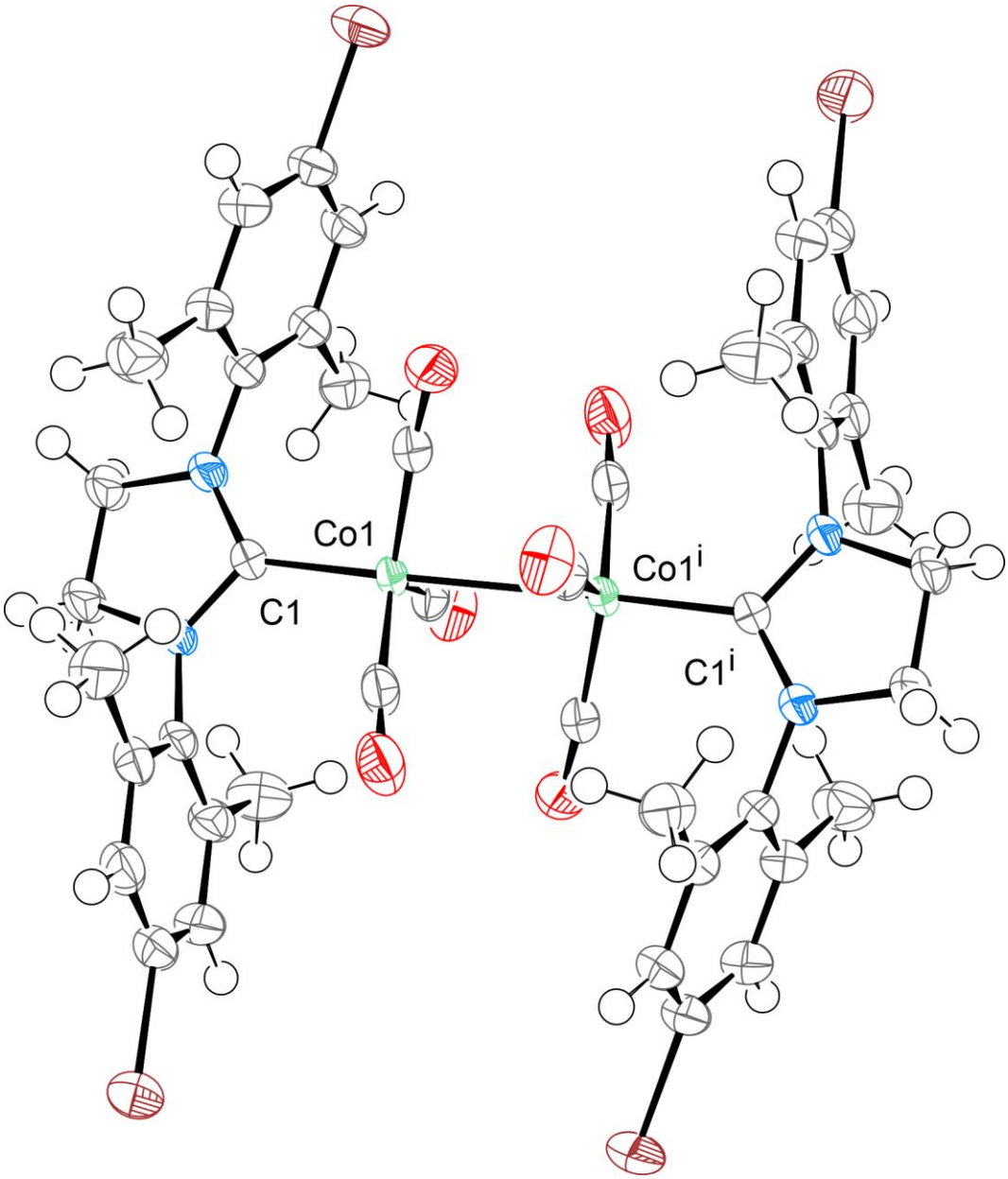

Figure S60. ORTEP of **2-Br** at 80 % probability level for non-hydrogen atoms according to single crystal X-ray diffraction data. Selected interatomic distances [Å]: Co1–C1 1.9392(11), Co1–Co1^{i} 2.7153(3).

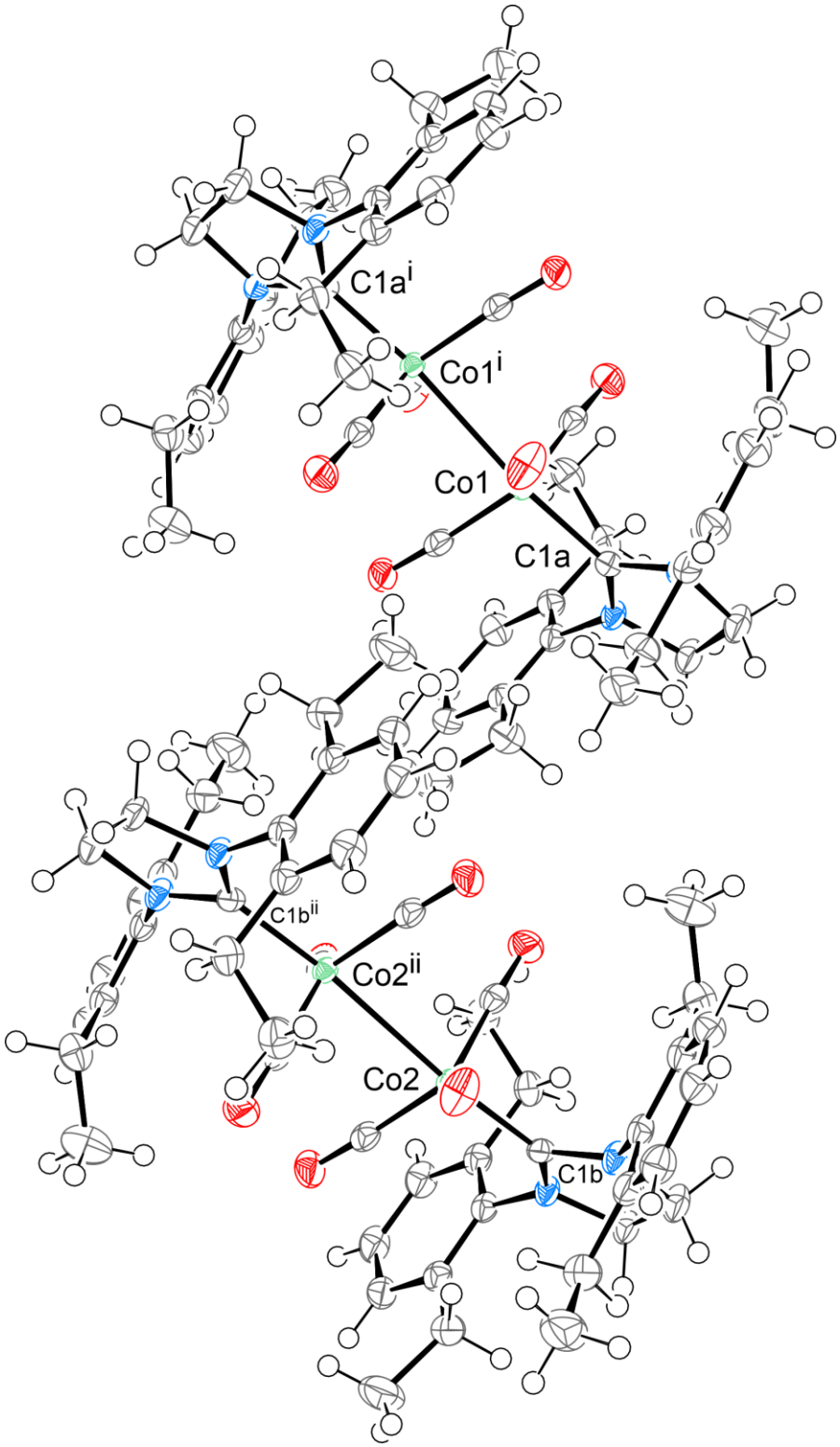

Figure S61. ORTEP of **2-Et** at 60 % probability level for non-hydrogen atoms according to single crystal X-ray diffraction data. Selected interatomic distances [Å]: Co1–C1a 1.9462(16), Co1–Co1^{i} 2.7461(4), Co2–C1b 1.9499(16), Co2–Co2^{ii} 2.7492(4).

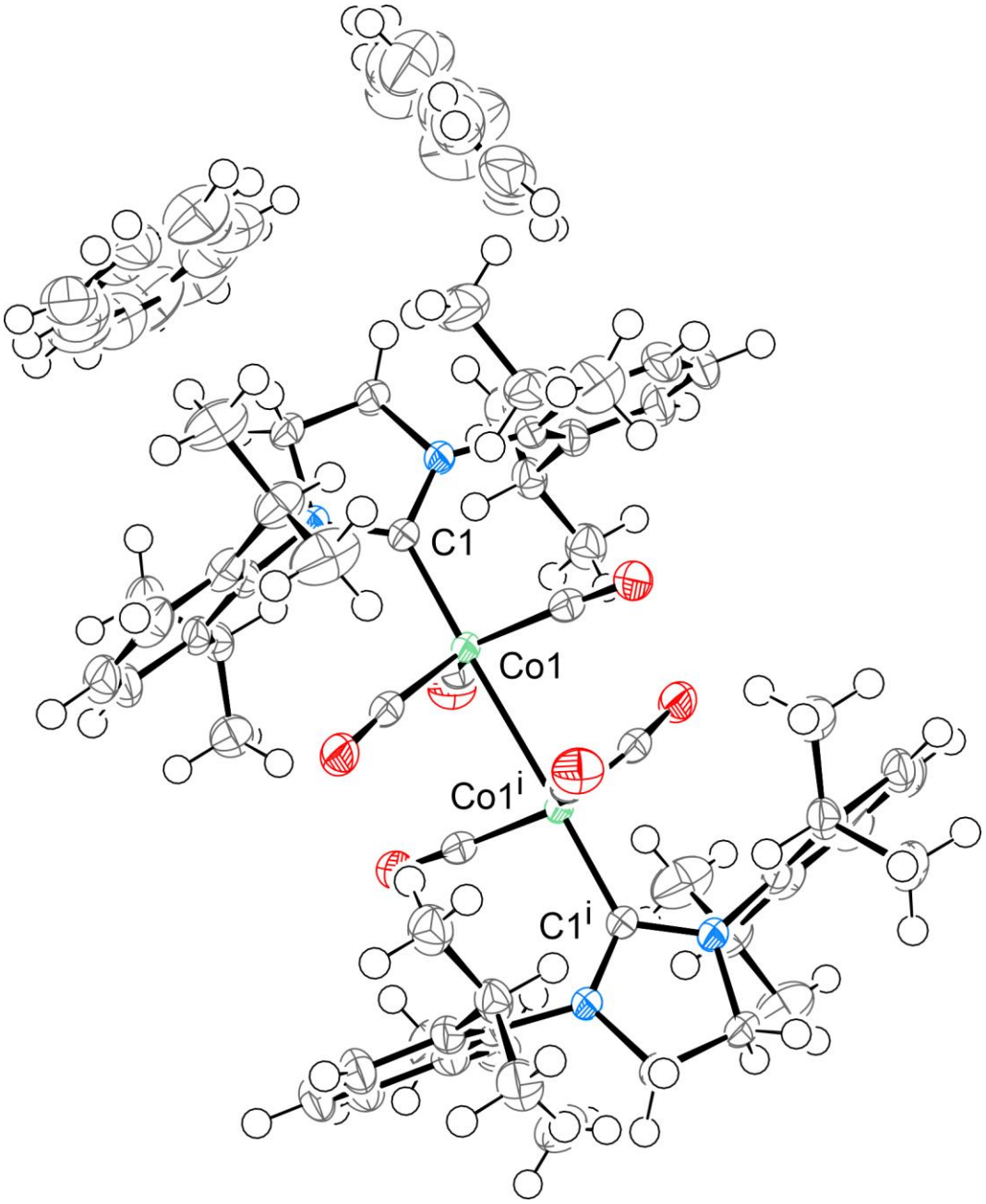

Figure S62. ORTEP of **2-^{i}Pr** at 80 % probability level for non-hydrogen atoms according to single crystal X-ray diffraction data. Selected interatomic distances [Å]: Co1–C1 1.9464(10), Co1–Co1^{i} 2.7512(3).

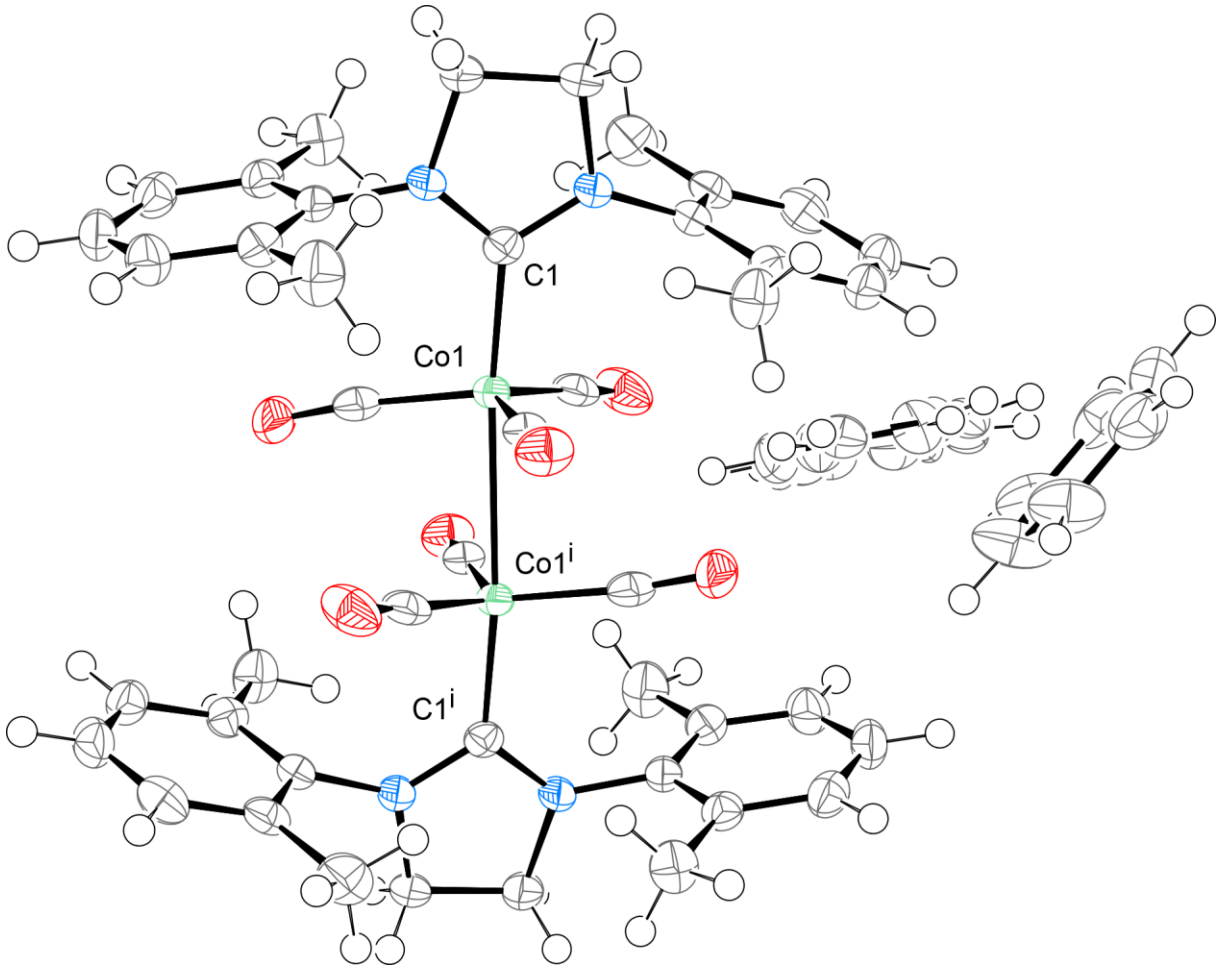

Figure S63. ORTEP of **2-Me** at 70 % probability level for non-hydrogen atoms according to single crystal X-ray diffraction data. Selected interatomic distances [Å]: Co1–C1 1.940(2), Co1–Co1^{i} 2.7183(6).

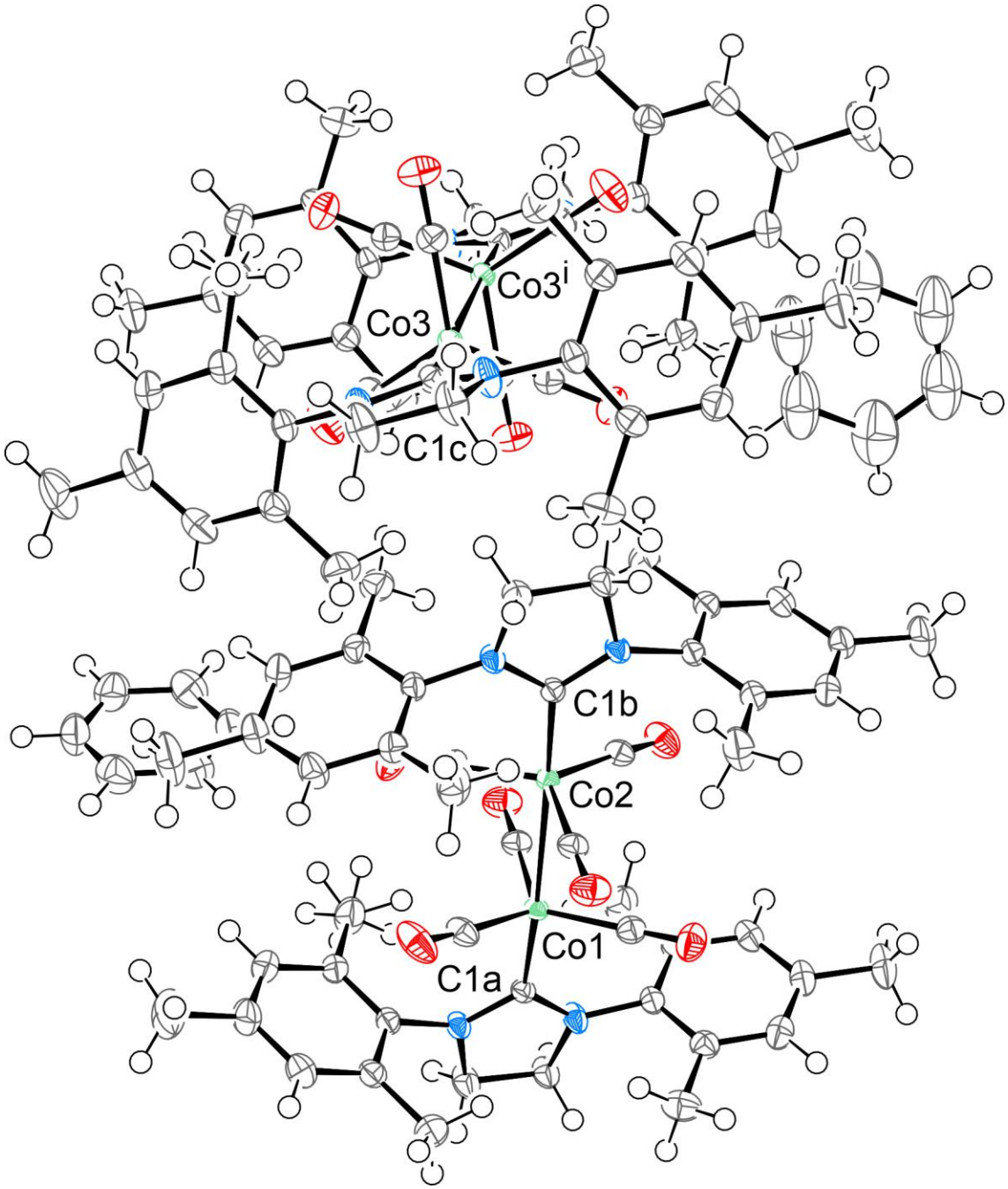

Figure S64. ORTEP of **2-Mes** at 70 % probability level for non-hydrogen atoms according to single crystal X-ray diffraction data. Selected interatomic distances [Å]: Co1–C1a 1.9390(9), Co2–C1b 1.9383(9), Co1–Co2 2.71989(18), Co3–C1c 1.9471(9), Co3–Co3^{i} 2.7520(2).

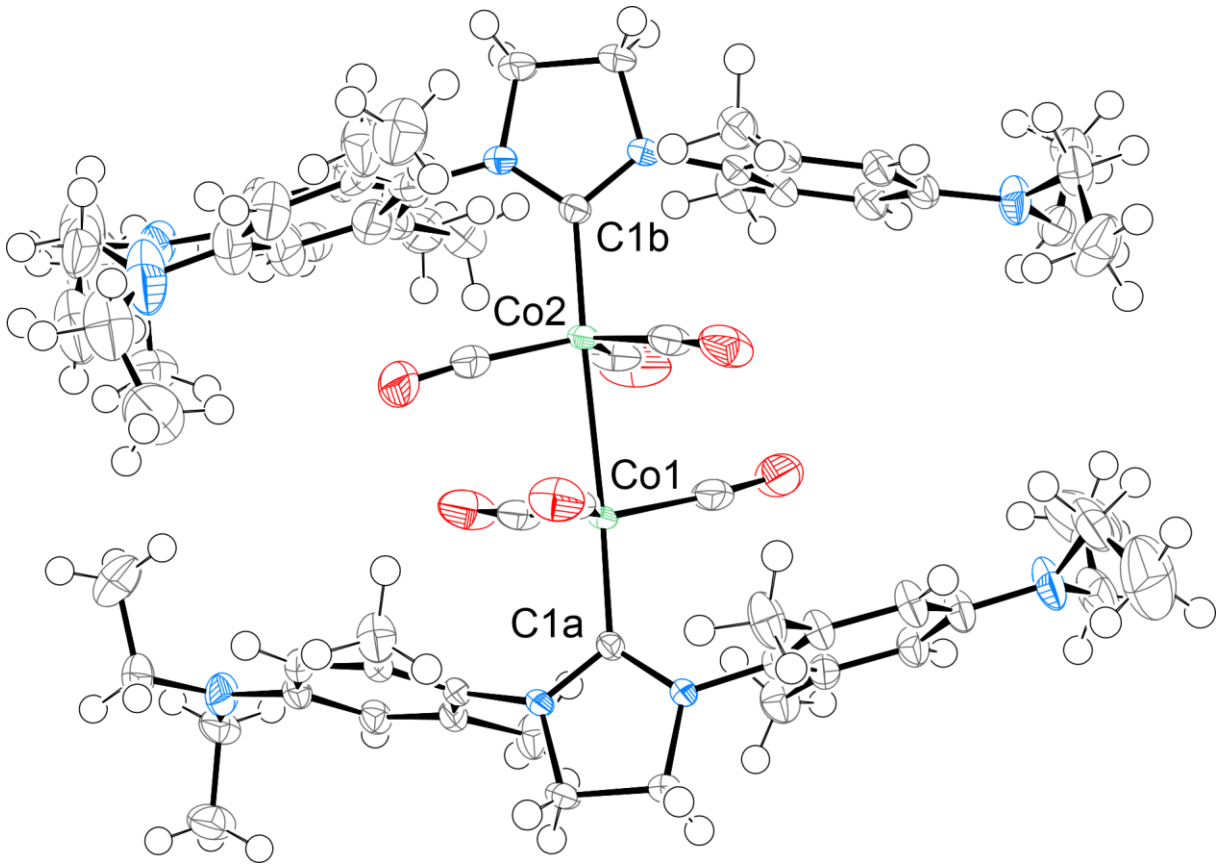

Figure S65. ORTEP of **2-NEt$_2$** at 80 % probability level for non-hydrogen atoms according to single crystal X-ray diffraction data. Selected interatomic distances [Å]: Co1–C1a 1.9388(9), Co2–C1b 1.9468(9), Co1–Co2 2.72357(18).

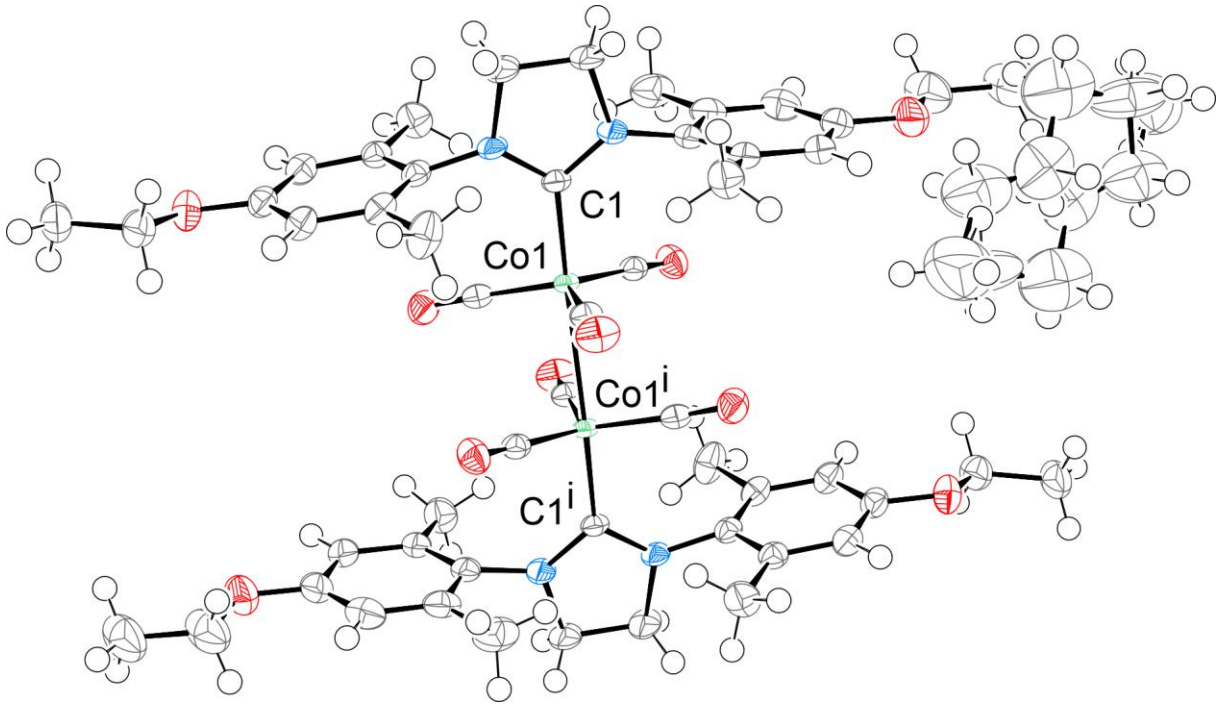

Figure S66. ORTEP of **2-OEt** at 80 % probability level for non-hydrogen atoms according to single crystal X-ray diffraction data. Selected interatomic distances [Å]: Co1–C1 1.9471(13), Co1–Co1^{i} 2.7431(3).

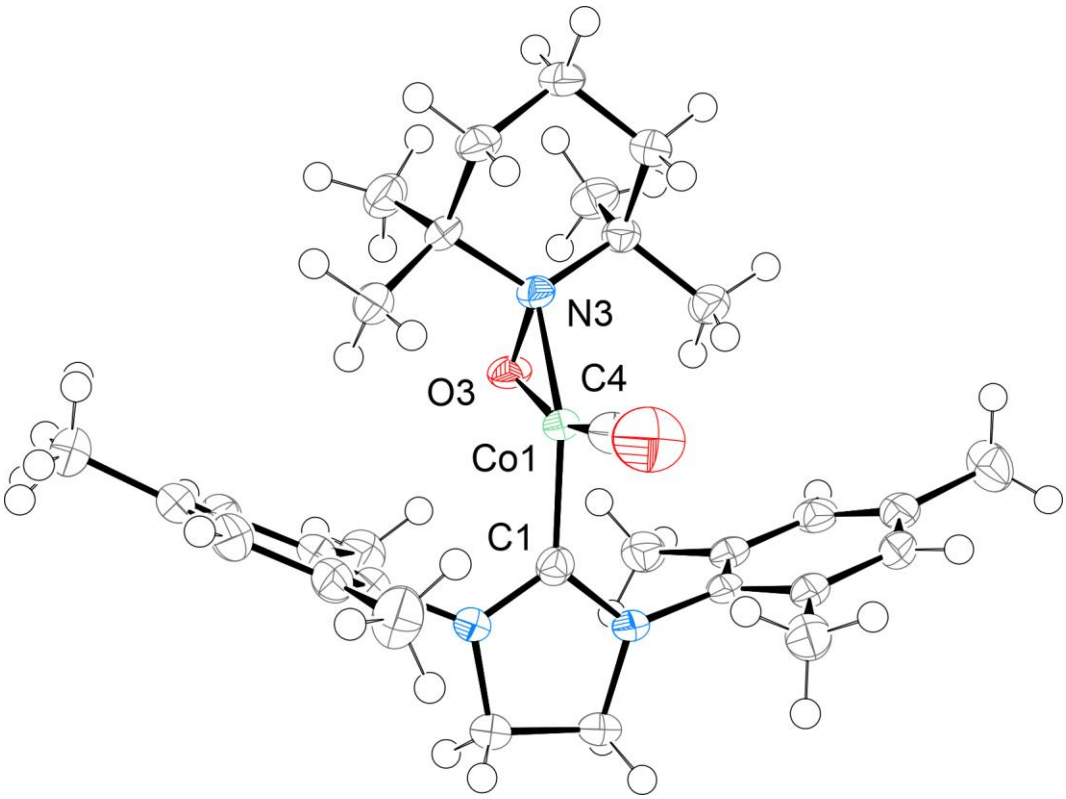

Figure S67. ORTEP of **3** at 70 % probability level for non-hydrogen atoms according to single crystal X-ray diffraction data. Selected interatomic distances [Å]: Co1–C4 1.6997(16), Co1–O3 1.8640(9), Co1–C1 1.8829(14), Co1–N3 1.9361(11).

8. References

1. P. Horeglad, M. Cybularczyk, B. Trzaskowski, G. Z. Żukowska, M. Dranka and J. Zachara, *Organometallics*, 2015, **34**, 3480-3496.
2. Z. Ouyang, J. Du, L. Wang, J. L. Kneebone, M. L. Neidig and L. Deng, *Inorg. Chem.*, 2015, **54**, 8808-8816.
3. M. Iglesias, D. J. Beetstra, J. C. Knight, L.-L. Ooi, A. Stasch, S. Coles, L. Male, M. B. Hursthouse, K. J. Cavell, A. Dervisi and I. A. Fallis, *Organometallics*, 2008, **27**, 3279-3289.
4. S. Leuthäußer, D. Schwarz and H. Plenio, *Chem. Eur. J.*, 2007, **13**, 7195-7203.
5. S. Takebayashi and R. R. Fayzullin, *Organometallics*, 2021, DOI: 10.1021/acs.organomet.0c00765.
6. G. W. Nyce, S. Csihony, R. M. Waymouth and J. L. Hedrick, *Chem. Eur. J.*, 2004, **10**, 4073-4079.
7. A. V. Zhukhovitskiy, J. Geng and J. A. Johnson, *Chem. Eur. J.*, 2015, **21**, 5685-5688.
8. Y. Zhang and S. T. Diver, *J. Am. Chem. Soc.*, 2020, **142**, 3371-3374.
9. M. Süßner and H. Plenio, *Chem. Commun.*, 2005, DOI: 10.1039/B512008J, 5417-5419.
10. M. Shang, J. Z. Chan, M. Cao, Y. Chang, Q. Wang, B. Cook, S. Torker and M. Wasa, *J. Am. Chem. Soc.*, 2018, **140**, 10593-10601.
11. R. Dorta, E. D. Stevens, C. D. Hoff and S. P. Nolan, *J. Am. Chem. Soc.*, 2003, **125**, 10490-10491.
12. R. E. Hoffman and E. D. Becker, *J. Magn. Reson.*, 2005, **176**, 87-98.
13. G. H. Imler, M. J. Zdilla and B. B. Wayland, *Inorg. Chem.*, 2013, **52**, 11509-11513.
14. G. Sheldrick, *Acta Crystallogr. A*, 2015, **71**, 3-8.
15. G. Sheldrick, *Acta Crystallogr. C*, 2015, **71**, 3-8.
16. L. J. Farrugia, *J. Appl. Crystallogr.*, 2012, **45**, 849-854.